Charles University in Prague

Faculty of Mathematics and Physics

DOCTORAL THESIS

Tomáš Špringer

IN SITU STUDY OF NUCLEIC ACIDS INTERACTIONS KEY FOR GENE EXPRESSION AND THERAPY BASED ON ITS SILENCING

Institute of Physics of Charles University

Supervisor: **Prof. RNDr. Josef Štěpánek, CSc.**

Charles University in Prague,
Faculty of Mathematics and Physics
Institute of Physics

Associate Supervisor: **Prof. Jiří Homola, Ph.D., DSc.**

Academy of Sciences of the Czech Republic, Prague
Institute of Photonics and Electronics, v. v. i.

Study programme: Physics

Specialization: Biophysics, Chemical and Macromolecular Physics

Prague 2014

ACKNOWLEDGEMENT

I would like to express my gratitude to my supervisor Prof. Josef Štěpánek from the Institute of Physics of Charles University for his continuous help and professional guidance. I would like to also extend my appreciation to Prof. Jiří Homola from the Institute of Photonics and Electronics of the AS CR, v.v.i., for his professional guidance and extensive support.

I am also grateful to my colleagues with whom I collaborated on multiple research projects during my doctoral studies. These people include Hana Vaisocherová, Marek Piliarik, Hana Šípová, Markéta Bocková, Kateřina Mrkvová, Maria Laura Ermini, Xue Song, Ludmila Jiráková, Veronika Ševců, Josefína Lamačová, Karel Chadt, Nicolas Scott Lynn, Barbora Špačková, Jana Jabloňová, Milan Vala, Pavel Adam, and others at the Institute of Photonics and Electronics of the AS CR, v.v.i. Special thanks also go to Dr. Ivan Rosenberg for the inspiring discussions and Pavel Novák at the Institute of Organic Chemistry and Biochemistry of the AS CR, v.v.i. Finally, I would like to thank Jan Vachoušek at the Institute of Physics of Charles University.

I am deeply grateful to my family, especially to my wife, who has a prodigious comprehension for my time-consuming efforts to solve scientific puzzles. Special thanks also go to my parents, who always supported me during all studies.

Try not to be a person of success,
but rather a person of virtue.

Albert Einstein

I declare that I carried out this doctoral thesis independently, and only with the cited sources, literature and other professional sources.

I understand that my work relates to the rights and obligations under the Act No. 121/2000 Coll., the Copyright Act, as amended, in particular the fact that the Charles University in Prague has the right to conclude a license agreement on the use of this work as a school work pursuant to Section 60 paragraph 1 of the Copyright Act.

In Prague Tomáš Špringer

Název práce: *In situ* studium interakcí nukleových kyselin významných z hlediska genové exprese a terapie založené na jejím potlačení

Autor: Tomáš Špringer

Katedra / Ústav: Fyzikální ústav Univerzity Karlovy

Vedoucí doktorské práce: Prof. RNDr. Josef Štěpánek, CSc., Karlova Univerzita v Praze, Matematicko-fyzikální fakulta, Fyzikální ústav UK

Abstrakt: V dizertační práci studujeme nová analoga odvozená od R06 aptameru cílící na TAR vlásenku HIV viru s použitím citlivého biosensoru s povrchovými plasmony, který umožňuje sledování molekulárních interakcí v reálném čase. Vyšetřujeme sedm různých modifikací, které jsou umístěné na devíti pozicích R06 aptameru, a odhalujeme jejich použitelnost při tvorbě účinných a stálých anti-TAR oligonukleotidů. Dále zjišťujeme, které pozice jsou vhodné pro nahrazení modifikací, a zároveň interpretujeme výsledky v kontextu lokální nukleotidové geometrie a interakcí v TAR/anti-TAR komplexu. V dizertační práci dále vyvíjíme nový fluidický systém, který eliminuje disperzi vzorku a míšení vzorků, a tak umožňuje přesné sledování molekulárních interakcí na povrchu SPR čipu. Pro charakterizaci podmínek měření na povrchu oligonukleotidového čipu studujeme stínící efekt jednomocných a dvoumocných kationtů, které jsou klíčové pro interakci záporně nabitých oligonukleotidů.

Klíčová slova: TAR vlásenka, modifikace, DNA/RNA čip, biosensor s povrchovými plasmony, mikrofluidika

Title: *In situ* study of nucleic acids interactions key for gene expression and therapy based on its silencing

Author: Tomáš Špringer

Department / Institute: Institute of Physics of Charles University

Supervisor of the doctoral thesis: Prof. RNDr. Josef Štěpánek, CSc., Charles University in Prague, Faculty of Mathematics and Physics, Institute of Physics

Abstract: In this doctoral thesis we study novel analogues based on R06 aptamers and targeting TAR hairpins of the HIV virus by means of surface plasmon resonance biosensor, which allows for sensitive and real-time monitoring of molecular interactions. We investigate seven different modifications placed at nine different positions on the R06 aptamer in order to find out their applicability in the construction of efficient and stable anti-TAR oligonucleotides. We also determine which positions are suitable for substitutions with a modification and interpret the results in the context of the local nucleotide geometries and interactions in the TAR/anti-TAR complex. In this doctoral thesis we further develop a new fluidic

system. This fluidic system eliminates sample dispersion and intermixing effects and thus enables accurate monitoring of molecular interactions on the surface of an SPR chip. We also characterize experimental conditions on the surface of an oligonucleotide chip and their relations towards bio-molecular assays. Specifically, we study the shielding effect of monovalent and divalent cations, which are crucial for the interaction of negatively charged oligonucleotides.

Keywords: TAR hairpin, modification, DNA/RNA chip, SPR biosensor, dispersionless microfluidics

Table of Contents:

1 Introduction

1.1 Nucleic acids

Nucleic acids are molecules which have essential function for storage and expression of genetic information in organisms [1]. The genetic information is stored in double-stranded deoxyribonucleic acid (DNA) in a genome. This information is transcribed into single-stranded messenger ribonucleic acid (m-RNA) and then translated into proteins in ribosome. The genetic information is duplicated during the process which is called DNA replication.

DNA and RNA have structure which consists of nucleobases that are connected to the sugar-phosphate backbone via N-glycosidic bond. DNA and RNA strand contains in a sugar-phosphate backbone deoxyribose and ribose, respectively. Nucleobases in DNA are C (cytin), T (thymin), A (adenin) and G (guanin). RNA contains C, U (uracil), A and G. DNA basically forms double-stranded molecules while RNA is found single-stranded in a living cell. The duplex is stabilized mainly by base-pairing, stacking, ionic and hydrophobic interactions in aqueous environment. Base pairing is sequence specific where A forms two hydrogen bonds with T and C three hydrogen bonds with G (see Figure 1). The first model of DNA duplex structure was described by James Watson and Francis Crick in 1953 [2].

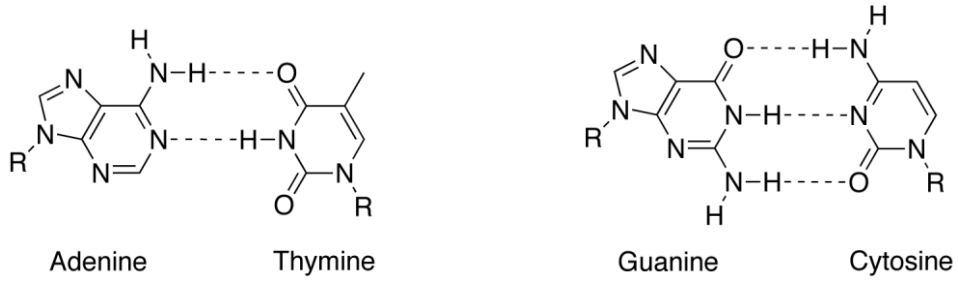

Figure 1. Canonical Watson-Creek base pairing in nucleic acids.

Nucleic acids are further stabilized by non-canonical base pairing such as Hoogsteen or wobble interactions. Hoogsteen base pairing is typically observed in triplex structures where the third strand binds around the duplex in the major groove [3-5]. Homopurine and homopyridines sequences (e.g. poly- dT•dA*dT or poly-

rC•rG*rC$^+$) are employed in these structures. Hoogsteen base pairing is also observed in quadruplexes which are formed by the strands abundant in guanines [6, 7]. These structures were found in telomeres of living organisms. Wobble base pairing is the other example of non-canonical interaction of nucleic acids [8]. This base paring, which occurs for instance between guanine-uracil, hypoxanthine-cytosine, hypoxanthine-adenine and hypoxanthine-uracil, is employed between codon and anti-codon interaction during RNA translation.

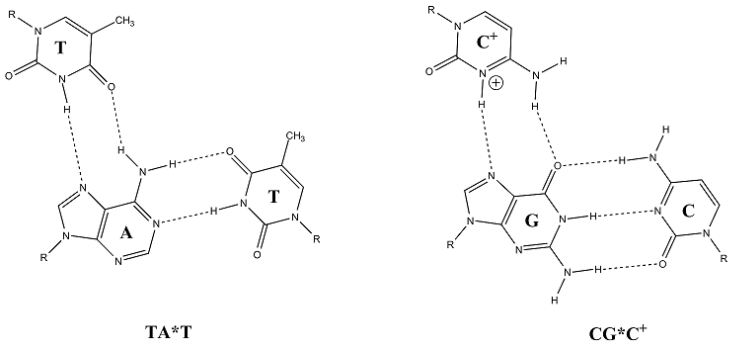

*Figure 2. Hoosteen base pairing of poly- dT•dA*dT or poly- rC•rG*rC$^+$.*

Nucleic acid duplexes form different conformation under specific conditions [1]. Most common conformation of DNA duplex is B-form, which is found under the physiological conditions in cells. When DNA is dehydrated, A-form is adopted. DNA duplex might also adopt Z-form which forms left-handed structure in contrary to A-DNA and B-DNA.

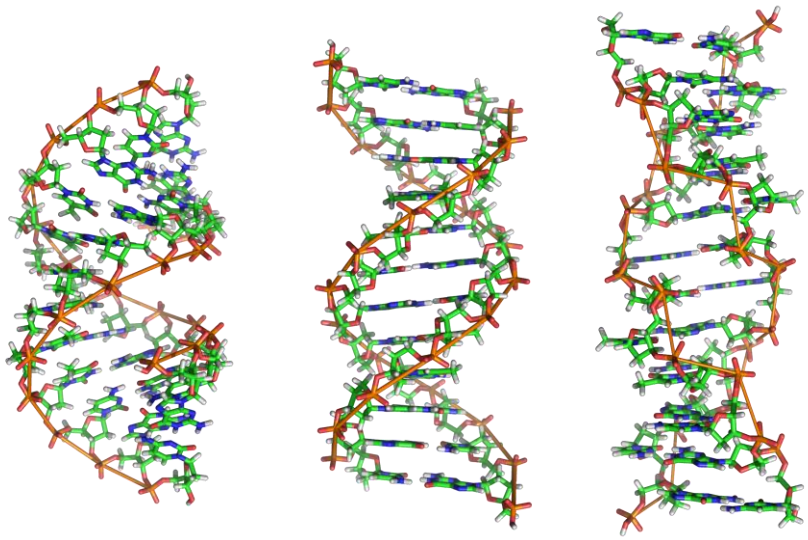

Figure 3. A- , B- and Z-form of nucleic acids.

Interactions of nucleic acids are affected by many factors such as temperature, type and concentration of salts and pH of environmental, hydration of the nucleic acids and last but not least the base composition of nucleic acid strands [1, 9-11]. For the investigation of the nucleic acid interactions, short sequences of nucleic acids about 8-30 nucleotides, which are called oligonucleotides, are typically used. The general parameter which characterizes the complexes of nucleic acids is melting temperature [9]. The complexes are formed under the low temperature conditions. When the system is heated, the thermal motion overcomes the binding forces and the structure is denatured into single strands. The melting temperature of the system is defined as the state when the half of the complexes is compact and the half is denatured into single strands.

1.2 Hybridization of oligonucleotides

The complex formation of nucleic acid strands, called hybridization, is a fundamental process which is employed in many applications from DNA biosensor or DNA microarray technology [12-15] to therapeutic strategies [16-18]. Formation of duplexes with complementary base sequences, which is the main type of oligonucleotide hybridization, have been deeply studied in a solution [9-11, 19], however, significantly lower effort has been paid to investigation of hybridization on a surface of RNA/DNA chip [20, 21].

1.2.1 Hybridization of oligonucleotides in a solution

Hybridization of oligonucleotides in a solution is nowadays fairly well understood [9-11, 19]. In these studies the method such as UV-Vis spectroscopy or calorimetry has been typically applied. As known the oligonucleotides are negatively charged molecules, therefore, the cations in their vicinity are crucial for shielding of the repulsive forces and subsequent efficient hybridization of complementary oligonucleotides.

In 2006 and 2008, SantaLucia, Jr., et al. [9, 11] presented the nearest-neighbor model to predict the duplex stability. This model was derived from the melting studies employing the UV-Vis absorption spectroscopy for concentration of monovalent cations (Na^+) up to 1M. The validity of this model was lately extended

for other monovalent cations by Nakano et al. [19]. In this study it was shown that the effect of monovalent sodium, potassium and cesium cations on duplex stability was the same. Recently Owczarzy et al. [10], based on the analysis of a large set of UV absorption spectra, proposed an empirical formula for oligonucleotide duplexes enabling the prediction of melting temperatures, transition enthalpies, entropies and free energies in buffers containing magnesium and monovalent cations. Moreover, it was observed the competition of monovalent sodium and divalent magnesium on duplex stability. For certain combination of monovalent sodium and divalent magnesium the stability of a duplex was not a superposition of both cations but paradoxically the stability decreased [10].

Not only the empirical models have been developed to predict the duplex stability in a solution but also some theoretical models have been established. Two major types of polyelectrolyte theories for studying the nucleic acid helix stability have been proposed: the Poisson-Boltzmann (PB) theory [22-25] and the counterion condensation (CC) model [26]. The CC theory is based on the assumption of two-state ion distribution and is a double-limit law, i.e., it is developed for dilute salt solution and for nucleic acids of infinite length. The PB theory is a mean-field theory that ignores ion-ion correlations, which can be important for multivalent ions (e.g., magnesium). Recently, Tan and Chen proposed optimized tightly bound ion model (TBI), which employs separate treatments for tightly bound ions and for diffuse ions surrounding DNA molecules [27, 28]. This model accounts for discrete modes of counterion binding. Fluctuations and correlations between the ions tightly bound to DNA are considered, while these effects were neglected in other models based solely on the meanfield approach of the Poisson-Boltzmann equation.

1.2.2 The effect of DNA chip surfaces on a oligonucleotide hybridization

Although the underlying hybridization process is fairly well understood in a bulk solution, the understanding of solid-phase (SP) hybridization (hybridization of oligonucleotides on a DNA/RNA chip) in the presence of cations is much less developed [20, 21]. The presence of a surface in DNA/RNA chips has great effect on observed interactions. The immobilized probes (the oligonucleotides which are attached to the surface of DNA chip surface) are typically densely immobilized on a

surface of DNA/RNA chip. Typically, DNA probe layers are characterized by a surface density of 10^{12}–10^{13} probes/cm^2 and a layer thickness of several nanometers [20, 29], which correspond to a local concentration of oligonucleotides about 0.1 M. For comparison the typical experiments in a solution are performed for μM concentrations [9, 10]. Therefore all interactions that proceed on a surface of DNA/RNA chip are spatially restricted. Moreover, the oligonucleotides contain negatively charged phosphate groups. Together with the high density of immobilized oligonucleotides it represents an environment with high density of negative charges, where the electrostatic effects play a crucial role. Under these conditions it is not surprising that the role of the cations, which effectively shield the negative charges, is emphasized.

Several experimental and theoretical works have demonstrated the repulsion of the immobilized probes and its destabilizing effect on duplexes, and related it with the cation shielding [20, 30-33]. Peterson et al. [32] and Yu et al. [30] reported that the hybridization efficiency (HE), which is the ratio of hybridized targets (the oligonucleotide sequence which binds to the probe) to the probes on a surface, decreases with an increase of the surface probe density. Peterson et al. [32] showed that the yield of the probe immobilization on the surface increases with an increase of the concentration of monovalent sodium in the immobilization buffer. The dependence of HE on sodium concentration in the range of 0–500 mM was studied in the work of Okahata et al. [31]. In agreement with the electrostatic theory, it was determined that the HE increases with an increase of the sodium concentration. Recently Cho et al. [33] used a surface plasmon resonance (SPR) sensor to demonstrate that the key factor influencing the probe density and subsequent SP hybridization is the total concentration of sodium, whereas the type of buffer had only a minor effect.

For SP hybridization of complementary oligonucleotides, several theoretical models have been also developed. Vainrub and Pettitt [34] developed a macroscopic theoretical model considering the repulsion between the charged immobilized probe layer and the target as the main factor influencing the hybridization yield and the binding kinetics on a DNA chip. This model was subsequently improved by Halperin et al. [35] who treated the immobilized probes as a 3D layer.

In summary, the experimental and theoretical works dealing with the cation effect on SP hybridization published so far have focused more on the probe density,

while the role of different types and concentrations of cations has been addressed to a lesser extent. Beyond these progresses the further study of oligonucleotide interactions on a DNA chip surface is needed. For example, the effect of multivalent or simultaneous effect of monovalent and multivalent cations on duplex stabilization has not been fully explained.

1.3 Short nucleic acids as a therapeutic agent

Oligonucleotides are very often considered as potential agents in therapeutic strategies. They can create variety of structures from linear geometries to complex three dimensional ones. Moreover, they are easily chemically prepared and modified. In the general concept, oligonucleotides are introduced to the cell in order to interact with nucleic acids or proteins, which results in the modulation or inhibition of expression of pathogenic proteins [16-18].

1.3.1 Basic therapeutic strategies

In this paragraph we will describe antisense strategy, which utilizes the oligonucleotides complementary to the specific sequences [16, 17], and the strategy based on application of aptamers (oligonucleotides with specific three-dimensional structures) [18].

The typical target in antisense strategy is a messenger m-RNA which has a crucial function in a protein expression. Messenger m-RNA is transcribed from a human genome, transported into endoplasmatic reticulum and finally employed in protein synthesis [1]. We can distinguish three types of anti-sense strategies [36-39]: i) the use of single stranded anti-sense oligonucleotide (AS-ON), ii) the triggering of RNA cleavage through catalytically active ONs referred as ribozymes, iii) RNA interference (RNAi) induced by small interfering RNA (siRNA) molecules. The differences among the approaches are summarizes in Figure 4. In the further text, the two main antisense mechanisms, which use single stranded As-ON, are briefly described.

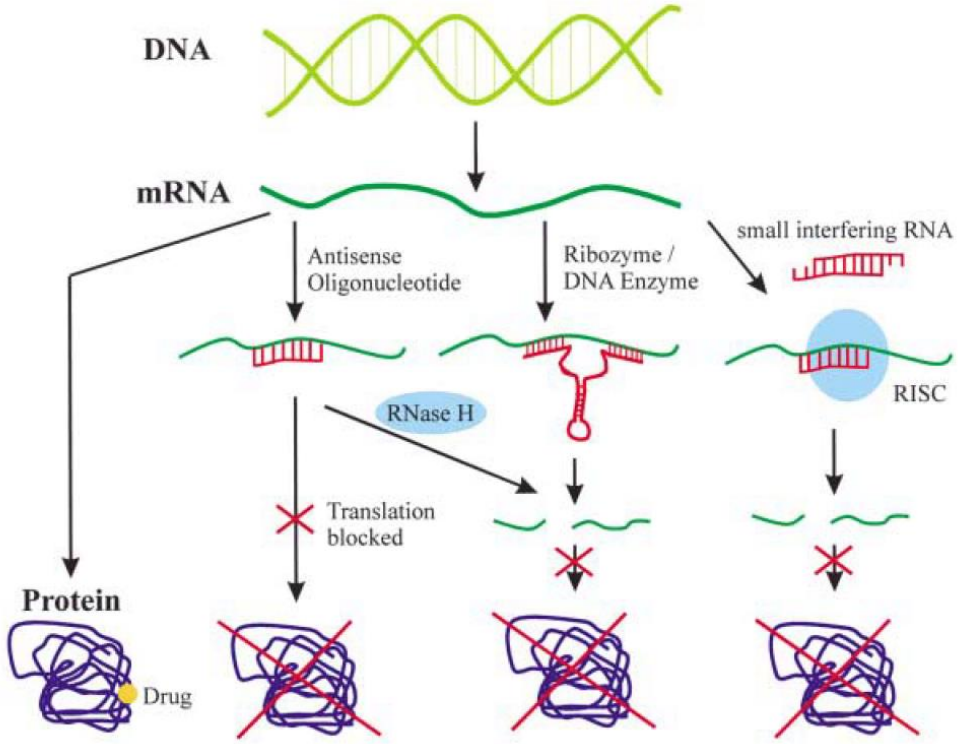

Figure 4. Comparison of different antisense strategies. While most of the conventional drugs bind to proteins, antisense molecules pair with their complementary target RNA. Antisense-oligonucleotides block translation of the mRNA or induce its degradation by RNase H, while ribozymes and DNA enzymes possess catalytic activity and cleave their target RNA. RNA interference approaches are performed with siRNA molecules that are bound by the RISC and induce degradation of the target mRNA (reprinted from [37]).

In the first mechanism As-ONs activating RNase H enzyme are used. RNase H belongs to endonucleases. It naturally recognizes RNA/DNA hybrid duplex and cleaves the RNA molecule while the DNA molecule is not affected [40]. After the degradation of m-RNA molecule in the hybrid RNA/As-ON duplex, the complex is split and the free intact As-ON is prepared for binding to the next m-RNA molecule. The same As-ON can be many times recycled which leads to high efficiency of this strategy. In special cases the protein synthesis might be downregulated up to 85%-95% of the control level [38] .

The second mechanism is based on inhibition of protein expression by a steric blocking with As-ON. As-ON is bound to the specific complementary sequence of m-RNA which leads to termination of the m-RNA maturation and thus inhibits the protein synthesis. For instance, one of the potential target steps is m-RNA splicing when the non-coding sequences of m-RNA are cleaved. To block m-RNA splicing, As-ON, which physically prevents the cleavage of m-RNA or does not enable the

binding of essential factors, is bound to the specific sequence of m-RNA [39]. As-ONs might also downregulate the protein synthesis by inhibition of m-RNA translation as demonstrated in [41]. As-ON is directed to the translation initiation codon of m-RNA which leads to termination of protein translation.

The antisense strategy was firstly demonstrated by Paterson et al. in 1977 who used synthetic single-stranded DNA to inhibit m-RNA translation [42]. A year later, Zamecnik et al. showed that the replication of Rous Sarcoma virus could be inhibited by synthetic oligonucleotide [43].

The therapeutic strategy based on application of aptamers uses the three-dimensional structure of oligonucleotides to treat diseases [18, 44-46]. Originally, aptamers were chosen as an agent that bound to the target protein and inhibited its function. Nowadays, this method is widened for usage in nucleic acid binding, small molecule binding or cell binding [47, 48]. The effective aptamers for binding to specific molecule can be found by SELEX method (System Evolution of Ligands by EXponencial enrichment) [49]. SELEX method starts with the pool of random sequences (typically about 10^{14}-10^{15} different sequences), which is allowed to bind with the target molecule. The oligonucleotides with highest affinities are bound to the target molecule and amplified by PCR method. The selected oligonucleotides are again allowed to incubate with the same target molecule. These steps are several times repeated until favorite oligonucleotides, which have high affinity and specificity to the initial target molecule, are obtained. The application of aptamers was demonstrated for basic fibroblast growth factor (bFGF) which was implicated in neovascularization of tumors as well as other disease processes [50]. Optimized aptamer binds specifically to the heparin-binding site of bFGF and does not interfere with the other members of the FGF family.

1.3.2 Chemical modifications of oligonucleotides

The effective oligonucleotides applicable in therapeutic strategies have to fulfill several requirements: a) ability to bind specifically and with high affinity to the target partner b) resistance against nucleases in organism c) nontoxicity for the organism d) ability to penetrate into a cell e) ability to activate RNase H enzyme (only for As-ON activating RNase H) [51, 52]. Because not all these requirements

are fulfilled for native oligonucleotides (especially they are quickly degraded by cellular nucleases), various chemical modifications of oligonucleotides have been proposed, synthesized, and tested.

General, we can distinguish three types of modification of ribonucleotides: analogs with unnatural bases, with modified sugars (with special attention to 2′position of ribose) and with altered phosphate backbones. The analogues with modified unnatural bases exhibited low stability against nucleases, therefore, this approach did not seem to be promissing [36]. Nowadays, chemical modifications are applied to modify sugars or phosphate backbone, where we can distinguish three generations of modifications (see Figure 5) [36, 38]. In the first generation one of the non-bridging oxygen in the phosphate group is replaced with either sulphur group (phosphorothioates), methyl group (methylphosphonates) or amines (phosphoramidates). This modification improves the resistance against nucleases and many of them activates RNase H [17, 37, 38]. This group contains the only one antisense oligonucleotide, Vitravene, which has been so far approved by United States Food and Drug Administration (as a drug against cytomegalovirus). Over the indisputable progress in the first generation of oligonucleotides, these modifications significantly suffer from *in vivo* side effects. Second generation involves oligonucleotides which are modified at 2′ position of ribose. Most often used modifications are 2′-O-methyl and 2′-O-methoxyethyl ribose. These modified oligonucleotides have higher affinity to m-RNA sequence, better tissue uptake, increased resistance to nucleases, longer *in vivo* half-life and lesser toxicity than the first generation [38, 53]. On the other hand, these modifications do not activate RNase H. In the third generation, chemical modifications of furanose ring, phosphate linkages and riboses are employed. Most famous third-generation oligonucleotides are locked nucleic acid (LNA), peptide nucleic acid (PNA) and morpholino phosphoroamidates (MF). These oligonucleotides have high resistance to nucleases in cellular environment and high affinity to target RNA sequence [38, 54]. However, the third generation of oligonucleotides does not activate RNase H, therefore the biological effect is caused mainly by the steric hindrance.

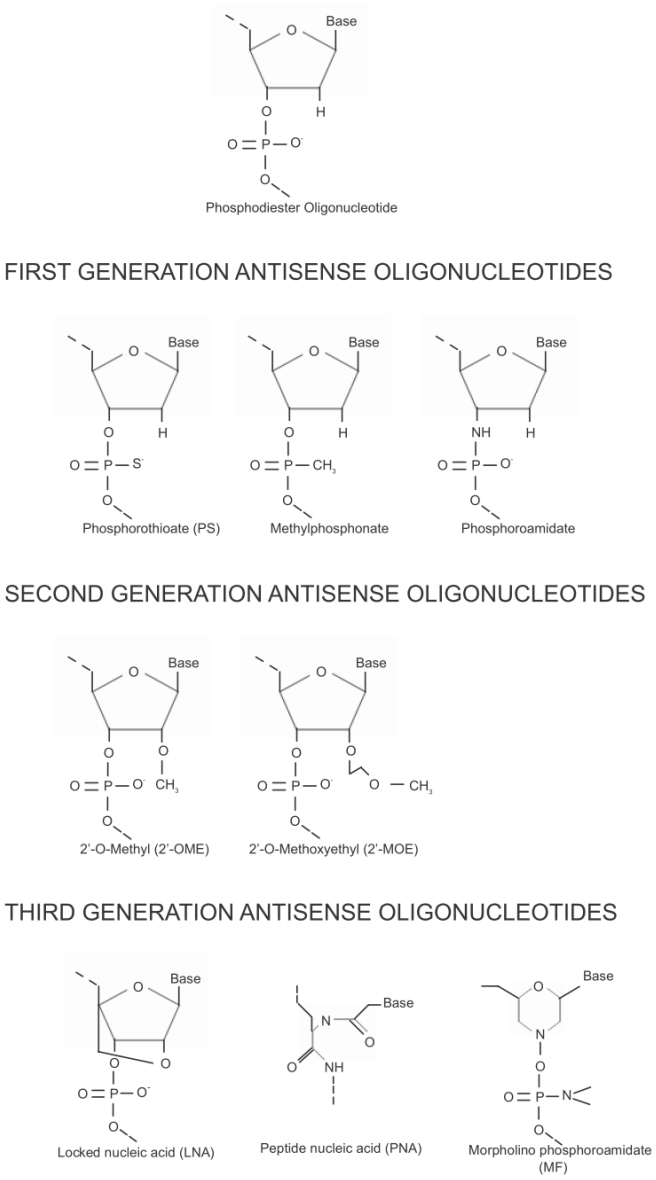

Figure 5. The chemical structures of selected modifications in the first, second and third generation. The natural nucleotide is shown on the top (reprinted from [38]).

To combine the chemical properties of different modification, chimeric strategy was developed [55]. In this approach, a chimeric ON analogue is composed of the segments with different modifications. For instance, Wu et al. used ON with central segment consisting of DNA or phosphorothioate-DNA monomers and with the flanking ends consisting of 2′-O-methyl RNA. They found that the ends ensured high resistance to nucleolytic degradation and the central segment of the length of four or five deoxy-residues was sufficient for activation of RNase H [56].

1.4 HIV virus

Human immunodeficiency virus (HIV) is a lentivirus from retrovirus family. If human being is infected the virus causes acquired immunodeficiency syndrome (AIDS) [57-59]. In this state of the organism the immunity is weakened and the additional diseases are life-threatening. According to the annually report of the Joint United Nations Programme on HIV/AIDS (UNAIDS), all over the world 35.3 millions of people lived with HIV virus in 2012. In this year 2.6 million were newly infected and 1.8 million died due to AIDS related infections [60]. These data demonstrated the widespread and dangerousness of this disease.

HIV virus has various genetic variants [61]. This high diversity is caused by the origin of HIV virus and also by high mutation rate of reverse transcriptase. HIV virus is divided into two major groups, HIV-1 and HIV-2. HIV-1 is probably derived from chimpanzee viruses (SIVcpz) and HIV-2 from sooty mangabey viruses (SIVsm). HIV-1 is more virulent and infective therefore the prevalence of HIV-1 is global while HIV-2 virus is rather localized to West Africa. HIV-1 is further classified into three subgroups: M (main), N (new), and O (outlier).

1.4.1 HIV morphology

HIV virus is a spherical particle with diameter from 100 to 120 nm [58, 59, 62, 63]. The virus genome is composed of two identical single-stranded RNA molecules, which are enclosed by conical capsid created from viral capsid protein CA (p24). The capsid also encloses proteins Vif, Vpr, Nef, Vpu (Vpu for HIV-1, Vpx for HIV-2), nucleocapsid protein NC (p7), some cellular factors, and viral enzymes that are essential for the replication of HIV in human cell: reverse transcriptase (RT), integrase (IN) and protease (PR). Matrix surrounding capsid is composed of matrix protein MA (p17), which ensure the integrity of the viral particle. The outer envelope of the virus is created from a lipid bilayer which was formed from the host membrane during the budding of virus. The lipid bilayer envelope contains glycoproteins gp120 and gp41, which are responsible for the recognition of CD4 receptor of T cells during the entry to the host cell.

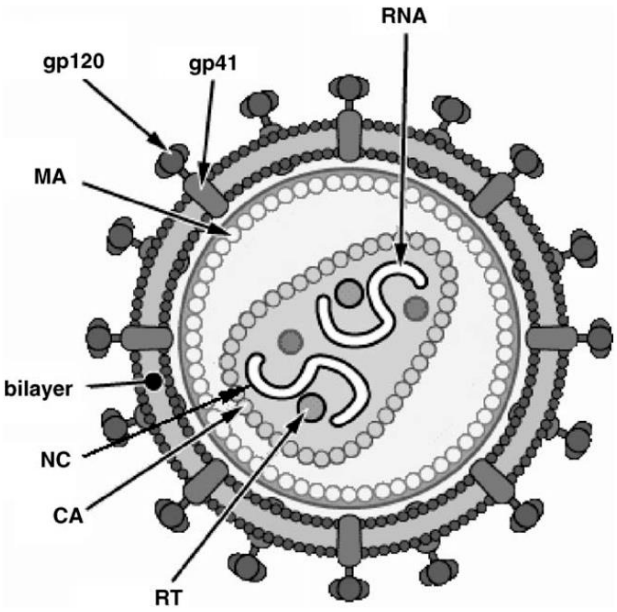

Figure 6. Schematic representation of HIV virus. The description of Figure is written in the text (reprinted from [58]).

1.4.2 HIV live cycle

HIV attacks macrophages and CD4 T cell in living organism [58, 59, 64, 65]. The entry of HIV virus to the cell begins with high-affinity attachment of viral protein gp120 to CD4 receptor of the cell [64, 66]. This initial binding is followed by subsequent interactions and structural changes of the viral particle, which allows for the fusion of viral and cell membranes and the entry of the capsid into the cell. By this way the viral RNA, proteins and enzymes such as RT, IN and PR are transported to the cell. In the cell, viral RNA is transcribed into a full-length double-stranded DNA by RT. The fidelity of the reverse transcription is affected by cellular protein APOBEC3G. To decrease this retroviral effect viral Vif is employed to suppress the expression of this protein. In general, the reverse transcription is highly error-prone process. This explains the variety of mutations, which leads to the drug resistance. Subsequently, viral DNA is directed by viral Vpr into the nucleus and integrated by the viral IN into the host genome. In this phase the HIV might be latent in the host genome for several years. In the first stage of viral transcription by cellular RNA polymerase II, only multi-spliced m-RNA is produced which allows to express the regulatory proteins at a basal level. Tat protein binds to the trans-activation response element (TAR) of proviral RNA and encourages transcription of viral genes. Rev is also regulatory protein. When Rev reaches the sufficient level, Rev binds to RRE

(Rev responsive element) on non-spliced or single spliced viral RNA and protect viral RNA from splicing. Rev also facilitates the transport of viral RNA from nucleus into the cytoplasm. Then, gp160 protein, which is precursor of gp120 and gp41, is produced together with Gag and Gag-Pol polyproteins. Gag and Gag-Pol polyproteins are precursors for structural proteins and enzymes RT, PR and IN. Before the viral budding Nef, Vpu and gp160 proteins are employed to decrease the number of CD4 molecules in the celular membrane in order to avoid interactions between gp120 and CD4. The bugging induces PR activity to cleave the Gag and Gag-Pol polyproteins, which leads to formation of new virion.

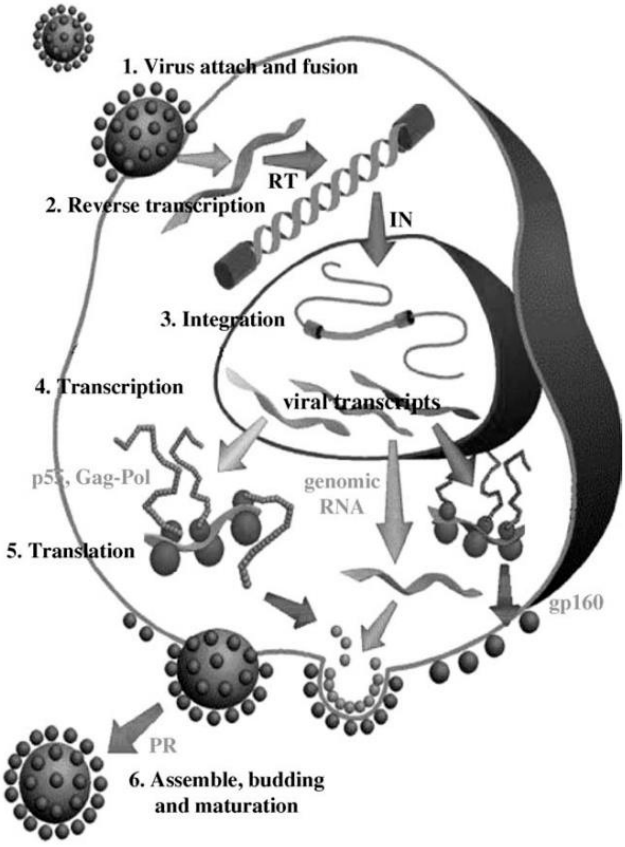

Figure 7. Life cycle of HIV virus in a human cell (reprinted from [58]).

1.4.3 Genome of HIV virus and its TAR element

HIV genome is composed of two identical 9.2kb nucleotides which codes nine genes (*gag*, *pol*, *env*, *tat*, *rev*, *nef*, *vif*, *vpr*, *vpu* (HIV-1) or *vpx* (HIV-2)) [58, 59]. Three of these genes - *gag*, *pol*, and *env* - contain information that is employed for

development of structural proteins in HIV virus**.** The other six genes - *tat*, *rev*, *vpr*, *nef*, *vif* and *vpu* (or *vpx* in the case of HIV-2) - are genes which are employed to regulate the different steps of the HIV replication.

Several hundred anterior nucleotides of HIV RNA at 5′ end is a non-coding sequence [58, 59]. Nevertheless, this part of HIV RNA contains essential structural and functional regions such as TAR, PBS, DIS and SD. TAR (nucleotides 1-59) is the binding site for the Tat protein and thus this region is responsible for activation of viral RNA transcription. PBS (primer bind site, 182-199) is important for initialization of reverse transcription. DIS (dimerization initial site, 248-271) is employed in dimerization of the two copies of viral RNAs into virion. SD (spliced donor site, 290) is used to generate all subgenomic spliced m-RNAs. Due to the essentiality for HIV reproduction, these regions are very often targets of nucleic-acid based strategies [18, 67-70]. For instance, in recent years TAR and DIS region have been widely studied as a target of aptamer strategy [18, 70].

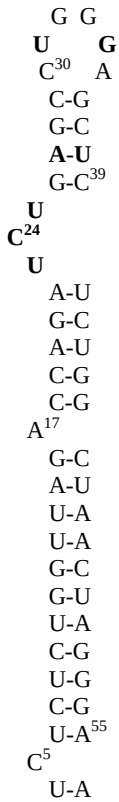

TAR region is the sequence of the initial 59 nucleotides at 5′side of HIV-1 RNA. It forms a hairpin structure with 6-nucleotide hairpin loop, hairpin stem and side bulge [59, 71-75]. The structure of TAR region of HIV-1 is shown in Figure 8. TAR hairpin is an essential structural and functional motive which is employed in transcription of viral RNA. TAR hairpin serves as a scafold for binding of Tat protein and subsequent cellular cyclin T1. These two proteins form complex that enable interaction with CDK9 (Cyclin Dependent Kinase 9). Bound CDK9 kinase hyperphosphorylates the cellular RNA polymerase II (its C-terminal domain), which enables effective function of RNA polymerase II. Without this step, the transcription is prematurely terminated.

Figure 8. The structure of the full-length TAR segment of HIV-1 RNA.

1.4.4 Tat protein

Tat protein is a regulatory protein targeting the TAR motive which enables the transcription of viral RNA [75-78]. Tat protein, especially basic amino acids 48-57, primarily binds to UCU bulge on at 5′ side of a stem. This leads to conformation changes and formation of base triplex U_{23}-A_{27}-U_{38} which is in contact with arginine group on Tat protein. If any other proteins are not present, Tat protein binds almost exclusively to the bulge region. When the cyclin T1 is present, the additional stabilization interactions are formed. Cyclin T1 primarily binds nucleotide U31 on TAR motive. Cyclin T1 also interacts with Tat protein, which encourages Tat protein to bind G34 with Lys-50. Cyclin T1 and Tat interaction is highly cooperative. It means that Tat binds to TAR hairpin very weakly without cyclin T1 and cyclin T1 does not bind TAR in the absence of Tat protein.

The binding of Tat protein to TAR hairpin is assumed to be crucial for the formation of the complex with cyclin T1 and CDK9. Therefore TAR is very often the target of antiviral strategies aiming to protect TAR hairpin against binding of Tat protein/cyclin T1 complex [18]. In general, there are reported two approaches. In the first approach the substrate with high affinity to Tat protein is offered. This strategy leads to consumption of free Tat protein. For instance, Yamamoto et al. reported the aptamer with affinity to Tat protein with K_d =0.12 nM, which is about of two orders better than that of TAR-Tat interaction [79]. The second approach is based on a substrate which binds directly TAR hairpin [80-82].

1.4.5 R06 aptamer and its kissing complex with TAR

Several papers focused their effort to find a suitable oligonucleotide with a high affinity and specificity to TAR hairpin [81-83]. Darfeuille et al. used SELEX method that is able to select the oligonucleotide with high affinity and a specificity to TAR from a huge pool of random sequence [82]. Darfeuille et al. employed DNA and RNA libraries containing more than 10^{11} sequences. The set of eleven RNA and DNA oligonucleotides were selected under the physiological ionic conditions. The selection buffer contained 140 mM potassium acetate, 20 mM sodium acetate, 3 mM magnesium acetate and 20 mM Hepes (pH 7.3 at 20°C). These oligonucleotides exhibited antisense and kissing interaction with target TAR hairpin. In general, RNA

molecules were found to have higher affinity than DNAs. The privileged oligonucleotide was found R06 aptamer with hairpin structure, which formed so-called kissing complex with TAR. The sequence of R06 aptamer is shown in Figure 9. The central 8-nucleotide loop of R06 aptamer contains the sequence 5′-UCCCAG-3′, which is fully complementary to the apical loop of TAR hairpin, and two adjacent bases forming "GA pair", which is very important for the stability of the kissing complex.

Figure 9. Class A of RNA oligonucleotides binding to TAR found with SELEX method. The sequences in a black box are complementary to the apical loop of TAR motive (reprinted from [81]).

In further studies the aspects such as the minimal length of R06 stem and the different combinations of the bases adjacent to the central six bases were investigated. In the study of Darfeuille et al. the minimal length of R06 aptamer, which ensured the same stability as the untruncated version of R06 aptamer, was investigated [84]. In these studies the central apical loop was conserved and the adjacent stem was shortened. The sequences with lengths from 24-mer ($R06_{24}$) to 8-mer ($R06_8$) were investigated (see Figure 10). These oligonucleotides were incubated with TAR hairpins and the stabilities of kissing complex were determined. This study revealed that $R06_{16}$ is the minimal motive which offers nearly the same stability (K_d = 7.0±1.8 nM) such as the full-length $R06_{24}$ (K_d = 6.2±0.9 nM). Therefore, $R06_{16}$ was very often used as the aptamer sequence in further studies.

R06 RNA	Sequence 5′-3′	K_d (nM)
$R06_8$	5′ GUC C C 3′ AGA	>1000
$R06_{12}$	GUC 5′ CG C 3′ GC C AGA	53.1 ± 6.4
$R06_{14}$	GUC 5′ ACG C 3′ UGC C AGA	9.1 ± 1.1
$R06_{16}$	GUC 5′ CACG C 3′ GUGC C AGA	7.0 ± 1.8
$R06_{24}$	GUC 5′ UCAACACG C 3′ AGUUGUGC C AGA	6.2 ± 0.9

Figure 10. The truncated sequences of R06 aptamer and corresponding equilibrium dissociation constants K_d of their complex with TAR (reprinted from [84]).

In published studies it was observed that high affinity aptamers conserved the motive where G and A bases are adjacent to 5′ and 3′ end of the central 6-mer apical loop [81-83]. This observation was confirmed in the study of Duconge et al. where all combinations of adjacent bases were investigated [85]. It was found that "GA pair" is crucial for the stability of the kissing complex and any other combination of bases decreased the stability of the complex. The stability of the complex was lowered in the following order AG > GG > GU > AA > GC > UA >> CA, CU. The origin of high stability of "GA pair" was clarified in the later studies [86, 87]. It was assumed that incorporation of "GA pair" releases the internal structure of R06 aptamer so that the additional stacking interactions and non-canonical base pairing are facilitated between R06 aptamer and TAR hairpin.

The structure of the kissing complex between TAR and R06 aptamer was described in several publications where RTG crystallography, NMR and molecular dynamic (MD) simulations were employed [85-88]. The formed kissing complex of these two hairpins is illustrated in Figure 11. The analysis of data from X-ray crystallography showed that the complex has the conformation of A type except the bases between the stems and the loops [89]. The analysis of the kissing complex also showed the bend between the helices of TAR hairpin and R06 aptamer. This bend between both hairpins was determined to 28.1°, 47.6° and 3.8° with X-ray crystallography, NMR and MD simulations, respectively. The other bend was found in the sugar-phosphate backbone of individual hairpins. The bend was observed

between C4 and C5 at TAR hairpin and G5* and U6* at R06 aptamer (the asterisk denotes the bases belonging to R06 aptamer). This structural feature enables non-canonical base pairing and stacking.

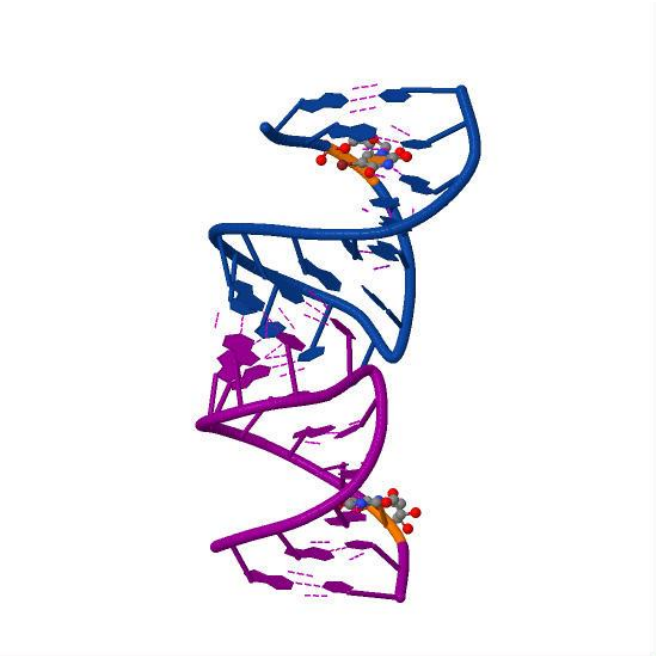

Figure 11. 3D structure of the kissing complex between TAR hairpin and R06 aptamer, which was obtained with RTG crystallography (the code in pdb: 2jlt). TAR hairpin and R06 aptamer is denoted by purple and blue color, respectively. Dashed lines represent hydrogen bonds between complementary bases.

In the kissing complex there were found the following interactions. The basic interaction between TAR hairpin and R06 aptamer is canonical base pairing of six central bases of kissing complex 5′-CUGGGA-3′ (TAR) and 5′-U*C*C*C*A*G*-3′ (R06) [87, 89]. The kissing complex is further stabilized by the non-canonical interactions in the proximity of the bend in sugar-phosphate backbone of individual aptamers. It was revealed that G5*(H-O2′) might form hydrogen bond with C5(O2p) or C4(O3′) and C4 (H-O2′) with U6* (O1p) or U6*(O2p). To confirm this assumption R06 aptamer was modified by 2′-O-methyl to prevent the hydrogen bonding. For the methylation of –OH at G5*, K_d increased more than 10 times and the melting temperature decreased about 11 °C. For methylated C4 (H-O2′), the destabilization was not so high. It thus indicated that G5*(-OH) forms the hydrogen bond while hydrogen bonding of C4 (H-O2′) is not conclusive. Kissing complex was also stabilized by stacking interactions. The inter-molecular stacking between TAR and R06 was observed. Due to the local bending (C4/C5 and G5*/U6*) and

conformation changes the authors supposed that this interaction occurs between G5* and C5. And last but not least, the kissing complex is stabilized by the intra-molecular stacking interactions of adjacent bases in the individual TAR hairpin and R06 aptamer.

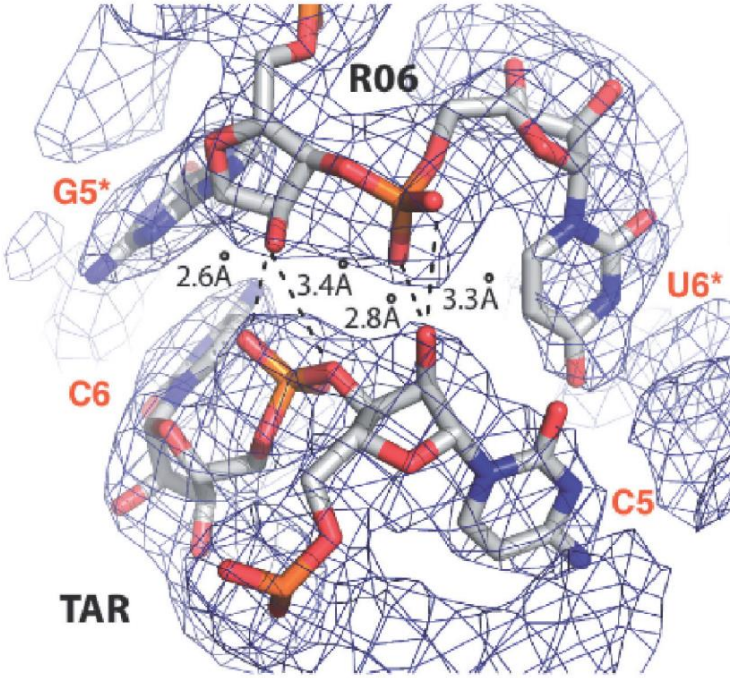

Figure 12. Potential non-canonical hydrogen bonding between TAR hairpin and R06 aptamer which were determined by X-ray crystallography (reprinted from [89]). Note that C5 and C6 in Figure correspond to C4 and C5 in our nomenclature, respectively.

1.4.6 Analogues of R06 aptamer

The aptamer R06, which was deeply discussed in previous text, represents RNA sequence. However, the natural RNA sequence is not a suitable agent in therapeutics strategies for its low resistance against nucleases. Therefore, the structure of R06 aptamer was chemically modified. Recently, several papers have presented different analogues of R06 aptamer [84, 90-93].

In 2002 Darfeuille et al. published 2′-O-methyl analogues of RNA aptamer [90]. The structure of the modification is shown on Figure 13. In the study, 24-mer aptamer $R06_{24}$ was used. Stability of the complex between TAR and this analogue was characterized by using UV absorption and SPR spectroscopy. The stability was characterized by K_d = 9.9±1.0 nM with kinetic constants k_{on} = 9.0±0.3 M^{-1} s^{-1}, k_{off} = 8.9±0.6 $10^{-4}s^{-1}$. This meant that the complex revealed slightly lower stability than complex between TAR and parent R06 aptamer (K_d = 6.9±2.9 nM). It was also

shown that 2′-O-methyl analogue selectively inhibit the tat-mediated transcription of a DNA template. It was observed that 50% inhibition was reached for aptamer concentration of 388 ± 33 nM. For unmodified RNA $R06_{24}$ the same inhibition effect was observed for concentration over 4 μM. The authors supposed that this low inhibition might be caused by a degradation of unmodified RNA sequence in the cell-free extract. The stability of 2′-O-methyl analogue was tested in HeLa cell nuclear extract and no degradation was observed up to 80 minutes.

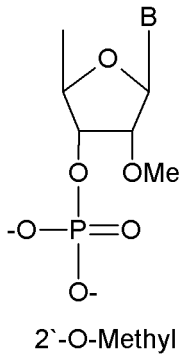

Figure 13. Chemical structure of 2′-O-methyl RNA analogues (reprinted from [90]).

In 2002, N3′→P5′ deoxyphosphoramidate (NP-DNA) analogue of $R06_{24}$ aptamer was published [93]. It was determined by SPR spectroscopy that dissociation constant K_d was 3.4 ± 0.3 nM, which is slightly lower that the stability for parent RNA $R06_{24}$ (K_d = 6.9 ± 2.9 nM). The ability of NP-DNA aptamers to compete with tat peptide was demonstrated *in vitro* in a competition assay. It was also demonstrated that NP-DNA is capable to inhibit the tat-dependent in vitro transcription in HeLa cell nuclear extract with IC_{50} = 400 nM.

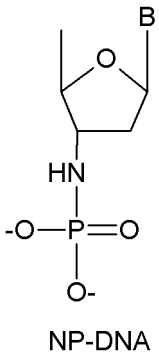

Figure 14. Chemical structure of NP-DNA analogues (reprinted from [93]).

In 2004 LNA/DNA chimeric aptamers were published by Darfeuille et al. [84]. LNA and DNA bases were varied in the shorten 16-mer aptamer sequence $R06_{16}$. The stability of privileged aptamers LNA4 and LNA5 reached 64.1±2.8 and

21.1±2.1 nM, respectively. The susceptibility of LNA5 was also monitored and no significant degradation was observed up to 50 h in bovine serum.

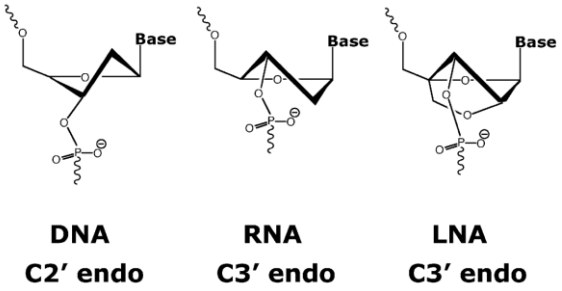

Figure 15. Chemical structure of LNA bases (reprinted from [84]).

In 2007 a systematic screening of 64 different LNA/2′-O-methyl chimeric aptamers (derived from $R06_{16}$) corresponding to all possible combinations of 6-nt loop sequence complementary to the TAR element of HIV-1 was performed by SPR spectroscopy [92]. This study was focused on the determination of TAR-aptamer complex stability of the synthesized aptamers. For majority of aptamers it was found that $K_d > 1$ nM. Three combinations of LNA/2′-O-methyl nucleoside analogues displayed the affinity which was below K_d of unmodified RNA aptamer (K_d = 1.31± 0.15 nM under the conditions of the measurement). It was also demonstrated that one of these chimeric aptamers inhibited the TAR-dependent luciferase expression in a cell assay.

2 Objectives

On the road to the understanding of molecular mechanisms of gene expression and regulation, the quantification of the structural, thermodynamic, and kinetic characteristics of formation and dissociation of complexes between nucleic acids, their modified analogues, enzymes and other molecules, presents an important milestone. The goal of this doctoral thesis is to contribute to the understanding of interaction properties of nucleic acids by investigating selected interactions involving nucleic acids by means of SPR spectroscopy. SPR spectroscopy is an optical technique allowing for the observation and quantification of molecular interactions in real-time and without the use of labels. In order to achieve this goal, several technical objectives have been also set.

The first technical objective is to optimize the SPR biosensor instrumentation and experimental methodologies to enable routine measurements of nucleic acid interactions with a high degree of accuracy and repeatability. Optimization of the biosensor instrumentation includes the optimization of a microfluidic system to eliminate undesirable effects, including as sample dispersion and inter-sample mixing. These undesirable effects act to hamper the measurements of both the association and dissociation phase of the investigated interactions and thus influence the kinetic and equilibrium constants obtained with the SPR biosensor. Optimization of experimental methodologies includes the characterization of nucleic acid interactions on the surface of an SPR chip, especially the effect of cations.

Another important objective of this doctoral thesis is to use the optimized SPR biosensor for a comprehensive study of anti-TAR oligonucleotide analogues (based on the R06 aptamer) with novel modifications that attack therapeutically relevant TAR motives of the HIV virus. These modified oligonucleotides are provided by the research group of Dr. Ivan Rosenberg at the Institute of Organic Chemistry and Biochemistry AS CR. In these oligonucleotides, selected modifications are sequentially placed either in a singular internucleotide linkage of the R06 loop, between the loop and the adjacent GA basepair, or between the GA basepair and the stem. This objective includes i) the evaluation of modifications with respect to their potential for the construction of efficient anti-TAR oligonucleotides, ii) the suitability of R06 aptamer positions for substitution with modifications, and

iii) the interpretation of results in the context of local nucleotide geometries and interactions in the TAR/anti-TAR complex.

Results obtained by the author during the doctoral research that resulted in publications are enclosed in the appendix of this doctoral thesis.

3 Surface plasmon resonance (SPR) biosensor

3.1 SPR setup and principle of operation

During the thesis a laboratory four-channel SPR biosensor PLASMON IV, which was developed at the Institute of Photonics and Electronics, Prague, Czech Republic, was used. The SPR biosensor combines three main compartments: optical system, fluidic system and bio-recognition element.

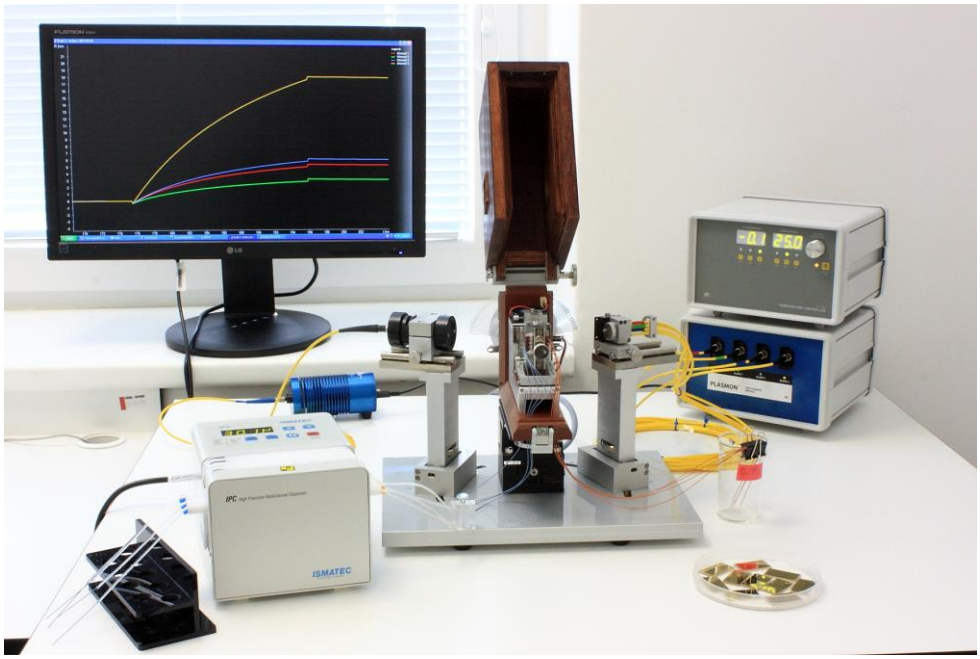

Figure 16. Photograph of the surface plasmon biosensor Plasmon IV.

3.1.1 Optical system

The SPR biosensor is based on the wavelength spectroscopy of surface plasmon resonance and the attenuated total reflection method [94, 95]. The broadband light generated in a halogen lamp is transmitted through a multimode optical fiber, collimated, polarized and illuminates the sensor chip through the optical prism (see Figure 16 and Figure 17). The sensor chip consists of a glass plate coated with an adhesion-promoting titanium layer (thickness: 1 nm) and a gold layer (thickness: 50 nm). On the gold layer the light beam is reflected from four independent spots. The reflected light is collected by optical fibers and transmitted into the four-channel spectrometer.

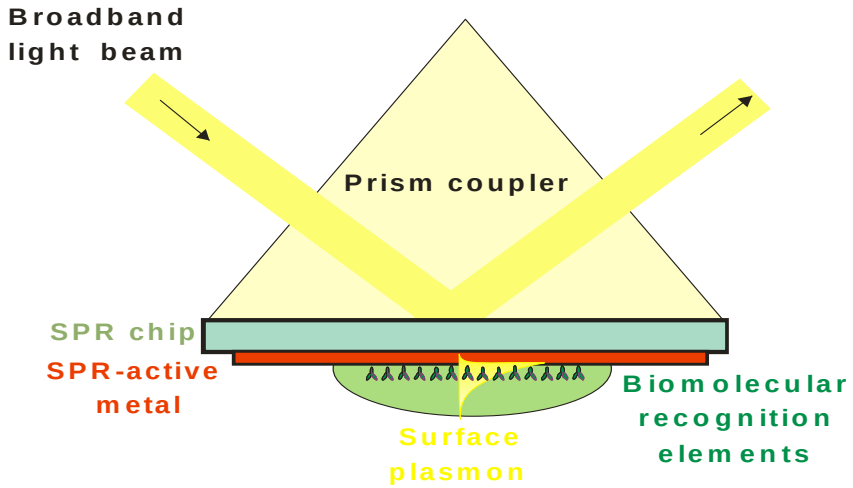

Figure 17. Schema of SPR biosensor.

Excitation of the surface plasmon (the collective oscillations of valence electrons on the gold-dielectric interface) is manifested as a distinct dip in the spectrum of the reflected light. Energy transfer between the light wave and surface plasmon occurs only when these two waves are phase-matched, i.e. for certain wavelength in case for a fixed angle of incidence. This resonant wavelength is dependent on refractive index changes in the proximity of gold layer. When the refractive index increases the position of the resonant dip is shifted to the red region of the spectrum and vice versa (see Figure 18). The SPR biosensor is also equipped with the temperature stabilization, which enables to control the temperature stability better than 0.01 °C.

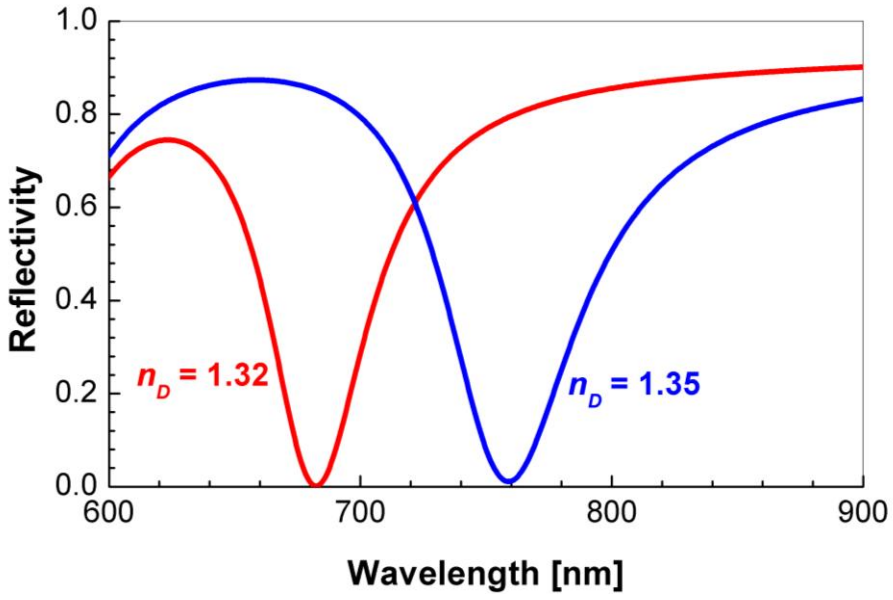

Figure 18. Shift of the resonant dip caused by a refractive index change of the solution in contact with the gold layer.

SPR biosensor is employed in an experimental practice where binding of the molecules to a surface of SPR chip locally changes the refractive index (see Figure 19). During experiments, the spectral position of the minimum of the resonant dip is monitored in time. When an analyte is not present in a solution, no binding of analyte occurs and the sensor response is stable. If the analyte is injected, the analyte is bound on a surface of chip and the minimum of the resonant dip is red-shifted. And finally for solution without the analyte, the dissociation of the analyte from a surface of chip is observed as an SPR shift back towards blue region. The SPR sensor response is proportional to the amount of bound molecules [94, 96, 97]. For SPR biosensor based on the wavelength interrogation near the wavelength of 750 nm, a 1-nm SPR wavelength shift represents a change in the protein surface coverage of 17 ng/cm^2.

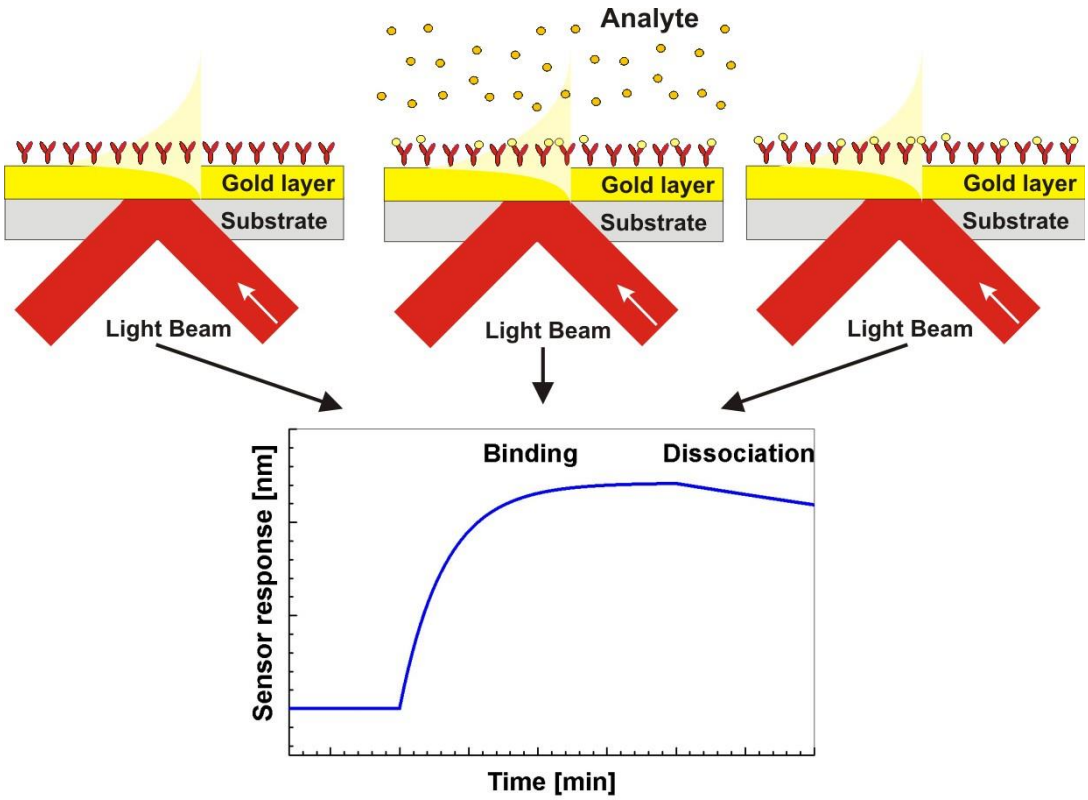

Figure 19. SPR sensor response to binding and dissociation of analyte on a surface of SPR chip.

3.1.2 Fluidic system

Conventional SPR biosensor Plasmon IV contains four independent flow-through channels which enable to simultaneously monitor four different interactions (see Figure 20). Each channel with the dimension of 2 mm (width) x 6 mm (length) x 60 μm (height) is formed from an adhesive foil which is stuck to the plexiglass flow-cell and pressed against the chip on a glass prism. It means that the volume of a channel is less than 1 μL. Each channel has one inlet and one outlet on the opposite sides. To deliver solutions to a chip surface, a four-channel peristaltic pump is employed. The inlets and outlets are connected to peak tubings with inner diameter 0.01 and 0.02 inch, respectively. The solutions are typically pumped with the flow rate from 10 to 60 μL/min.

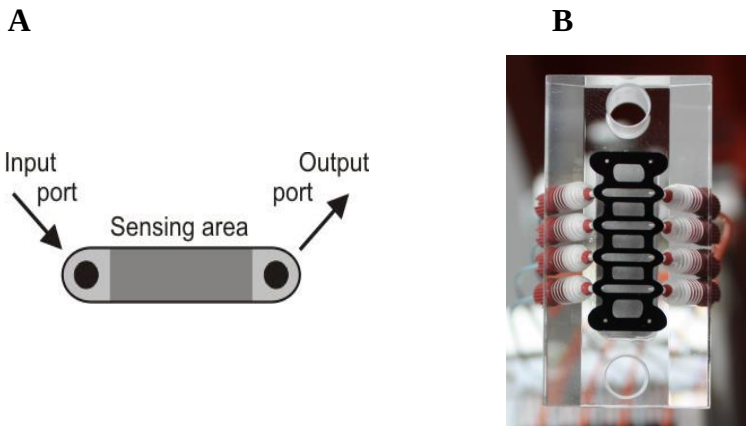

Figure 20. (A) Schema of one channel in the conventional flow-through fluidic system where a sample is transported through the sensing area from the input to output port. (B) Photography of the real arrangement.

3.1.3 Biorecognition element

Biorecognition element is an interface between optical device and biological systems which ensures the specific and sensitive binding of analytes from solution to the surface of chip. For this purpose many different chemistries with immobilized receptors (interacting partner to analyte in a solution) are commonly used [94]. We distinguish two-dimensional surfaces such as self-assembled monolayers (SAMs) of alkanethiolates or disulfides [98-100] or three-dimensional matrixes such as

carboxymethylated dextran [101] or non-fouling zwitterionic [96] and methacrylate polymers [102].

In the thesis the surface chemistry based on streptavidin-biotin interaction was mainly used [98] (see Figure 21). Streptavidin is a tetrameric molecule with four high affinity binding pockets to biotin. The equilibrium dissociation constant K_d of biotin-streptavidin is approximately 10^{-15} M. During the functionalization of a surface of SPR chip a neat gold chip is immersed into the solution of mixed carboxy- and hydroxy- terminated thiols to form SAM on a surface of SPR chip. Carboxyl groups serves as functional groups while hydroxyl groups are employed to lower the nonspecific binding of molecules. Then the carboxyl group is activated by *N*-hydroxysuccinimide (NHS) and *N*-ethyl-*N'*-(3-diethylaminopropyl) carbodiimide (EDC) reagents (amine coupling chemistry) and streptavidin is covalently bound via amino group to a chip surface. This streptavidin modified chip surfaces enable binding of biotinylated receptors to a surface of SPR chip such as DNA/RNA oligonucleotide probes, antibodies or proteins. Nowadays, this chemistry offers stable and reproducible surface together with easy and routine preparation [98].

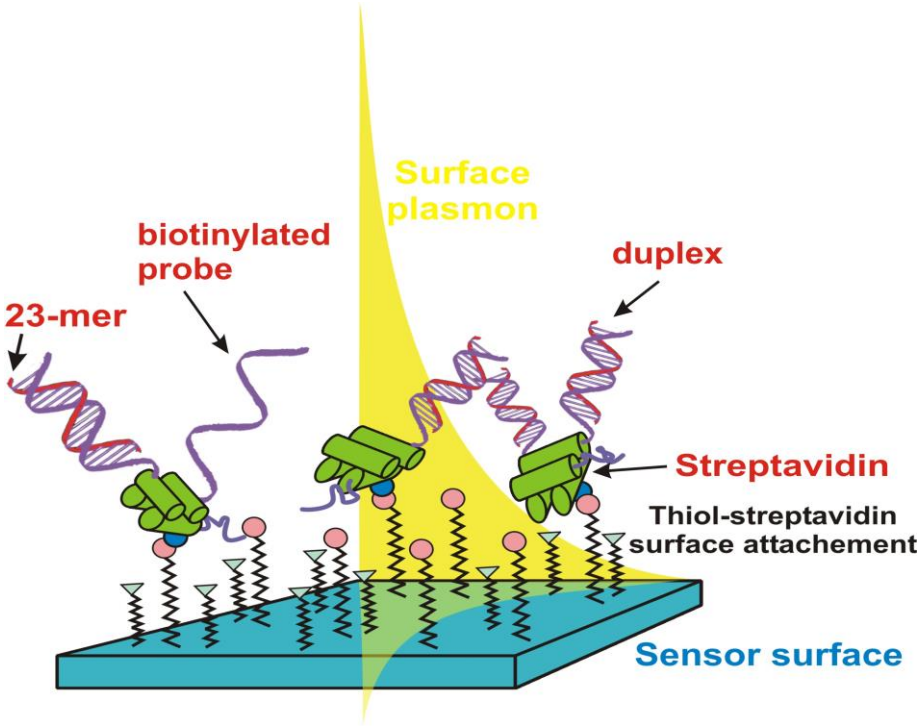

Figure 21. Streptavidin modified SPR chip with immobilized DNA probe and hybridized complementary DNA sequence forming duplex.

3.2 Theoretical description of molecular interactions on a surface of SPR chip

SPR spectroscopy is a real-time and label-free technique where the sensor response is directly proportional to the amount of bound molecules on a chip surface [94]. The SPR spectroscopy so presents a unique tool for monitoring of molecular interactions.

To quantify the molecular interactions on a chip sensor, it is necessary to develop theoretical description for observed interactions [94, 103-105]. These models are based on the monitoring of an actual amount of bound molecules of an analyte on a chip surface in a time in dependence on the concentration of analyte in a solution and free binding sites of receptors on a surface of a chip.

The most common model (*pseudo first-order model kinetics*) assumes two interacting partners (one analyte A in a solution and one receptor R immobilized on a surface of a chip) which form a complex in 1:1 stochiometric ratio on a chip surface. For instance, this model involve the binding of DNA strand to a complementary probe (duplex formation) or binding of antigen to antibody on a chip surface. In this model two processes are considered: (a) the association process when the analyte A binds to free receptor R immobilized on a surface of a chip and (b) the dissociation process when the complex AR dissociates into individual partners A and R. These processes might be symbolically expressed as:

$$A + R \underset{k_d}{\overset{k_a}{\Leftrightarrow}} AR \tag{1}$$

As indicated both processes occur simultaneously and affect the actual surface concentration of formed complexes γ on a surface of a chip. The changes of surface concentration of formed complexes γ in time might be written as:

$$\frac{d\gamma}{dt} = \frac{d\gamma_a}{dt} + \frac{d\gamma_d}{dt} = k_a \alpha_0 (\beta - \gamma) - k_d \gamma , \tag{2}$$

where γ_a and γ_d is amounts of associated and dissociated complexes, k_a and k_d are association and dissociation rate constants, α_0 is injected analyte concentration and β is the surface concentration of receptors. In equation (2) the difference β-γ presents the surface concentration of free unbound receptors. Rate constants k_a and k_d, which are independent of time and concentration of reactants, characterize the association and dissociation kinetics, respectively. This equation was derived by Langmuir for

molecular interactions of receptors immobilized on a surface with analyte in a solution.

For the state when the association and dissociation of complexes is in the equilibrium the actual surface concentration of complexes is stable [94, 103, 104]. This state, which is called equilibrium state, is expressed as:

$$K_A = \frac{k_a}{k_d} + \frac{\gamma_{eq}}{\alpha_0(\beta - \gamma_{eq})}, \quad (3)$$

where K_A is the equilibrium (association) constant, and γ_{eq} the concentration of complexes in the equilibrium state.

The equation (2) assumes that the free analyte, which is in the proximity of a surface of SPR chip, is constant and is equal to the concentration of injected analyte. However, if we consider the effect of mass transport, the diffusion of analyte to a surface of a chip is limited and the concentration of analyte increases gradually after the analyte injection. In general, the concentration of free analyte at a chip surface varies in time as written:

$$\frac{\partial \alpha(x,y,t)}{\partial t} = D\left(\frac{\partial^2 \alpha(x,y,t)}{\partial x^2} + \frac{\partial^2 \alpha(x,y,t)}{\partial y^2}\right) - 4v_{\max}\frac{y}{h}\left(1-\frac{y}{h}\right)\frac{\partial \alpha(x,y,t)}{\partial x}, \quad (4)$$

where D is diffusion coefficient, v_{max} maximum velocity of laminar flow, x and y are space coordinates in the direction of an analyte flow and perpendicular to a surface of a chip, respectively, and h is the height of a flow cell. Equations 2 and 4 thus offer the full description (full model) of molecular interactions on a chip surface. The solving of the equations lead to fundamental partial differential (PDE) coupled with the relevant kinetic equations [106]. These types of equations can be solved only by numerical methods, which are extremely time-consuming. Therefore the simplifications of equations were developed. The models with simplified mass transport were offered to obtain the accurate results in a reasonable time [107, 108].

In reality, we also observe the situations that do not correspond to *pseudo first-order model kinetics.* Therefore the different models of molecular interactions are considered [94]. *Zero order reactions* involve the situation where the conformation changes of the AR complex occur. This model has been applied for the description of experiments where the physico-chemical properties of receptors on a surface of a chip are changed after analyte binding [109, 110]. The other model (*model of parallel pseudo first-order reactions*) involves the situation where

molecular interactions with different rate constants proceed simultaneously. It corresponds to situation where an analyte binds to different kinds of receptor sites or different states of analytes to a receptor with one binding site [111]. The model of *multivalent receptor binding* describes the situation where a receptor binds more than one analyte. This model involves the formation of triplexes where the oligonucleotide probe attached to a surface of a chip binds two oligonucleotide sequences [98].

4 Results

4.1 New dispersionless microfluidics

In the conventional SPR systems the flow-through format, where buffers and samples are sequentially delivered through the identical tubing to the sensing area, is used (Figure 20). This conventional system offers easy handling with SPR biosensor, which thus explain the popularity of this arrangement in laboratory practice [94]. However, this system may cause some problems when the analysis of SPR data such as determination of association and dissociation constants is demanded.

In the theory of the kinetics analysis, it is assumed that the analyte at a constant concentration is injected to the sensing area during the measurement. This scenario is not often realized for the conventional flow-through system. When the analyte is transported as a plug inserted between two segments of buffers through the relatively long tubings, the sample dispersion and inter-sample mixing occurs [112-114]. These effects result in a variation of the sample concentration during the experiment, especially the concentration is depleted at the beginning of the sample injection. To eliminate these undesirable effects, novel dispersionless microfluidic system was proposed.

4.1.1 Architecture of the dispersionless microfluidics

The concept of the dispersionless microfluidics is illustrated in Figure 22. Each sensing channel contains two input and two output ports. The input and output ports are connected by tubings to two independent pumps and to regulatory valves, respectively. In experiment, two different liquids are introduced to the microfluidic channel through the two input ports. In state A, output port 2 is opened and output port 1 is closed, which makes liquid #1 flow through the sensing area and then to the waste container while liquid #2 flows directly to the waste container. In state B, the direction of flow is reversed, output port 1 is opened and output port 2 is closed, which makes liquid #2 flow through the sensing area. When the microfluidics is switched between states A and B, the change of liquids takes place in the close

proximity to the sensing area. It results in injection of liquids to the sensing area without the liquid dispersion and intermixing.

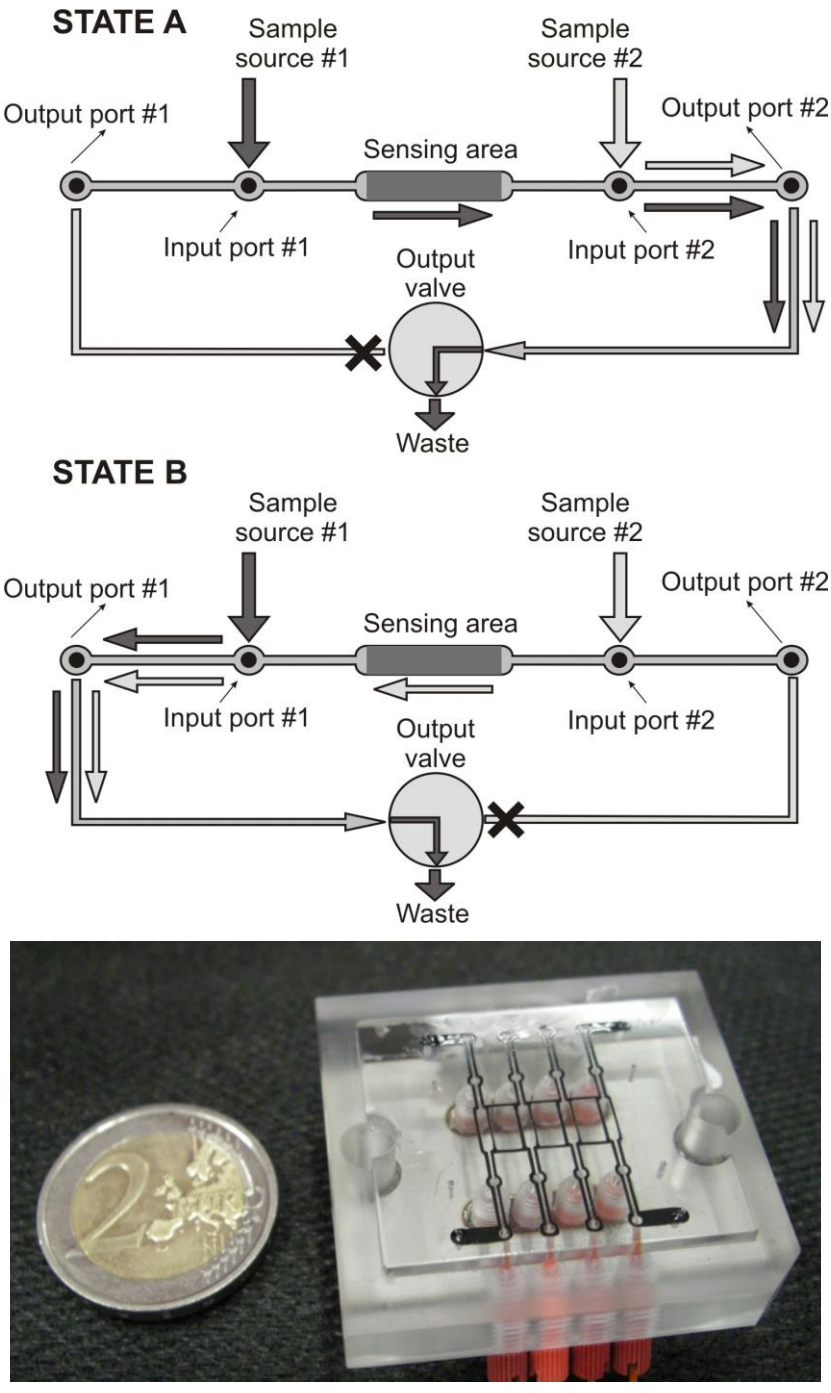

Figure 22. Principle of operation of the novel dispersionless microfluidic system and the photograph of four-channel flow-cell based on this approach.

A prototype of the four-channel microfluidic flow-cell is shown in Figure 22. The microfluidic structure is formed from 60-μm-thick self-adhesive vinyl foil which is attached to the surface of a polished acrylic manifold. The input ports are

connected to two multichannel peristaltic pumps Ismatec. The two output ports of each sensing channel are connected to microelectric valves (VICI Valco Instruments Co. Inc., USA) in such a way that one output port is always opened to the waste container while the other is closed allowing the simultaneous switching in all sensing channels.

4.1.2 Materials and methods

Oligonucleotides

In SPR experiments DNA biotinylated 20-mer and hybrid DNA/RNA 47-mer oligonucleotide probes with the sequence of biotin-$(TEG)_2$-5′-TAT TAA CTT TAC TCC CTT CC-3′ (B-E441) and biotin-(TEG)-5′-CCC CCC CrArA rArArA rArArA rArArA rArArA rACC ACC ACC ACC ACC ACC ACC ACC AC-3′ (P_1) were used, respectively. DNA 20-mer and 15-mer oligonucleotide targets with the sequence of 5′-GGA AGG GAG TAA AGT TAA TA-3′ (E441C) and 5′-**T**^TT TTT TTT TTT TTT-3′ (ON428g- chimeric complementary strand to the central part of P_1) were employed, respectively. T represents DNA strand. **T**^ denotes deoxy-3′-phosphonate modification, which improves the stability of oligonucleotide against nucleases. Reference 26-mer DNA oligonucleotide P_{ref} with the sequence of $BdTG_{25}$ was also used. B-E441 and E441C oligonucleotides were purchased from LMFR Masaryk University in Brno, Czech Republic. P_1 and P_{ref} were obtained from IDT Inc., USA. ON428g was obtained from the Institute of Organic Chemistry and Biochemistry AS CR, v.v.i., Prague, Czech Republic. All oligonucleotides were in HPLC purity.

SPR experiment

The streptavidin-modified surface, which was prepared according to the procedure described in part 3.1.3, was used for this study.

To demonstrate the fluidic performance, two different flow-cells (dispersionless and conventional) were used during the SPR experiment. Buffer $Tris_{500}$ (10 mM Tris with 500 mM NaCl, pH 7.4) was pumped for at least 15 minutes. Then, 100 nM probe B-E441 was introduced to the surface of SPR chip for 15

minutes. Subsequently, $Tris_{500}$ and 100 nM target E441C for 250 s, and $Tris_{500}$ were injected at flow rate of 10 μL/min.

To demonstrate the performance of new microfluidics for kinetic analysis, dispersionless flow-cell was used. Buffer PBS (137 mM NaCl, 1.4 mM KH_2PO_4, 8 mM $Na_2HPO_4.12\ H_2O$, 2.7 mM KCl, pH 7.4 at 25°C) was injected for 15 minutes to the surface of SPR chip. Then, 50 nM P_1 or P_{ref} was injected for 5 minutes into the detection and reference channel, respectively. Subsequently, hybridization buffer (75 mM KCl, 50 mM Tris-HCl, 3 mM $MgCl_2$, pH 7.4 at 25°C) was injected. Finally, ON428g at concentrations of 5, 10, 20, 50 and 100 nM for 600 s and hybridization buffer for at least 15 minutes was pumped into both detection and reference channels.

4.1.3 Kinetic analysis with dispersionless microfluidics

The effect of newly developed microfluidic system on binding of analytes was demonstrated on a model system of complementary DNA strands. DNA probe B-E441 was attached to the streptavidin modified chip surface. Then, the complementary strand E441C was pumped along the surface of SPR chip and the hybridization of the complementary strand was monitored. The typical experimental results are shown in Figure 23 where the dashed and full curves were obtained by using the conventional microfluidics and the newly developed dispersionless microfluidic system, respectively. The conventional microfluidics possessed retarded initial slope of the binding curve. As mentioned this retardation was caused by the dispersion between the two solutions and the adsorption of the analyte to the wall of input tubings during the sample delivery. These effects significantly affected the binding kinetics. As shown in Figure 23, these processes could be fully eliminated by the implementation of the dispersionless microfludics. The maximal slope was reached immediately after the analyte injection.

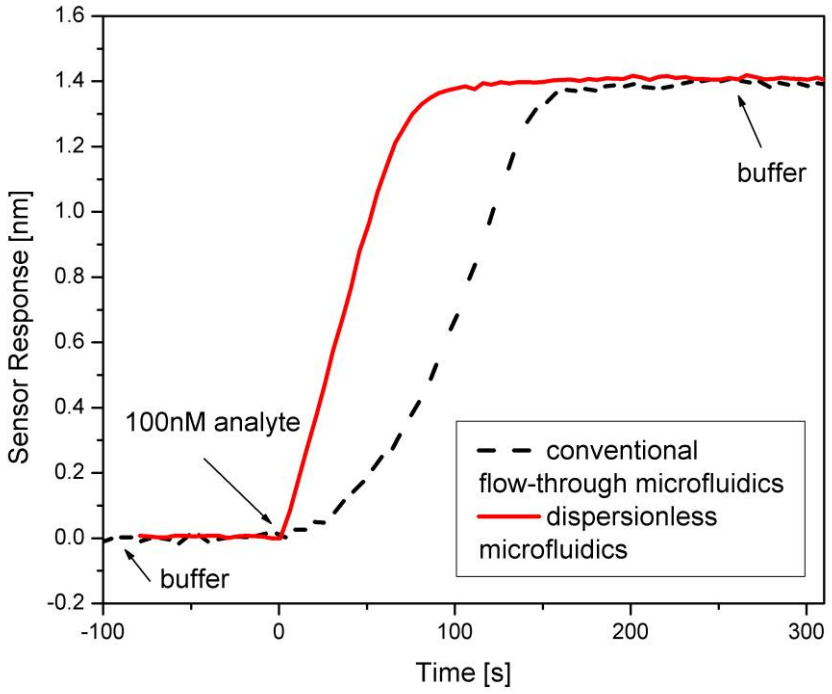

Figure 23. Sensor response to 100 nM target oligonucleotide E441C, which was injected to the sensing area using the dispersionless microfluidics (full red line) and the conventional microfluidics (dashed black line). Flow rate 10μL/min.

Dispersionless microfluidics was further applied for the kinetic analysis of the oligonucleotide binding. The biotinylated RNA probe P_1 was attached to a surface of SPR chip via biotin streptavidin interaction. The complementary target ON428g (15-mer) with one modified nucleotide, which improves the resistance against nucleases, was injected at different concentrations from 5 to 100 nM. The SPR sensor response was monitored and association and dissociation rate constant k_a and k_d and equilibrium dissociate constant K_D were calculated to 6.21×10^{5} $M^{-1}s^{-1}$, 8.72×10^{-3} s^{-1} and 1.4×10^{-8} M, respectively. BIAevaluation software from Biacore was used for the data processing.

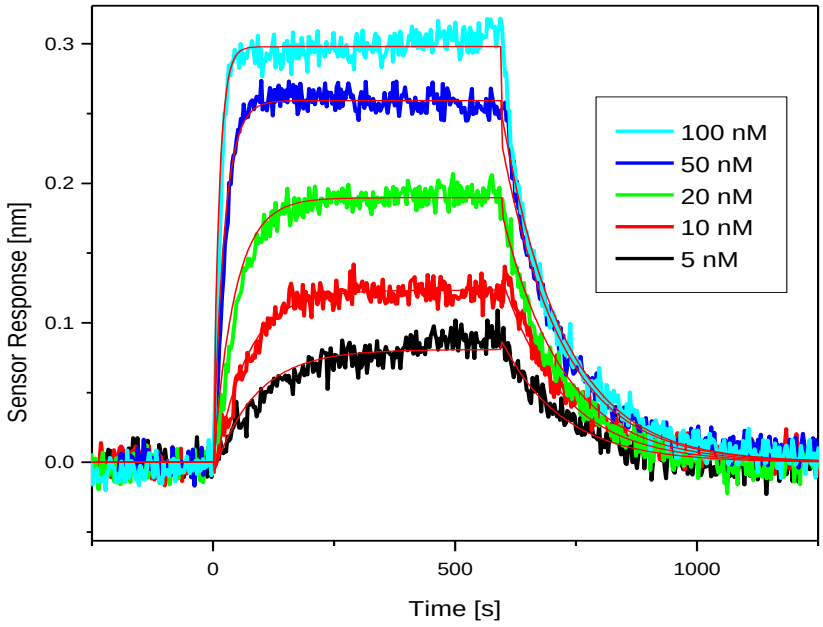

*Figure 24. Binding of chimeric sequence (5'-**T**^TT TTT TTT TTT TTT-3') to P_1 probe immobilized on surface of SPR chip. **T**^ denotes deoxy-3'-phosphonate modification. Flow rate 20 µL/min and temperature 20 °C was set during the SPR experiment.*

4.1.4 Conclusions - new dispersionless microfluidics

We demonstrated that dispersionless microfluidics allows for the analyte binding to the receptor on a surface of a chip without the sample dispersion. The system enables to monitor accurately the kinetics of molecular interaction. The design and application of the dispersionless microfluidics were published in [115, 116] (Appendix II and III). The setup was further employed in the study of the kissing complex between TAR and R06 aptamer and in the characterization of new modified R06 analogues.

4.2 Interaction of oligonucleotides on a surface of DNA chip

Majority of SPR experiments in the framework of the doctoral thesis was performed on DNA or RNA chips. In these systems the target in a bulk typically binds (SP hybridizes) to the biotinylated oligonucleotide probe which is attached to a surface of SPR chip. It is supposed that the presence of the surface of SPR chip influences the conditions for oligonucleotide interactions and that these conditions significantly differ from the experiments in a solution [20, 117-119]. It is therefore important to evaluate the effect of a surface of DNA/RNA chip on oligonucleotide interactions and to provide this knowledge to the DNA/RNA chip practice.

We decided to investigate the shielding effect of cations on interactions of oligonucleotides on a surface of DNA chip. The individual and simultaneous effect of monovalent sodium and divalent magnesium was monitored. The results were also compared with the situation in a solution. For this purpose, two oligonucleotide systems were chosen. In the first system, heterogeneous 23-mer oligonucleotides that form duplexes were used. Specifically, we used biotinylated 23-mer probe which formed the fully matched duplex with 23-mer target or partly mismatched complexes with two, three and four base mismatched targets. In the second system, homogenous 23-mer oligonucleotides which form triplexes were studied. Specifically, biotinylated homogenous 23-mer adenine probe which binds two homogenous 23-mer thymine target were used. Results of SPR experiments were completed with solution hybridization measurements using UV absorption spectroscopy.

4.2.1 Materials and methods

Oligonucleotides

In duplex formation experiments biotinylated 23-mer oligonucleotide probe BdO_{23} with the sequence biotin-$(TEG)_2$-5´-d(CAG TGT GGA AAA TCT CTA GCA GT)-3´ was used. This base sequence is a crucial for replication of the human immunodeficiency virus (HIV) [120]. The subsequent DNA oligonucleotide targets were used: (a) the fully matched target 5´-d(ACT GCT AGA GAT TTT CCA CAC TG)-3´ (CdO_{23}), (b) the partly mismatched target containing two purine–pyrimidine point mismatches (the mismatched bases are underlined) 5´-d(GCC AGA GAT TTT CTA CAC TG)-3´ (Mism2) (c) the partly mismatched target containing three purine–

pyrimidine point mismatches 5´-d(ACT GCC AGA GAT CTT CCA TAC TG)-3´ (Mism3), (d) the partly mismatched target containing four purine–pyrimidine point mismatches 5´-d(ACT GCC AGA AAT TCT CCA TAC TG)-3´ (Mism4). In triplex formation experiments, 23-mer oligonucleotide probe BdA_{23} with the sequence biotin-$(TEG)_2$-5´-dA_{23}-3´ and target dT_{23} was applied. The oligonucleotides were purchased from LMFR Masaryk University in Brno, Czech Republic. All oligonucleotides were in HPLC purity.

Immobilization of probes and hybridization of targets on an SPR chip

The streptavidin-modified surface of SPR chip, which was described in part 3.1.3, was used. Then, 10 mM Tris buffer (or 10 mM PBS, 10 mM HEPES or 10 mM cacodylate) containing 20 different sodium-magnesium cation compositions (0, 50, 150, 500 and 1000 mM sodium, and 0, 1.5, 5, and 15 mM magnesium) was injected for at least 10 minutes. Then, 100 nM biotinylated probes BdO_{23} (or BdA_{23}) was pumped for 35 minutes to allow the immobilization to a gold chip via high affinity biotin-streptavidin interaction. Subsequently, fully matched CdO_{23} targets or targets containing two (Mism2), three (Mism3) and four (Mism4) point purine-pyrimidine mismatched base pairs or dT_{23} targets were allowed to hybridize with probes on a surface of SPR chip. Both probe immobilization and target hybridization was performed for 35 minutes which was sufficient to obtain the maximal sensor response. During the experiments the flow rate was 30 μL/min and temperature was stabilized to 25°C. The typical SPR sensor response to immobilization of BdO_{23} probes and subsequent binding of fully matched target CdO_{23} is shown in Figure 25. Figure 25 also schematically presents the process of calculation of Gibbs energy. The *HE*, i.e. the ratio of formed duplexes to immobilized oligonucleotide probes, was calculated as $HE = (B \times M_{probe})/(A \times M_{target})$, where *A*, *B*, M_{probe} and M_{target} correspond to the sensor responses of probes and targets and molecular weights of probes and targets, respectively. Considering the duplex formation as a pseudo first-order process, its equilibrium association constant *K* is given by *HE* according to the formula $K = HE/[c_{target} \times (1\text{-}HE)]$, where c_{target} is the concentration of targets (c_{target} = 100 nM in our experiments). The decrease of Gibbs energy ΔG_T associated with the

duplex formation was determined using the van't Hoff equation $\Delta G_T = RT\ ln(K)$, where R and T are the gas constant and temperature.

Probe density D was determined according to equation $D = k_{BdO23/BdA23} \cdot A$, where $k_{BdO23} = 1.42 \cdot 10^{12}$ or $k_{BdA23} = 1.41 \cdot 10^{12}$ probe/cm^2/nm are the calibration coefficients for BdO_{23} and BdA_{23}, respectively. Calibration coefficients k_{BdO23} and k_{BdA23} were calculated for used SPR sensor system Plasmon IV taking into account the molecular weight of the probes. Details of the calculation are given in [94].

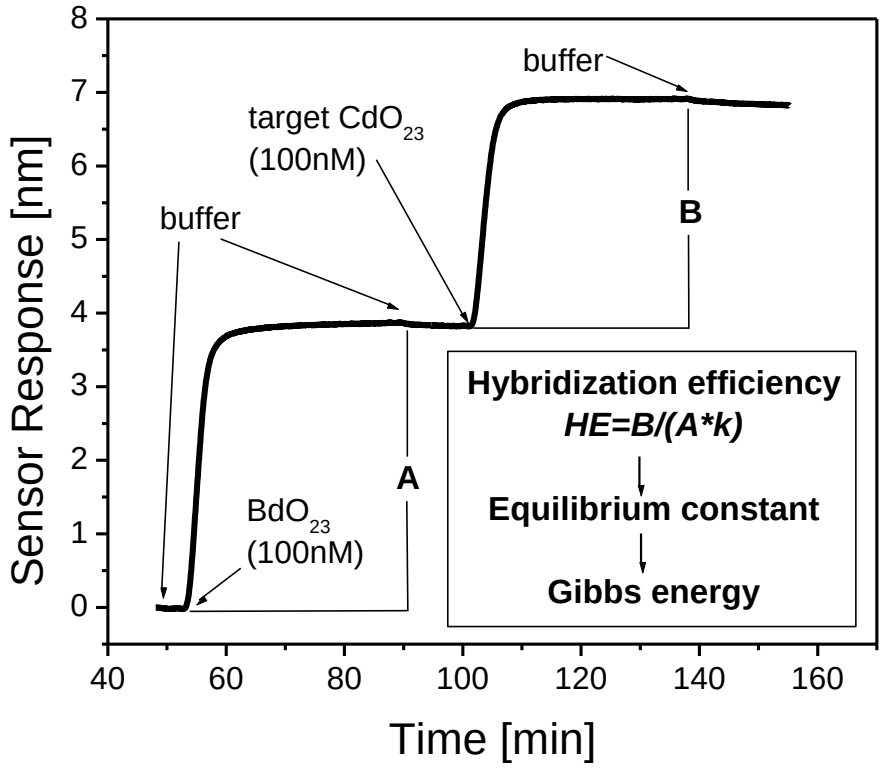

Figure 25. *Immobilization of BdO_{23} probe and subsequent hybridization of fully complementary sequence CdO_{23} for 0 mM NaCl/15 mM $MgCl_2$ in a buffer. Temperature 25°C and flow rate 30 µL/min. The schema of the calculation of Gibbs energy is also shown.*

UV absorption measurements

The complementary oligonucleotides BdO_{23} and CdO_{23} were prepared in 10 mM tris with 1000 mM NaCl (without magnesium) or with 15 mM $MgCl_2$ (without sodium). The equimolar solutions with a total strand concentration of 0.5, 1, 2 and 5 µM, and with total strand concentrations of 0.3, 0.6, 2 and 6 µM, were

prepared in Tris containing sodium and magnesium cations, respectively. The absorbance at the wavelength of 260 nm was measured with the UV-VIS absorption spectrometer Varian 4000 in cuvettes with 1-cm optical length. The heating cycles were performed at the temperature range from 30 to 90 °C with a heating rate of 1°C/min. Each sample was measured twice. The standard derivative method was used for the calculation of melting temperature. Gibbs energies ΔG_{298} were calculated from UV absorption measurements according to the description from SantaLucia [9, 11].

4.2.2 Results and Discussion

Hybridization of fully matched oligonucleotides

Target CdO_{23} with fully complementary sequence to immobilized probe BdO_{23} was primarily chosen to determine the effect of cations on formation of duplexes. The concentration of cations was varied from 0 to 1000 mM sodium and from 0 to 15 mM magnesium.

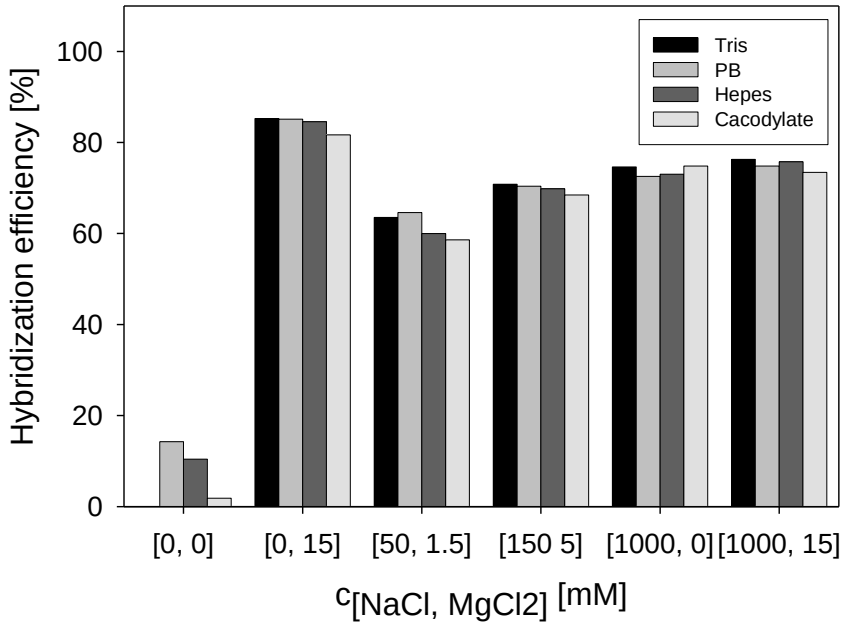

Figure 26. Hybridization efficiency of fully matched oligonucleotides hybridizing with probe BdO_{23} in various 10 mM buffers: Tris, phosphate buffer (PB), HEPES and cacodylate. The SPR experiments were performed in five different saline conditions (0 mM/15 mM, 50mM/1.5mM, 150 mM/ 5mM, 1000 mM/0 mM, 1000 mM sodium/15 mM magnesium) at 25ºC and flow rate 30 µL/min.

Prior to the main study, the effect of four different 10 mM buffers (Tris, phosphate buffer, HEPES and cacodylate) was tested for six concentrations of sodium and magnesium. The obtained hybridization efficiencies are presented in Figure 26. As shown the type of buffer had significantly weaker effect on binding of target CdO_{23} to probe BdO_{23} than used sodium or magnesium cations. This observation agrees with the previously published experiments [33]. The only exception which was observed is the case where no sodium and no magnesium cations were added to buffers (see [0, 0] in Figure 26). For this condition the binding of target is clearly affected by used buffers. Phosphate, HEPES and cacodylate buffer enabled slight binding of target CdO_{23} while no binding was observed for Tris buffer. This difference might be explained by the natural presence of cations in a buffer (phosphate buffer) or by the addition of cations during the adjustment of pH. For this reason we decided to use Tris buffer for the study of effect of cations on binding of oligonucleotides on a surface of DNA chip.

The typical hybridization experiment, where CdO_{23} target binds to previously immobilized BdO_{23} for sodium from 0 to 1000 mM and without magnesium cations, is shown in Figure 27.

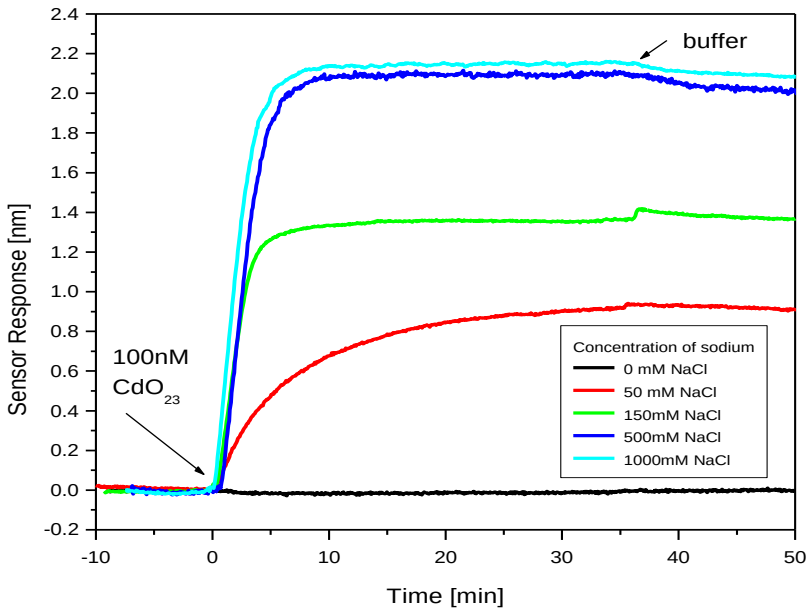

Figure 27. Hybridization of CdO_{23} sequence complementary to previously immobilized BdO_{23} for different concentrations of sodium and without magnesium. Temperature 25°C and 30 µL/min.

From the experimental data the stabilities of fully matched target for all sodium and magnesium concentrations were calculated according to van't Hoff equation and are shown in Figure 28a. As expected the stability increased with the amount of cations in a solution. This observation was in accordance with the previously published experiments where SP hybridization increased with the concentration of cations [20, 31, 33]. The dependence also clearly demonstrated that SP hybridization was more efficient for magnesium than for sodium cations. For instance, 15 mM magnesium stabilized duplexes more effectively than even high concentrated 1000 mM sodium. This aspect will be discussed further.

The local minima were also found when the magnesium concentration was fixed and sodium cations were varied. Specifically, the minima were observed for 50 mM sodium/1.5 mM magnesium, 150 mM sodium/5 mM magnesium and 500 mM sodium/15 mM magnesium. It is interesting that all these combinations correspond to a 30-fold excess of sodium over magnesium. As discussed in appendix IV these local minima were believed to be caused by the competition of sodium and magnesium cations in their binding to DNA duplexes. The competition of sodium and magnesium cations was described in [10, 22, 23] in a detail.

To compare the solid-phase results with the hybridization in a solution the stability of the duplex formation in a solution was calculated according to the prediction of Owczarzy et al. [10]. The obtained dependences are shown in Figure 28b. In Owczarzy's prediction the reference Gibbs energy $\Delta G_{298}^{solution}$, which was described in equation 23 in [10], was determined to -139±7 kJ/mol for 1 M concentration of monovalent sodium using UV absorption spectroscopy (see further). This value agrees with the prediction according to SantaLucia model [9] in a solution.

This comparison revealed several interesting features for SP hybridization, which differ to the experiments in a solution: (i) magnesium is more efficient in the duplex stabilization than even a much higher concentration of sodium, (ii) the absolute values of ΔG_{298} are substantially lower than those reported in a solution with the same cation content.

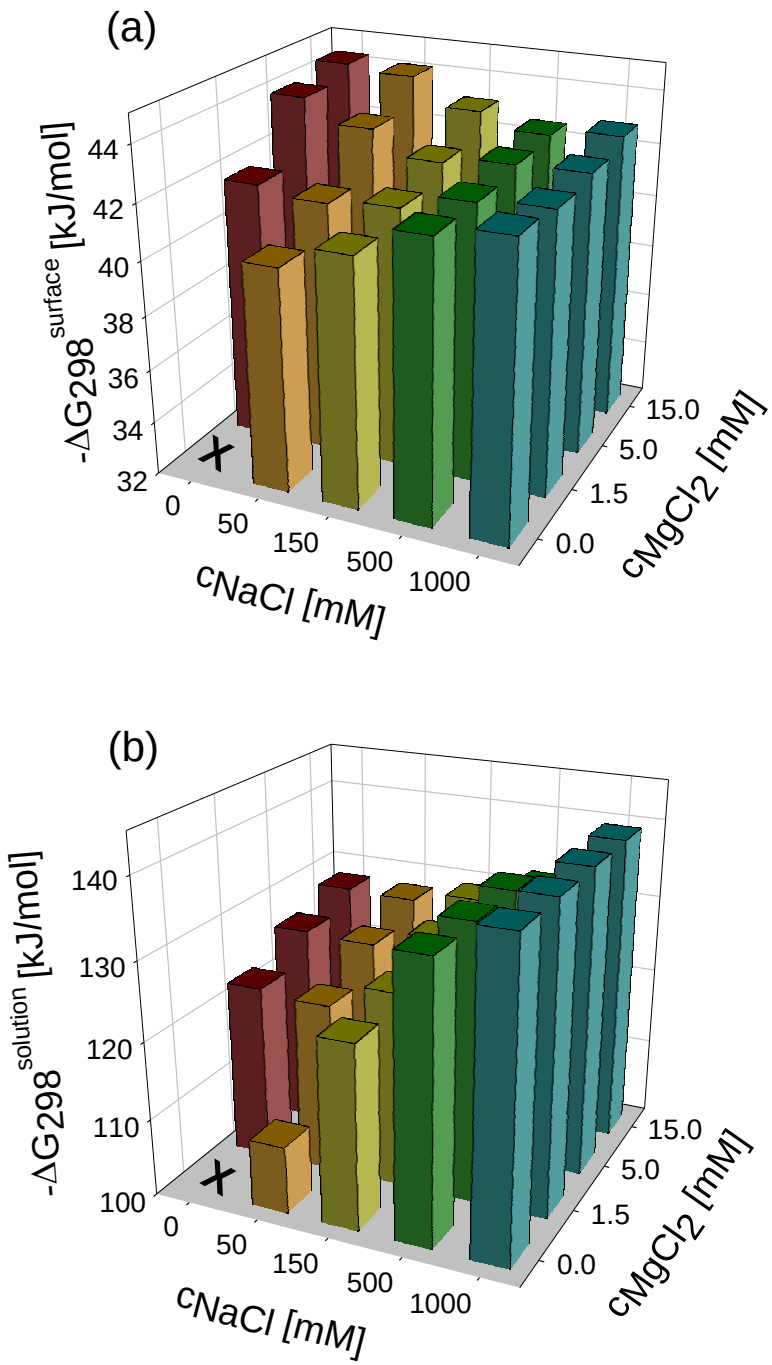

Figure 28. Gibbs energy ΔG_{298} of fully matched duplex formation CdO_{23}/BdO_{23} for different monovalent and divalent cation concentrations. (a) Gibbs energies on a surface of DNA chip obtained in hybridization study using the SPR sensor. (b) Gibbs energies in a solution calculated using the empirical formulas which was described by Owczarzy et al.[10]. The value for zero content of small cations is not shown, because no sensor response to hybridization was observed.

The observation that 15 mM magnesium (divalent) cation is more efficient in the duplex stabilization than even a highly concentrated monovalent sodium (1 M NaCl) is rather surprising and in the direct contradiction with the observation in a

solution. For oligonucleotide duplexes in a solution (present typically at micromolar concentrations), the opposite trend in cation efficiency has been described. Owczarzy et al. [10] observed that 1 M monovalent potassium, which is equivalent with sodium ions in the stabilization of duplexes in a solution [10, 19], is more efficient in the stabilization of the oligonucleotide duplexes than any concentration of divalent magnesium.

To confirm this observation several control experiments, where UV absorption of BdO_{23}/CdO_{23} duplex was used, were performed for selected cationic buffer composition (1000 mM sodium (without magnesium) and 15 mM magnesium (without sodium)). The melting temperatures of 75.3±0.5 °C and 70.1±0.5 °C corresponding to Gibbs energies ΔG_{298} of -139±7 kJ/mol and -130±6 kJ/mol for 1000 mM sodium and 15 mM magnesium, respectively, were achieved. The comparison of these results with the ΔdG_{298} values for SP hybridization obtained with the SPR sensor, i.e. -42.6±0.8 kJ/mol for 1000 mM sodium and -44.3±0.8 kJ/mol for 15 mM magnesium confirmed the opposite trend of the sodium and magnesium efficiency.

The UV absorption experiments also confirmed the significant lower duplex stability on a surface than in a solution. The destabilization was found 96.7 kJ/mol and 83.8 kJ/mol for pure 1000 mM sodium and 15 mM magnesium, respectively. This destabilization was previously observed in many publications [20, 117-119] and it is considered that the destabilization is caused by repulsion of negatively charged oligonucleotides on a surface of DNA chip.

Hybridization of partly mismatched oligonucleotides

To determine the cationic effect on stability of targets containing internal base mismatches, a series of SPR experiments with Mism2, Mism3 and Mism4 analogous to the experiments with fully matched oligonucleotides were carried out.

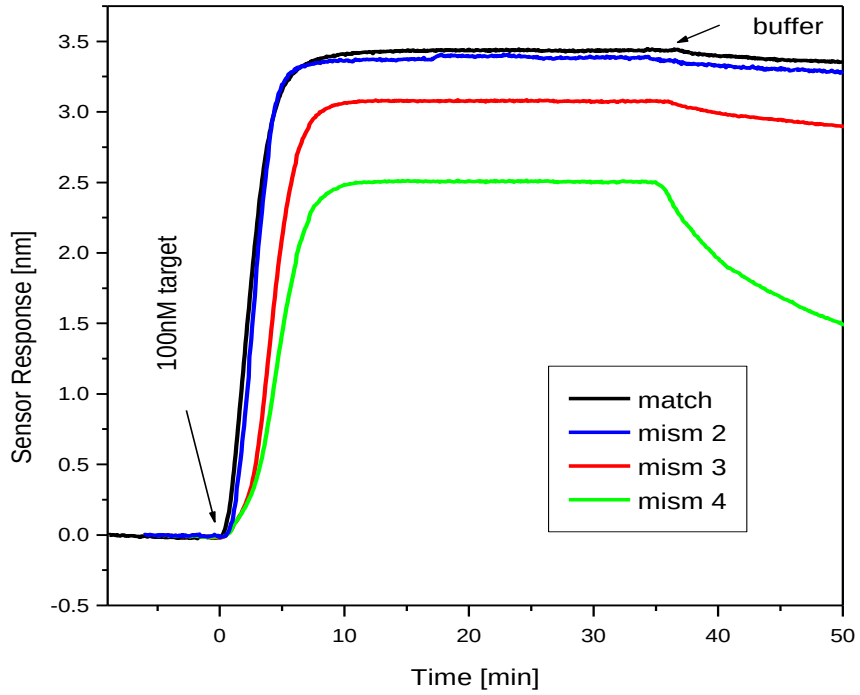

Figure 29. SP hybridization of partly mismatched oligonucleotides (Mism2, Mism3 and Mism4) to immobilized probes BdO_{23} on a surface of chip for buffer with 0mM NaCl/15mM $MgCl_2$. Temperature 20 °C and flow rate 30 µL/min.

In Figure 29 SPR sensor responses to Mism2, Mism3 and Mism4 for 15mM magnesium (without sodium) are shown. Mism2 reached nearly the same hybridization level as fully matched oligonucleotides while Mism3 and Mism4 had significantly lower stability. The same result was observed for other five combinations of cations [0/1.5, 0/5, 50/0, 1000/0, 1000/15] (data are not shown). This observation led us to the conclusion that Mism2 was not suitable for the study of the cationic effect on the stability of mismatched oligonucleotides and was excluded from further experiments.

In Figure 30 the stability of Mism3 and Mism4 oligonucleotides for all sodium/magnesium concentrations are shown. The overall trends of the duplex stability as a function of sodium and magnesium concentrations for Mism3 and Mism4 are similar, except the overall stabilities, which are lower than that for fully matched target. These include, in particular, the higher efficiency of magnesium over sodium and the stability minima when the sodium concentration was gradually varied and the magnesium concentration was fixed. This clearly indicates that the mechanism of sodium and magnesium shielding on duplex stabilities is the same both for fully matched and partly mismatched oligonucleotides.

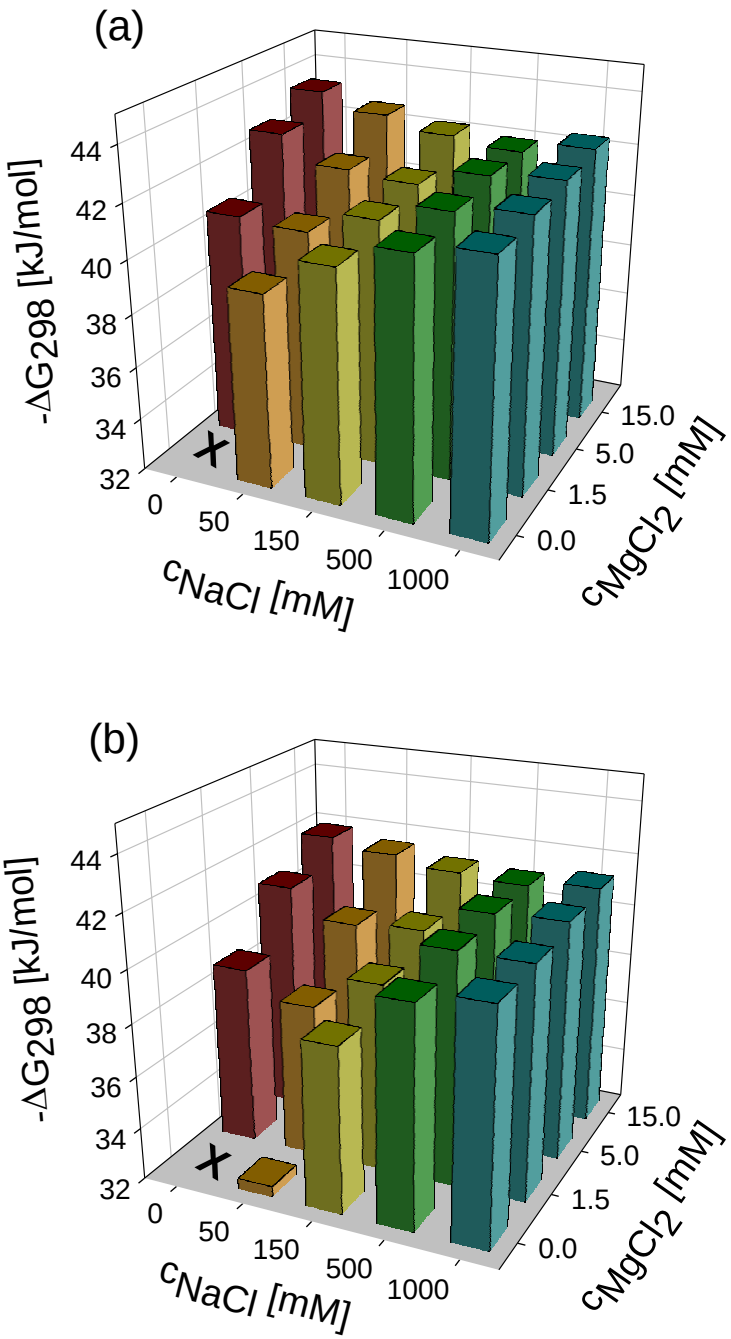

Figure 30. Gibbs energies ΔG_{298} of partly matched duplex formation on a surface of SPR sensor in the presence of various sodium and magnesium concentrations. The targets with three mismatches Mism3 (a) and four mismatches Mism4 (b) were used. The values for zero content of small cations are not shown, because no sensor responses to hybridization were observed.

In agreement with the previous DNA biosensor [30, 121] and microarray [118] studies, the total ΔG_{298} values were reduced due to the presence of mismatched base pairs. For instance, in the case of 15 mM magnesium without sodium, the

difference for three mismatches ΔG298(Mism3) – ΔG298(Match) = 0.84 kJ/mol is three times less than that for four mismatches ΔG298(Mism4) – ΔG298(Match) = 2.45 kJ/mol.

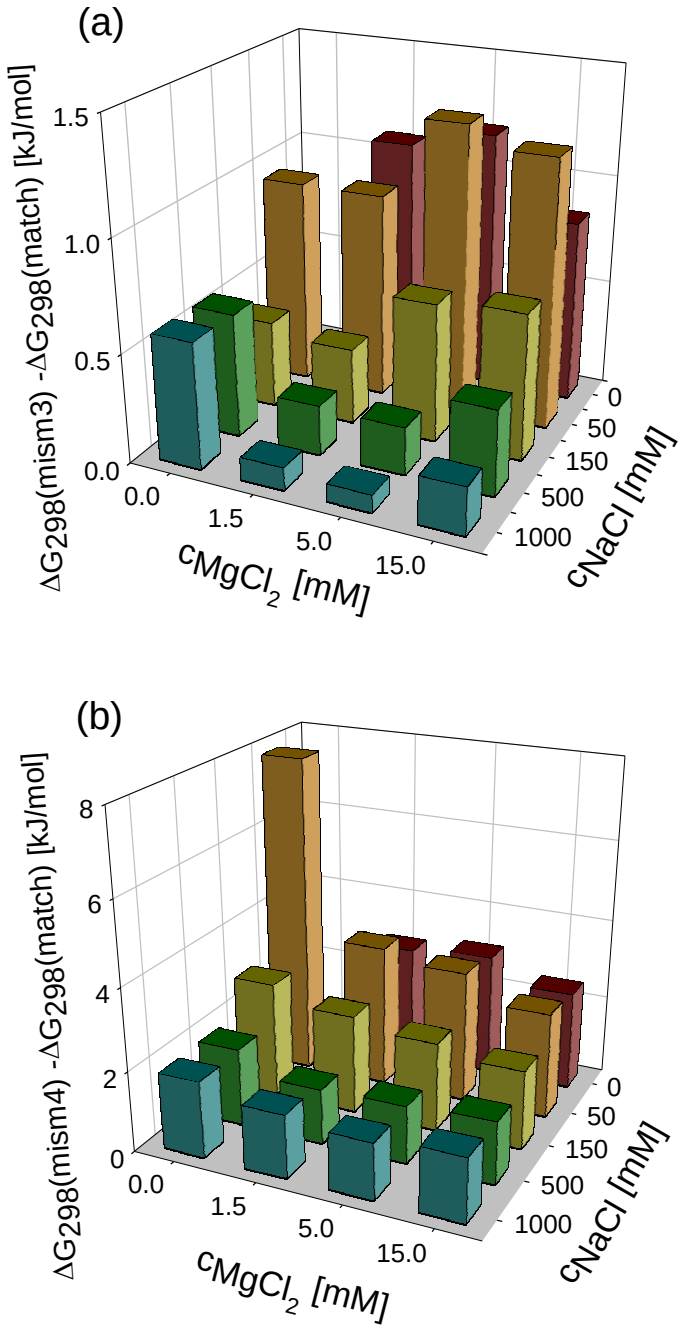

Figure 31. Differences between Gibbs energies ΔG_{298} of duplexes containing three (a) and four (b) internal mismatches and fully matched duplexes in the presence of various sodium and magnesium concentrations. Note that the horizontal axes were rotated for better visibility. The values for zero content of small cations are not shown, because no sensor responses to hybridization were observed.

Further, we decided to determine whether it is possible to improve the level of discrimination of partly mismatched and fully matched targets by optimizing the type and cation concentration in a hybridization buffer. The differences of the stabilities for three and four mismatched oligonucleotides and the fully matched oligonucleotides are shown in Figure 31. There is no clear dependence of the mismatched duplex destabilization on the magnesium concentration except for the case of 50/0 mM, in which, however, the stability of the used fully matched duplex is also substantially reduced. It is evident that at high sodium concentrations (higher than 100 mM) the destabilization of mismatched duplexes is lower in comparison with a low concentration of sodium (50 mM or less). In the optimization of the cation content for the discrimination of fully complementary and mismatched targets, the need for sufficiently high duplex stability has to be taken into account as well. The optimized cation composition yielding the highest level of discrimination between fully complementary and mismatched targets while maintaining a high hybridization signal is clearly the combination of the following cation concentrations, sodium: 0–50 mM and magnesium: 1.5 – 15 mM.

Probe immobilization

We also evaluated the effect of different cations on a probe immobilization. Probe BdO_{23} was immobilized to the covalently attached streptavidin layer via high affinity biotin-streptavidin binding. We used the same combination of sodium (0 to 1000 mM) and magnesium (0 to 15 mM) concentrations as in the hybridization studies. The probe densities for all sodium/magnesium concentrations are shown in Figure 32.

Figure 32 clearly demonstrates the significant effect of sodium and magnesium cations on the probe immobilization. This dependence is, surprisingly, very similar to the dependence which was determined in SP hybridization for fully matched duplexes BdO_{23}/CdO_{23}. This similarity includes increasing probe density with cationic concentration in a solution, higher efficiency of magnesium than sodium and the local minima (50 mM/1.5 mM and 150 mM sodium/5 mM magnesium). The trend where the probe immobilization increases with the concentration of cations was also found in previous publications by Peterson et al. [32] and Cho et al.[33]. They confirmed that monovalent sodium in a buffer has

positive effect on probe immobilization. This observation was explained by the effect of sodium to shield the negative charges of probes. However, up to date no publication has been found for the effect of multivalent cations on a probe immobilization.

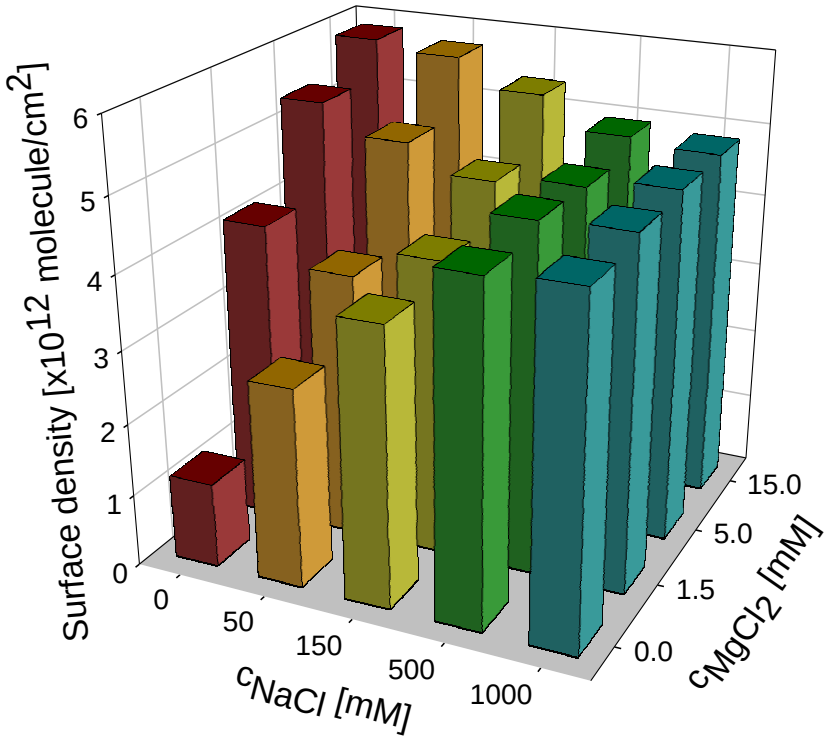

Figure 32. Density of immobilized probes for various sodium and magnesium concentrations after 35 minutes when the maximum probe density was reached.

If we compare hybridization and immobilization dependences only one exception in similarity was observed. The probes were successfully immobilized on a chip surface even without the presence of sodium or magnesium cations [0, 0]. The surface density reached about $1x10^{12}$ probe/cm^2, which is significantly lower than for buffers with cations. This observation clearly demonstrated that the probes might bind to a chip surface for low probe density when the repulsive forces are negligible. For higher probe density the cations are needed to shield the negative charges of probes.

These results demonstrate that the cations play a crucial role not only in hybridization processes but also in the immobilization of probes on a surface of a chip. The monovalent and divalent cations are able to shield the negative charges

during the immobilization in very similarly way as in hybridization study. Similarly to hybridization studies magnesium promoted higher shielding effect in comparison with sodium which results in higher probe densities on a chip surface. It is worth to mention that our results suggest that the probe immobilization is relatively non-affected for probe density lower than $1x10^{12}$ probe/cm^2 for our experimental conditions.

Considerations for interaction of duplexes on a surface of DNA chip

In SP hybridization experiments of fully matched oligonucleotides on a surface high efficiency of magnesium and lower duplex stability (in comparison with experiments in a solution) was observed. These both processes might be explained by the shielding effect of sodium and magnesium cations which effectively eliminate the repulsion of negatively charged oligonucleotides (see appendix IV).

On a surface of DNA chip all interactions proceeded in thin layer. We estimated from the characteristic dimension of the 23-mer oligonucleotide and streptavidin molecules that the thickness of this interaction layer is approximately 10 nm. Considering the observed values of probe coverage (~$5x10^{12}$ molecules/cm^2) and hybridization efficiencies of BdO_{23}/CdO_{23} duplexes (~75%), the molar concentration of duplexes in the active layer was 5 mM for 1000 mM sodium. This indicates that oligonucleotide duplexes occupy about 25% of the layer volume. Similar estimation might be done for 15 mM magnesium where even 35% of the layer volume is occupied. Considering that 75% of the active layer is freely accessible for cations and assuming that DNA duplexes form cylindrical polyanions with a radius of 10Å [22, 122] it is estimated that only a 6–8 Å thick shell surrounding each duplex is available on average for solvent with cations compensating for the negative charge of the DNA duplex. Using the Poisson–Boltzmann theory, Misra and Draper [122] determined concentration profiles for sodium and magnesium cations surrounding an isolated DNA duplex. These calculations showed that both sodium and magnesium cations effectively occupy an area up to 10 Å from the DNA duplex surface, which exceeds our estimated free zone. This suggests a spatial stress restricting the ability of cations to completely shield the negative charges on deoxyribophosphate backbones, which may explain the decreased stability of highly packed duplexes in comparison with lower

concentrations of oligonucleotides in a solution. It has been shown that the distribution of magnesium around an isolated DNA duplex is more compact than that of sodium [122]. Including two charges of magnesium it indicates that the total sum of positive charge is higher for magnesium under the restricted spatial conditions than for sodium. This can explain the stronger stabilization effect of magnesium over sodium on the duplex stability for solid-phase hybridization as well as the higher importance of the sodium–magnesium competition.

Interaction of oligonucleotides forming triplexes

We investigated the effect of monovalent and divalent cations on formation of DNA triplexes (dT_{23}•BdA_{23}*dT_{23}). For this purpose the experiments similar to the duplex formation was proposed. Biotinylated probe BdA_{23} was immobilized on a streptavidin modified chip surface and subsequently sequence dT_{23} was allowed to bind to BdA_{23} probe. Both processes were monitored. The experiments were performed in 10 mM Tris with the same cationic content as in the duplex hybridization study.

The hybridization efficiency is presented in Figure 33. The overall tendency is very similar to the duplex formation. The stability of the triplex formation increased with cationic content in a hybridization buffer, no binding of dT_{23} was observed for zero cationic content and magnesium supported higher stabilization effect than sodium cations. Small difference was observed for the positions of minima which were found for 150 mM/1.5 mM, 150 mM/5 mM and 150 mM sodium/15 mM magnesium.

Figure 33 shows that both high concentrated magnesium and high concentrated sodium strongly supported the formation of triplexes. For instance, the hybridization efficiency reached nearly 160% and 150% for pure 15 mM magnesium and pure 1000 mM sodium, respectively. It is worth to mention that an SPR sensor measures the amount of bound mass on a surface of SPR chip. Therefore, we cannot distinguish from the final sensor responses two limit states: i) all dT_{23} targets on a surface form triplexes (i.e., 75 % probes form triplexes and 25% are unoccupied for 1000 mM sodium) or ii) all probes are occupied (i.e. 50% probes form duplexes and 50% form triplexes for 1000 mM sodium). These limit cases are rather theoretical and the redistribution very probably occurs. And vice versa the hybridization below

100% does not mean that only duplexes are formed. The distribution of duplexes/triplexes on a surface of DNA chip might be obtained from SPR experiments, however, it was behind the scope of this study.

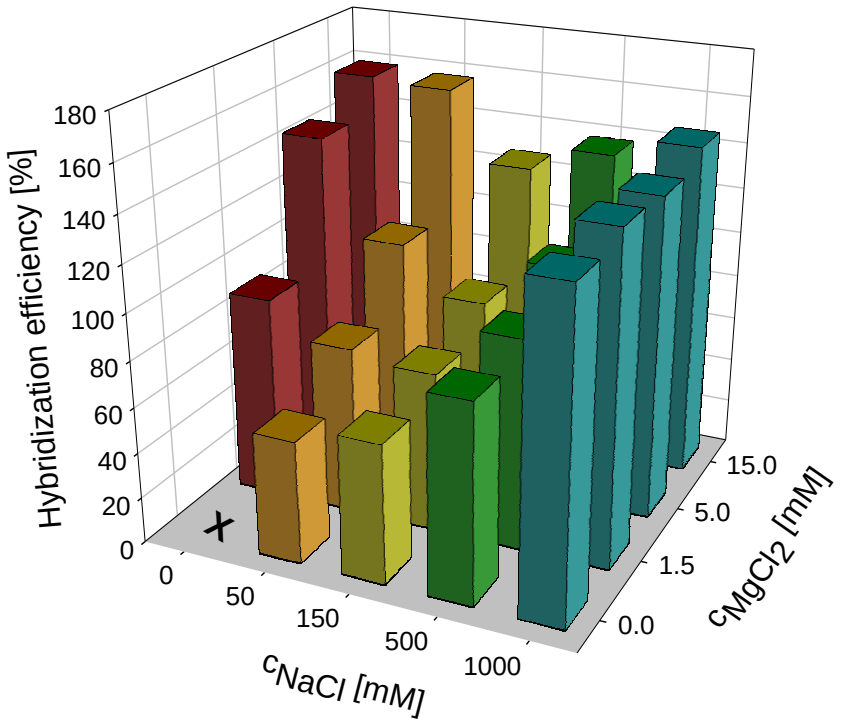

Figure 33. Hybridization efficiency for the binding of poly dT_{23} to BdA_{23} probe which was immobilized on a surface of SPR chip. The experiment was performed for 20 different concentrations of sodium and magnesium cations.

The immobilization of BdA_{23} probes was also monitored for different buffer compositions from 0 to 1000 mM sodium and from 0 to 15 mM magnesium. The obtained probe densities are presented in Figure 34.

The overall tendency is again very similar to the hybridization of BdO_{23}. It again included the tendency of increasing probe density with the concentration of cations and higher efficiency of magnesium than sodium. The minima of probe densities were also obtained for 50 mM/1.5 mM and 150 mM sodium/5 mM magnesium. These observations are not surprising because of the similarity of both sequences. Both BdO_{23} and BdA_{23} are DNA type and have the same length. These results demonstrate that the effect of cations shielding the negative charges during the probe immobilization is independent of base composition of probes.

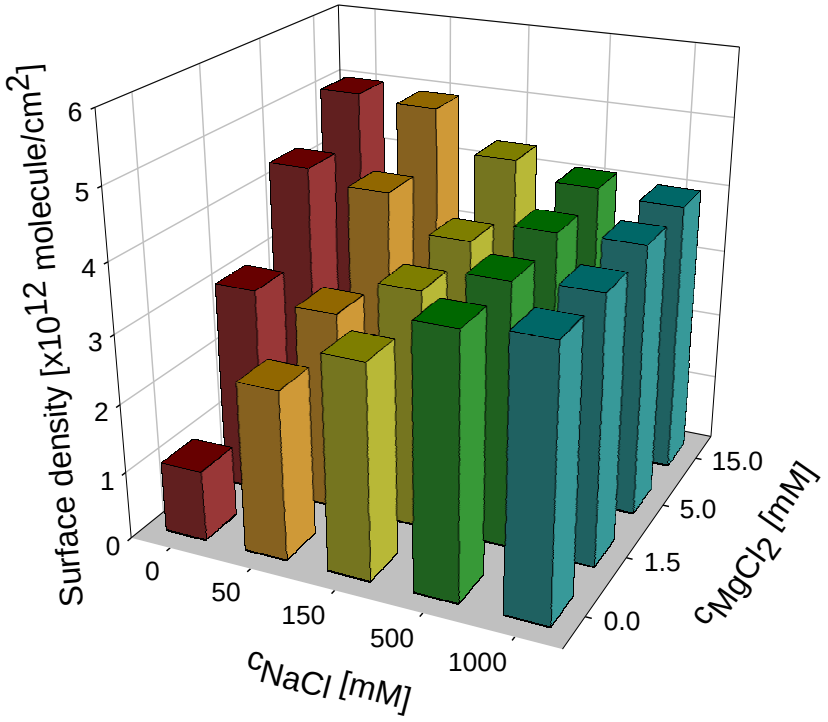

Figure 34. Surface density of immobilized BdA_{23} probes on a surface of DNA chip for 20 different concentrations of sodium and magnesium cations.

4.2.3 Conclusions - Interaction of oligonucleotides on a surface of DNA chip

This study has shown that the cationic shielding of repulsion of negative oligonucleotides was crucial for oligonucleotide interactions on a surface of DNA chip with high density of immobilized probes (~ $5x10^{12}$ molecules/cm^2). The spatial restricted conditions on a surface of DNA chip affected not only the duplex or triplex formation but also the immobilization of probes. These restricted conditions emphasized the role of divalent magnesium in the shielding of negative charges of oligonucleotides. It was demonstrated that magnesium is more effective than sodium, even for high concentration of monovalent cations. This observation significantly differs from the situation in a solution where high concentrated sodium had contrariwise higher stabilization effect than magnesium. The theoretical explanation of this phenomenon was proposed based on the assumption of surface restricted conditions. We published the interactions of oligonucleotides on a surface of DNA chip in [123] (Appendix IV).

4.3 Potential new therapeutics targeting TAR hairpin in HIV virus RNA

This work was focused on the study of new chemically modified oligonucleotides which are considered to be potentially employed as therapeutics against HIV virus. The modified anti-TAR oligonucleotides were derived from the parent RNA sequence of R06 aptamer which formed the kissing complex with TAR motive of HIV virus (see the schema in Figure 35). In the study the biotinylated RNA TAR sequence with 14 nucleotides, where four base pairs formed a stem and six nucleotides an apical loop, was used as a probe system.

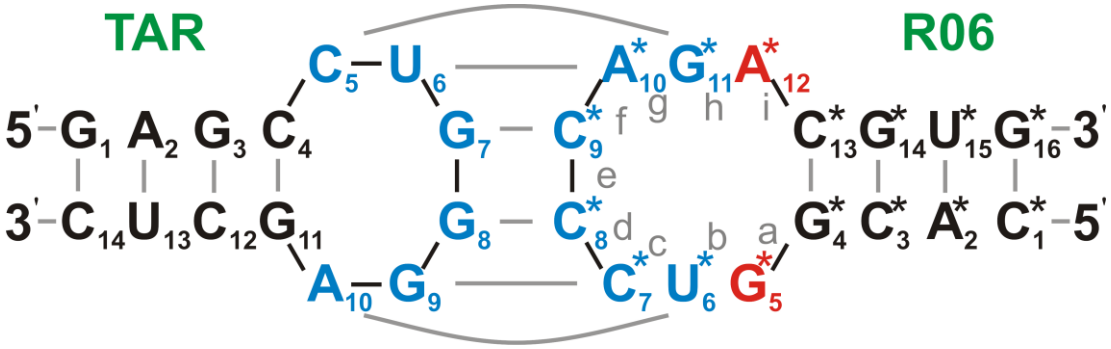

Figure 35. Schema of the kissing complex formed by the apical loops of TAR and R06 aptamer.

4.3.1 Materials and Methods

Oligonucleotides

In the study of TAR kissing complex with R06 aptamer and its analogs with new types of chemical modifications, 14-mer TAR probe with the RNA sequence biotin - TEG - TEG - 5′r-GAG CCU GGG AGC UC-3′ was employed. As the partner of TAR probe in the kissing complex, 16-mer RNA R06 aptamer with the 5′r-CAC GGU CCC AGA CGU G-3′ sequence was used [84]. The chemically modified anti-TAR oligonucleotides were of the same nucleobase sequence as RNA R06 aptamer with a single modification placed sequentially to individual nucleotide sites. Seven types of modifications, denoted as ON435, ON436, ON438, ON440, ON466, ON476 and ON477, each placed at nine positions (i.e. 63 various anti-TAR oligonucleotides) were examined.

The chemical structures of modifications are shown in Figure 36. In all cases the modifications of the sugar-phosphate backbone consisted in replacing the phosphate group by a phosphonate one at the 5´- or at the opposite (3´- and/or 2´-) site of the nucleotide. Most modifications consisted in elongation of the sugar-phoshate linkage with one chemical bond. The only exception was modification ON477 with a shorten linkage. The majority of modified linkages were isopolar with the natural ribose-phosphate linkage, in case of ON440, ON466, and ON477 2´-deoxyribose was used instead of ribose. The chemical modifications in studied anti-TAR oligonucleotides were placed gradually into the aptamer loop (see Figure 35 and Figure 37). The modified oligonucleotides were synthesized and HPLC purified at the Institute of Organic Chemistry and Biochemistry AS CR, v.v.i. (group of Dr. Ivan Rosenberg).

The 20-mer DNA probe biotin - TEG - TEG - 5′-TAT TAA CTT TAC TCC CTT CC-3′ (denoted as P_{ref}), which did not possessed any complementarity to the R06 aptamer sequence, was used as a reference probe in the reference channel. HPLC purified TAR probe and R06 aptamer were purchased from Dharmacon RNA Technologies, USA. HPLC purified P_{ref} probe was obtained from IDT technologies, USA, respectively.

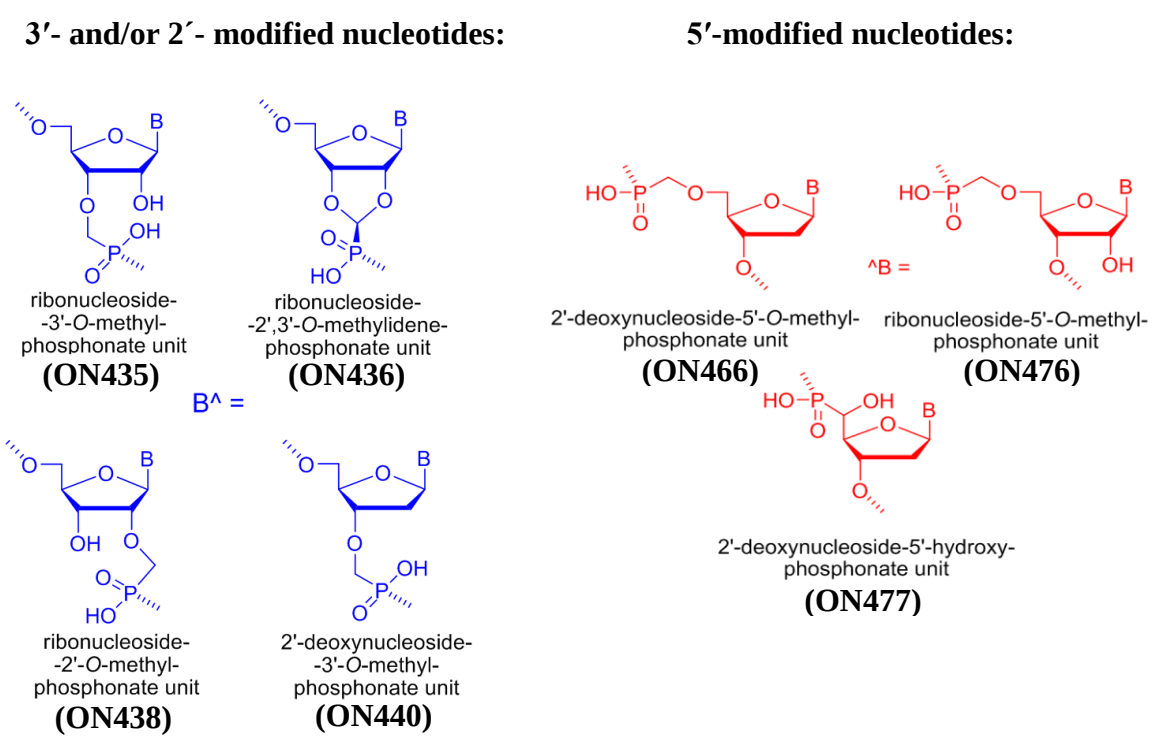

Figure 36. Structures of the studied chemical modifications.

Position of 3′/2′-modified nucleotides (ON435, ON436, ON438 and ON440) in anti-TAR oligonucleotides

a	5′r	CAC **G**^GU CCC AGA CGU G	3′
b	5′r	CAC G**G**^U CCC AGA CGU G	3′
c	5′r	CAC GG**U**^ CCC AGA CGU G	3′
d	5′r	CAC GGU **C**^CC AGA CGU G	3′
e	5′r	CAC GGU C**C**^C AGA CGU G	3′
f	5′r	CAC GGU CC**C**^ AGA CGU G	3′
g	5′r	CAC GGU CCC **A**^GA CGU G	3′
h	5′r	CAC GGU CCC A**G**^A CGU G	3′
i	5′r	CAC GGU CCC AG**A**^ CGU G	3′

Position of 5′-modified nucleotides (ON466, ON476 and ON477) in anti-TAR oligonucleotides:

a	5′r	CAC G^**G**U CCC AGA CGU G	3′
b	5′r	CAC GG^**U** CCC AGA CGU G	3′
c	5′r	CAC GGU ^**C**CC AGA CGU G	3′
d	5′r	CAC GGU C^**C**C AGA CGU G	3′
e	5′r	CAC GGU CC^**C** AGA CGU G	3′
f	5′r	CAC GGU CCC ^**A**GA CGU G	3′
g	5′r	CAC GGU CCC A^**G**A CGU G	3′
h	5′r	CAC GGU CCC AG^**A** CGU G	3′
i	5′r	CAC GGU CCC AGA ^**C**GU G	3′

Figure 37. Positions of 3'- and 5'-modified nucleotides in anti-TAR oligonucleotide.

SPR experiment

Streptavidin-modified chips, which were described in part 3.1.3, were used in this study. To obtain the reproducible surface conditions, streptavidin binding was stopped when 10 nm SPR sensor response, which corresponded to the surface density of 1.8×10^{12} molecule/cm^2, was reached. Then TAR buffer (= 20 mM Tris, 140 mM KCl, 20 mM NaCl, 3 mM $MgCl_2$, pH 7.4) was pumped along a surface of SPR chip for at least 15 minutes. In the detection channel 20 nM TAR probe was injected until the sensor response of 0.4 nm (~ 0.8×10^{12} probe/cm^2) was reached. In the reference

channel 40 nM P_{ref} probe was pumped for the same time. Target oligonucleotides were injected to the detection and reference channels for 10 minutes at concentration of 20, 50, 100, 200 or 500 nM for R06 aptamer and 100 nM or 300 nM for anti-TAR oligonucleotides (fast screening between 63 different oligonucleotides). Then, TAR buffer was again pumped. The chip was regenerated by the injection of 20 mM ethylenediaminetetraacetic acid disodium salt dihydrate (EDTA) for 5 minutes. During the SPR experiment both the association and dissociation phase were monitored in order to calculate kinetic constants. Each concentration was measured at least three times at the temperature of 23°C and the flow rate of 20 μL/min.

The obtained SPR sensor responses were employed to determine association and dissociation rate constants of monitored interactions. BIA evaluation software, version 4.1, from Biacore and 1:1 Langmuir model, which also considered the mass transport effects [94], was applied.

UV absorption measurements

UV absorption experiments were used for the determination of oligonucleotide concentrations. The absorbance at the wavelength of 260 nm was measured with the UV–VIS absorption spectrometer Varian 4000 in cuvettes with 1-cm optical length. Each sample was measured at least twice in pure water from Milipore Q, USA. Because only one substitution was performed in the sequence of R06 aptamer, the extinction coefficient of 151 400 L/(mole.cm) was used for R06 aptamer and all its analogs as well.

Molecular dynamic (MD) simulations

Analysis of the SPR results also uses MD simulations of kissing complexes formed by TAR and R06 or several its analogs, performed by Dr. Ivan Barvík at the Institute of Physics, Faculty of Mathematics and Physics of Charles University. The model systems of the kissing complexes were constructed using the crystal structure from Lebars et al. ([89], protein data bank 2JLT). It means that both oligonucleotides, TAR and aptamer, were in MD simulations lengthened in their stem of one base-pair in comparison with those used in SPR experiments. All simulated systems were surrounded by TIP3P [124] water molecules which extended to a distance of approximately 10 Å (in each direction) from the nucleic acids atoms.

This gave a periodic box size of ~75 Å, ~88 Å, ~70 Å for a simulated system consisting of ~40.633 atoms. New *.inpcrd (initial coordinates) and *.prmtop (molecular topology, force field [125-128]) files for the whole simulated system were created by means of the TLEAP module (the AMBER software package [129]).

Equilibration MD trajectories lasting for 5 ns were computed with the aid of the NAMD 2.7 software package [130]. For the production of MD runs ACEMD v. 2591 was used [131, 132]. Production runs were performed in the NVT ensemble, Langevin thermostat at 290/310 K, computing the electrostatic interactions with PME. The hydrogen mass repartitioning scheme used in ACEMD allowed an increased time step [131, 133]. Therefore, the integration time-step was set to 4 fs. Data were recorded every 100 ps. 300-500 ns MD trajectories were analyzed with the aid of the VMD 1.9 [134], CHIMERA 1.5.3 [135] and AMBER12/PTRAJ-CPPTRAJ [136] software packages.

4.3.2 Results and Discussion

SPR monitoring of TAR/R06 kissing complex formation

Prior to the study of anti-TAR oligonucleotides, the binding of parent R06 aptamer was investigated in details in order to obtain reliable reference data and to optimize the SPR measurement protocol. The SPR chip surface was prepared as written in Materials and methods. In the detection channel 20 nM TAR probe was injected until the sensor response of 0.4 nm was reached, which corresponded to approximately 20 % of the maximum surface density (~ 2.15 nm). The relatively low surface density of immobilized probes was used in order to reduce the effects of spatial restrictions and charge repulsion of neighboring probes, which affect the binding of the target oligonucleotides as discussed previously in section 4.2 and shown in [20, 123]. Within this study the dispersionless microfluidics developed within the framework of this doctoral thesis and described in section 4.1 was employed for the accurate monitoring of the binding kinetics.

Binding and dissociation to both immobilized TAR (detection channel) and P_{ref} probe (reference channel) was monitored for five R06 concentrations from 20 nM to 500 nM on four independent SPR chips. Duration of the association phase was set to 10 minutes. Typical experiment results from the detection channels are shown

in Figure 38. The reference channel did not indicate any unspecific binding of R06 aptamer to P_{ref} probes (data are not shown). The reference channels were therefore applied for the determination of general signal drifts or the effects of the refractive index differences between the sample and buffer solutions. All further figures are presented as a reference compensated.

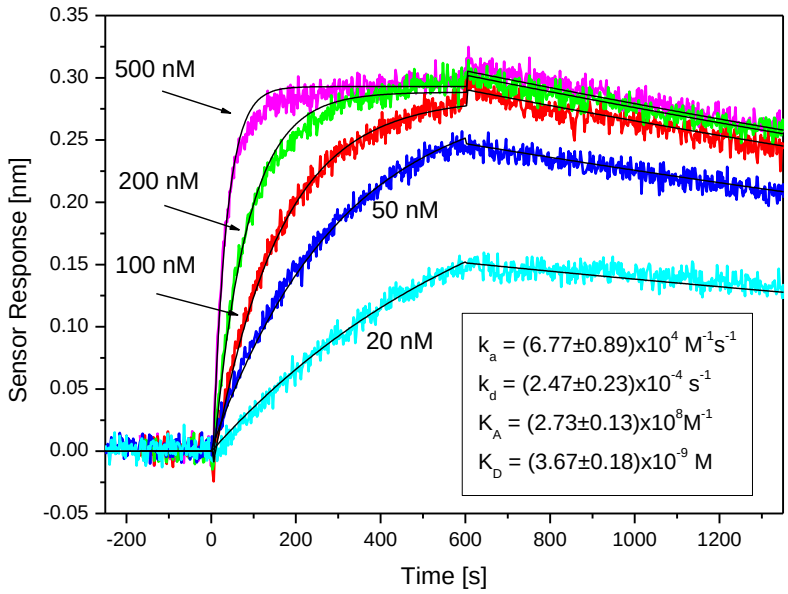

Figure 38. Typical SPR sensor response for association and dissociation of R06 aptamer on a TAR modified chip for concentrations from 20 nM to 500 nM. The black curves represent the fits obtained from the kinetic analysis. The shown kinetic and equilibrium constants were determined from four independent measurements, each on a separate chip. The temperature and the flow rate were set to 23°C and 20 μL/min, respectively.

As expected the binding rates increased with concentrations of R06 aptamers. The lowest sensor response was observed for the concentration of 20 nM while the saturation level was achieved for the concentration of 500 nM in a few minutes. When TAR buffer without R06 aptamer was injected, the dissociation of bound R06 aptamer from a surface of SPR chip occurred. The sensor responses to different concentrations were fitted by BIAevaluation software from Biacore (black curves in Figure 38). The association and dissociation rate constants and the association and dissociation equilibrium constants obtained from the series of independent experiments were k_a = (6.77±0.88) × 10^4 $M^{-1}s^{-1}$, k_d = (2.47±0.23) × 10^{-4} s^{-1}, K_a = (2.73±0.13) × 10^8 M^{-1}. and K_d = (3.67±0.18) × 10^{-9} M.

These values are in a reasonable agreement with those previously published in [84, 92, 137] by the group of prof. J.J.Toulmé. In [137], interaction of 24-mer R06 with 27-mer TAR hairpin was measured on an SPR chip. The determined values of

the constants were k_a = (3.9±0.9) × 10^4 $M^{-1}s^{-1}$, k_d = (2.6±0.5) ×10^{-4} s^{-1}, and K_d = (6.9±2.9) × 10^{-9} M. The dissociation kinetic constant k_d agrees perfectly with our result. The association kinetic constant is of the same order as that we obtained but somewhat lower, which can be attributed to different surface conditions. As a consequence of different kinetic association constants, the equilibrium dissociation constants K_d are also different. Later on, Darfeuille et al published in [84] the equilibrium dissociation constants obtained from gel mobility shift experiments for various lengths of R06 aptamer with 27-mer TAR hairpin. They obtained K_d = 6.2±0.9 nM for R06 24-mer and K_d = 7.0±1.8 nM for 16-mer version (which we used) of R06 aptamer. Taking into account the differences in the employed experimental techniques, the obtained value was in a surprisingly good agreement with SPR results. Simultaneously, their work demonstrated that shortening of the R06 stem (to four base pairs) reduced the thermodynamic stability of the kissing complex only very weakly. In the latest work [93], a substantially lower equilibrium dissociation constant, K_d = 1.31±0.15 nM, was reported for the kissing complex of R06 16-mer and 27-mer TAR. This value was determined from SPR experiment that was performed at almost the same conditions as in [137]. The only difference was that the sodium, potassium and magnesium salts used for preparation of reaction buffer were acetates in [137], while chlorides in [93]. The values of rate constants were not reported.

We can conclude that the precise values of the equilibrium and very probably also the rate constants depends sensitively on the conditions of the experiment. Considering this, our results concerning the kissing complex of TAR and R06 agreed well with the previously published results. It is also obvious that the effect of the chemical modifications of R06 should be evaluated in comparison with measurements on natural R06 performed at the same conditions and within the same series of experiments.

SPR characterization of the kissing complex formation with TAR probe for the whole set of 63 anti-TAR modified oligonucleotides required, however, simplified experimental procedure. We therefore tested the accuracy and reproducibility of kinetic and equilibrium constants determined from a simple SPR measurement using only one analyte concentration. Twelve cycles of R06 aptamer at selected 100 nM concentration were performed on seven different chips. The kinetic and equilibrium constants were determined for each individual curve. From this

experimental set we obtained the mean values with errors calculated as standard deviations: k_a = (7.14 ± 1.49) × 10^4 $M^{-1}s^{-1}$, k_d = (2.44 ± 0.67) × 10^{-4} s^{-1} and K_d = (3.44 ± 0.75) × 10^{-9} M. These results showed high reproducibility (see also Figure 39) and very good agreement with the values obtained by joint analysis of SPR curves for five different concentrations.

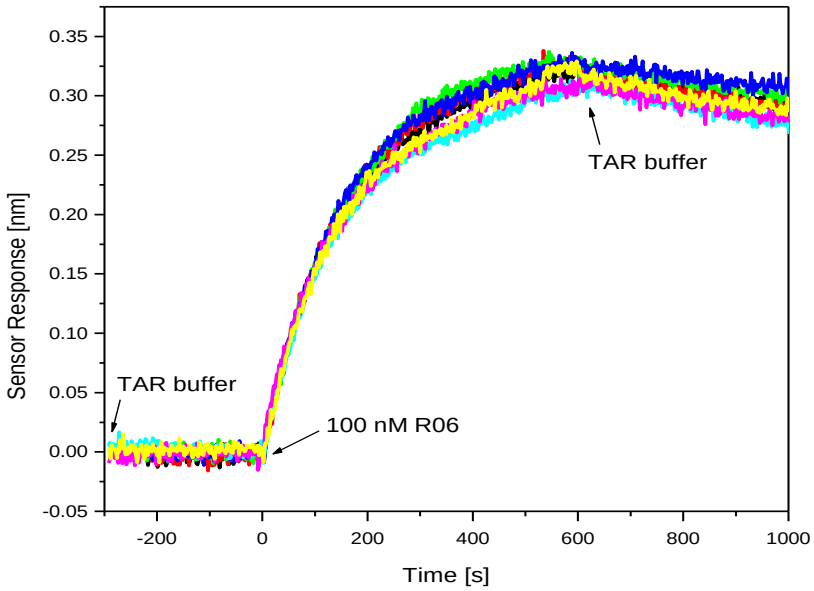

Figure 39. Reproducibility of measurement for six bindings of 100 nM aptamer R06 (two subsequent cycles, each with three bindings) during SPR experiment on one TAR-modified chip.

Kissing complex formation between TAR and anti-TAR modified oligonucleotides

The set of 63 modified anti-TAR oligonucleotides was screened by an SPR biosensor to characterize the effects of the type and position of modifications on the stability of the formed complex and kinetics of the complex association and dissociation. The simplified measuring procedure verified by the abovementioned measurements on the reference TAR/R06 complex, was employed. For each anti-TAR oligonucleotide it consisted of at least three independent binding cycles performed on at least three different chips using concentration of 100 or 300 nM. The concentration of 100 nM was used for nearly all anti-TAR oligonucleotides. The concentration of 300 nM was used only for anti-TAR oligonucleotides with very low stability (ON477b - ON477h). Figure 40 shows for illustration typical SPR curves obtained within a single binding cycle for the set of nine anti-TAR oligonucleotides containing ON435 modification at different positions. Variations of both the

association and dissociation rates in dependence on the position of the modification are obvious.

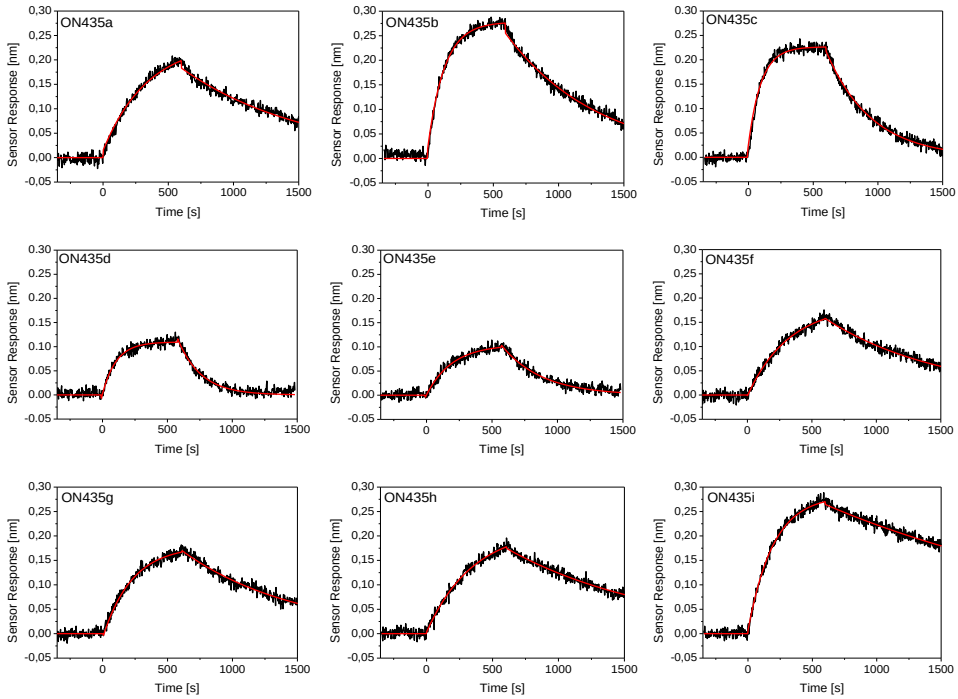

Figure 40. Example of SPR curves (in black) within a single binding cycle for different positions of the chemical modification in the anti-TAR oligonucleotide. Modification ON435, 100nM concentration. Results of the fit according to BIA evaluation software, 1:1 Langmuir model with mass transport effects are shown as red lines.

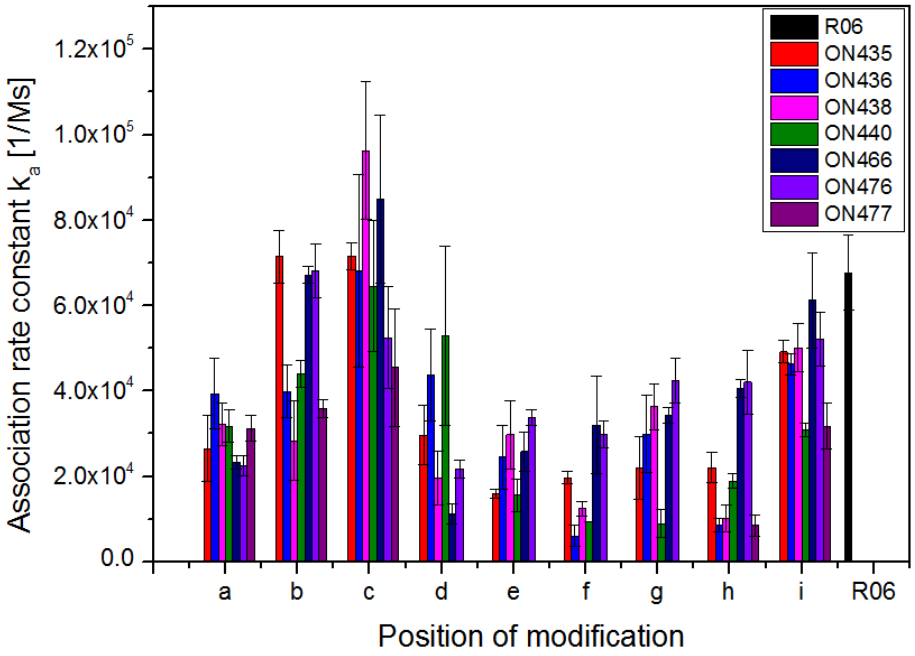

Figure 41 Association rate constants k_a for modifications ON435, ON436, ON438, ON440, ON466, ON476, ON477, and natural R06. Error bars present the standard deviations from at least three independent experiments.

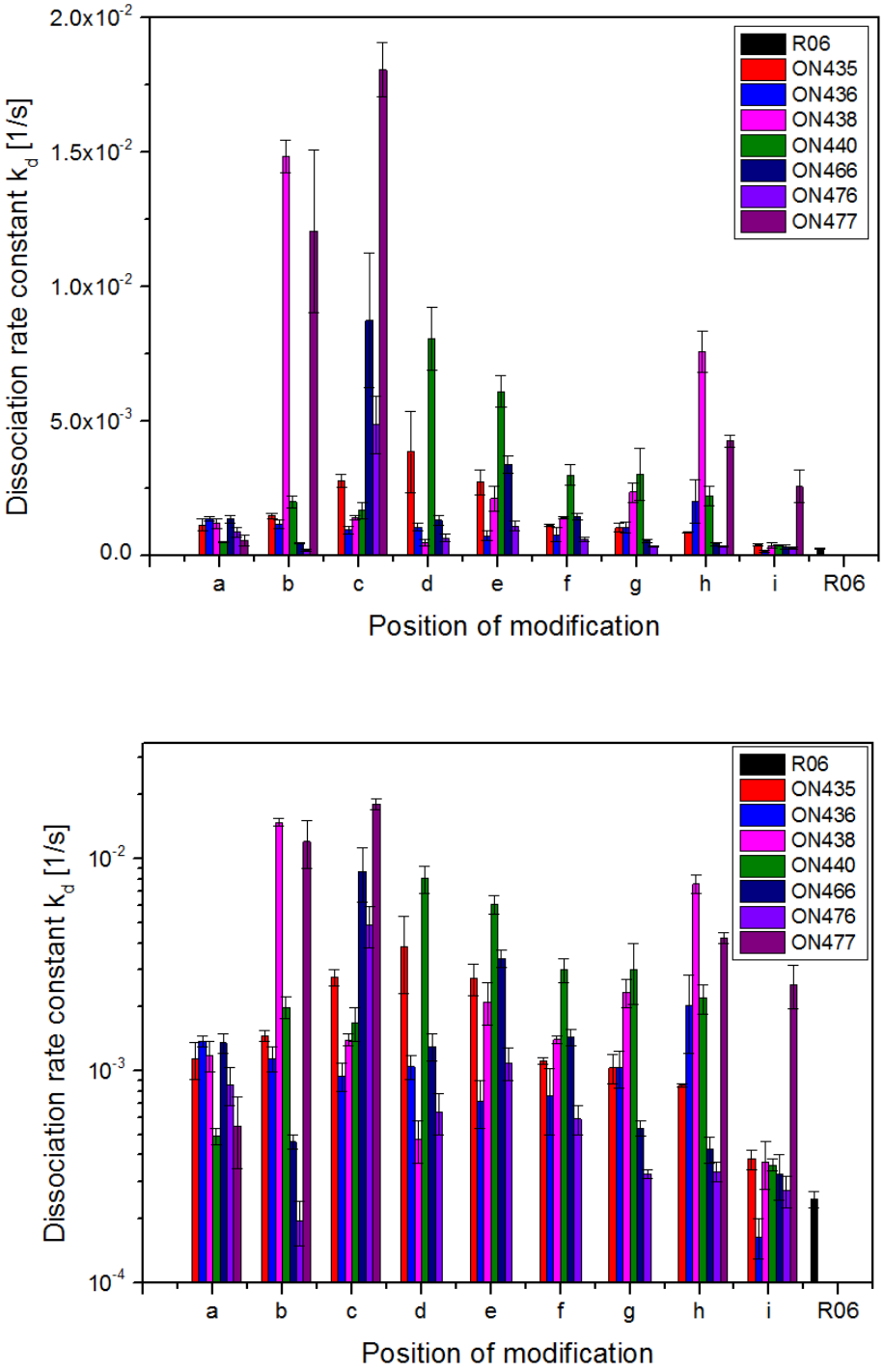

Figure 42. Dissociation rate constants k_d for modifications ON435, ON436, ON438, ON440, ON466, ON476, ON477, and natural R06 (linear scale (up), logarithmic scale (down)). Error bars present the standard deviations from at least three independent experiments.

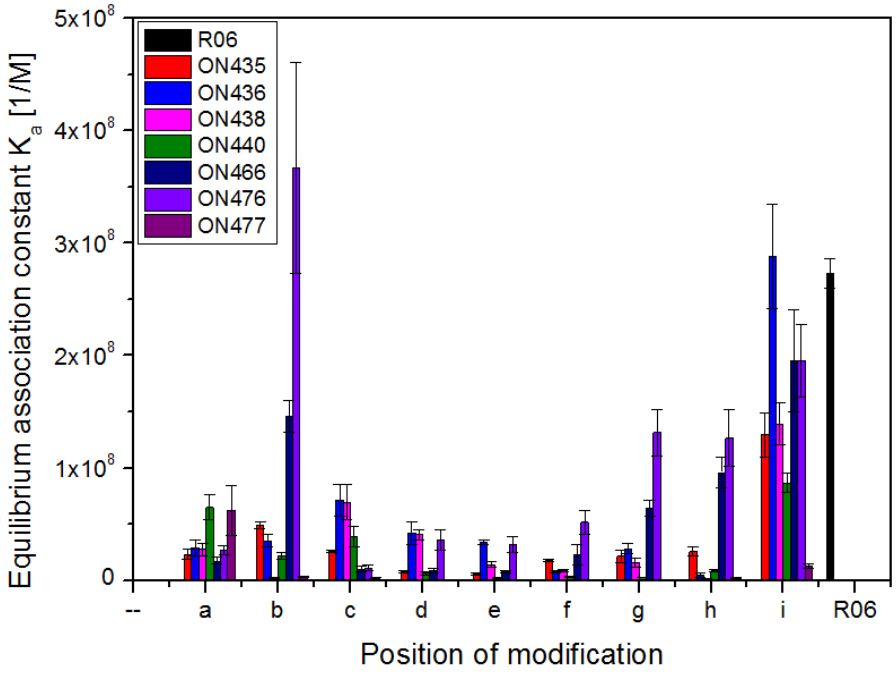

Figure 43. Equilibrium association constants K_a for modifications ON435, ON436, ON438, ON440, ON466, ON476, ON477, and natural R06. Error bars present the standard deviations from at least three independent experiments.

The kinetic and equilibrium constants for all modifications and positions are shown in Figure 41-Figure 44 and Table 1. For a clearer comparison, the values of the equilibrium association constant K_a are also shown despite that they represent the same information as K_d. All constants are obviously very sensitive to the type and position of the modification in the anti-TAR oligonucleotide. The constants were not determined for modification ON477 at positions from (d) to (g) because in these cases SPR experiments did not show any complex formation.

In general, the equilibrium constants indicated that the most of modifications decreased the thermodynamic stability of the kissing complex. Nevertheless, ten anti-TAR oligonucleotides exhibited stability comparable with R06, i.e. their dissociation equilibrium constants were lower than threefold value of that of R06 (11 nM). In the case of eleventh oligonucleotide, ON440i, this limit was within the range of the experimental error. For two modified oligonucleotides, ON436i and ON476b, the stability was not lower and was even higher, respectively, than that of the parent TAR/R06 kissing complex.

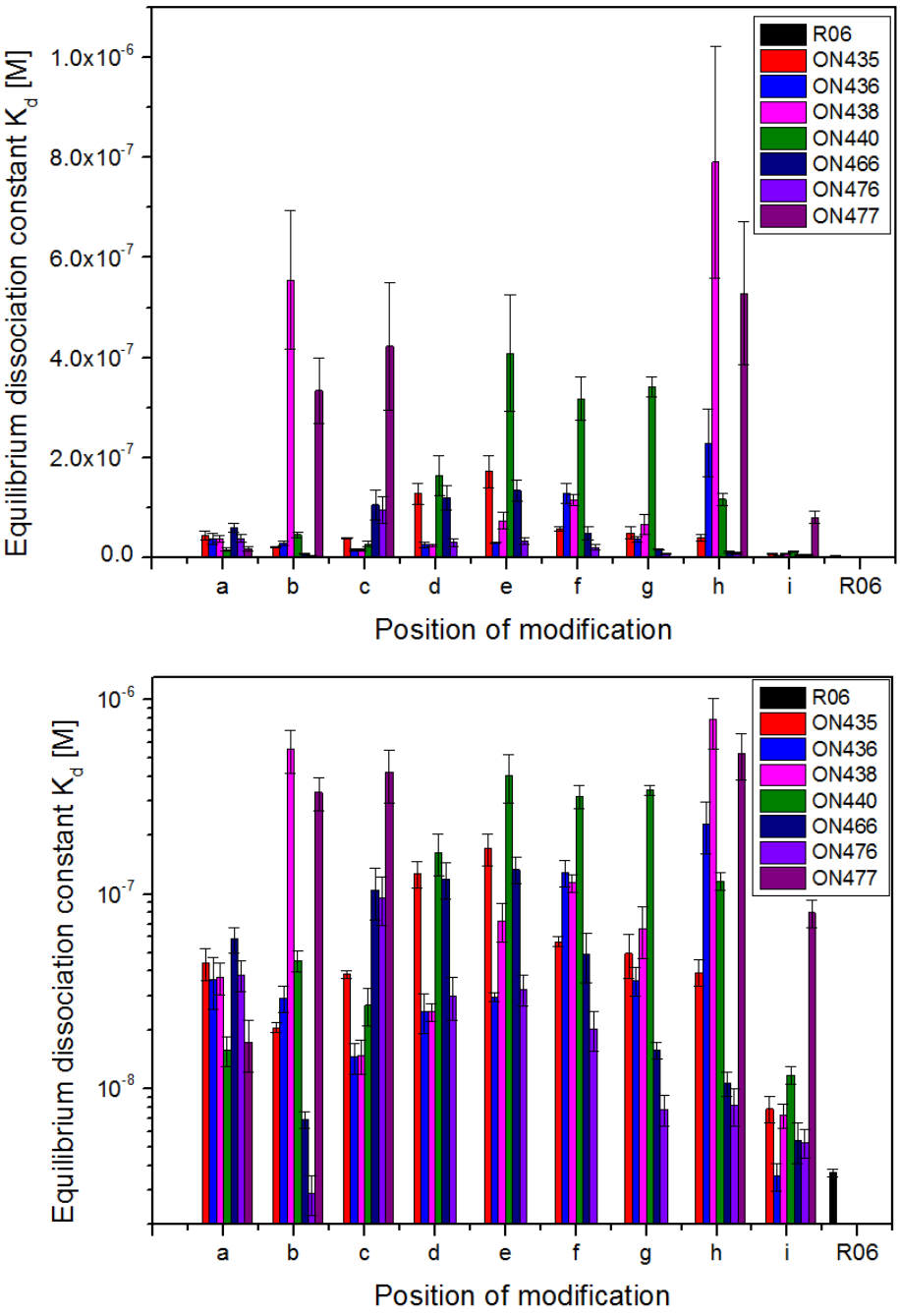

Figure 44. Equilibrium dissociation constants K_d for modifications ON435, ON436, ON438, ON440, ON466, ON476, ON477, and natural R06 (linear scale (up), logarithmic scale (down)). Error bars present the standard deviations from at least three independent experiments.

R06	k_a × 10^{+3} M^{-1} s^{-1}	k_d × 10^{-5} s^{-1}	K_a × 10^{+6} M^{-1}	K_d × 10^{-8} M
R06 full	67.7±8.9	24.7±2.3	273.2±12.9	0.37±0.02
R06 100nM	71.4±14.9	24.4±6.7	303.5±64.8	0.34±0.08

ON435	k_a × 10^{+3} M^{-1} s^{-1}	k_d × 10^{-5} s^{-1}	K_a × 10^{+6} M^{-1}	K_d × 10^{-8} M
ON435a	26,5±7,7	113,6±22,6	23,4±4,3	4,4±0,8
ON435b	71,4±6,2	146,0±8,7	49,0±2,8	2,0±0,1
ON435c	71,6±3,2	276,0±24,6	26,0±1,2	3,9±0,2
ON435d	29,6±6,9	384,3±152,2	8,0±1,2	12,7±2,0
ON435e	16,0±1,1	272,7±46,2	6,0±1,1	17,2±3,2
ON435f	19,7±1,5	111,3±4,0	17,7±1,0	5,7±0,3
ON435g	22,0±7,4	103,4±16,3	21,4±5,9	4,9±1,3
ON435h	22,0±3,5	85,5±1,5	25,8±4,4	3,9±0,6
ON435i	49,2±2,6	38,2±4,1	129,7±19,6	0,8±0,1

ON436	k_a × 10^{+3} M^{-1} s^{-1}	k_d × 10^{-5} s^{-1}	K_a × 10^{+6} M^{-1}	K_d × 10^{-8} M
ON436a	39,4±8,3	137,3±8,1	28,9±7,5	3,6±1,1
ON436b	39,8±6,2	114,5±15,3	35,1±5,5	2,9±0,5
ON436c	68,0±22,6	94,4±14,6	71,2±14,3	1,4±0,3
ON436d	43,7±10,7	104,5±13,9	42,0±9,7	2,5±0,6
ON436e	24,5±7,5	71,7±18,2	34,0±1,8	3,0±0,2
ON436f	6,1±2,5	76,2±26,3	7,9±1,1	12,9±2,0
ON436g	29,9±9,0	103,6±20,7	28,4±4,5	3,6±0,6
ON436h	8,6±1,6	202,0±81,4	4,7±1,6	22,9±6,7
ON436i	46,2±2,4	16,4±3,5	288,3±46,5	0,4±0,1

ON438	k_a × 10^{+3} M^{-1} s^{-1}	k_d × 10^{-5} s^{-1}	K_a × 10^{+6} M^{-1}	K_d × 10^{-8} M
ON438a	32,2±5,1	118,0±19,7	27,7±5,8	3,7±0,7
ON438b	28,4±9,3	1483,3±61,1	1,9±0,5	55,5±13,9
ON438c	96,3±16,2	139,7±9,1	69,6±15,3	1,5±0,3
ON438d	19,5±6,4	47,1±10,7	40,9±4,6	2,5±0,3
ON438e	29,8±8,0	211,8±47,7	14,2±3,0	7,3±1,6
ON438f	12,4±1,8	140,0±5,3	8,9±0,9	11,4±1,1
ON438g	36,3±5,3	234,7±36,1	15,9±4,1	6,6±2,0
ON438h	10,1±3,1	758,7±75,8	1,3±0,4	79,1±23,2
ON438i	50,2±5,6	36,8±9,3	139,3±19,0	0,7±0,1

ON440	k_a × 10^{+3} M^{-1} s^{-1}	k_d × 10^{-5} s^{-1}	K_a × 10^{+6} M^{-1}	K_d × 10^{-8} M
ON440a	31,8±3,7	49,2±4,2	65,1±10,9	1,6±0,3
ON440b	44,0±3,1	199,0±22,6	22,3±3,0	4,5±0,6
ON440c	64,5±15,3	168,0±30,4	38,7±9,2	2,7±0,6
ON440d	52,9±21,0	804,5±116,8	6,4±1,6	16,4±4,0
ON440e	15,6±3,7	610,0±60,3	2,6±0,6	40,9±11,6
ON440f	9,4±0,1	298,7±37,9	3,2±0,5	31,8±4,3
ON440g	8,9±3,3	301,0±96,6	2,9±0.2	34.1±2,0
ON440h	18,9±1,7	220,3±35,0	8,7±1,0	11,6±1,2
ON440i	31,0±1,6	35,9±2,3	86,7±8,5	1,2±0,1

ON466	k_a × 10^{+3} M^{-1} s^{-1}	k_d × 10^{-5} s^{-1}	K_a × 10^{+6} M^{-1}	K_d × 10^{-8} M
ON466a	23,3±1,6	135,3±14,1	17,4±3,0	5,9±0,9
ON466b	67,2±2,0	46,2±3,3	146,0±14,0	0,7±0,1
ON466c	84,8±19,7	874,8±248,4	10,1±2,6	10,5±3,1
ON466d	11,2±2,3	129,8±19,1	8,7±1,9	11,9±2,6
ON466e	25,8±4,5	338,5±32,8	7,6±1,1	13,4±2,1
ON466f	32,0±11,4	143,5±12,4	22,7±9,3	4,9±1,4
ON466g	34,3±1,9	53,5±4,5	64,5±6,9	1,6±0,2
ON466h	40,5±2,1	42,8±6,1	96,1±13,9	1,1±0,2
ON466i	61,3±11,2	32,4±7,9	195,6±45,6	0,5±0,1

ON476	k_a × 10^{+3} M^{-1} s^{-1}	k_d × 10^{-5} s^{-1}	K_a × 10^{+6} M^{-1}	K_d × 10^{-8} M
ON476a	22,5±2,3	85,7±17,5	26,8±4,1	3,8±0,7
ON476b	68,1±6,3	19,5±4,7	367,0±93,6	0,3±0,1
ON476c	52,5±11,8	485,1±106,2	11,2±2,6	9,5±2,7
ON476d	21,8±2,0	63,7±13,8	35,7±9,2	3,0±0,8
ON476e	33,7±1,8	108,5±18,8	32,1±7,2	3,2±0,6
ON476f	29,8±3,1	59,0±9,2	51,7±10,3	2,0±0,5
ON476g	42,5±5,3	32,4±1,5	131,6±20,5	0,8±0,1
ON476h	42,1±7,5	33,4±3,6	126,7±25,1	0,8±0,2
ON476i	52,2±6,3	27,1±4,7	195,7±32,5	0,5±0,1

ON477	k_a × 10^{+3} M^{-1} s^{-1}	k_d × 10^{-5} s^{-1}	K_a × 10^{+6} M^{-1}	K_d × 10^{-8} M
ON477a	31,2±3,0	54,8±20,2	62,3±22,1	1,7±0,5
ON477b	35,9±2,1	1210,0±301,0	3,1±0,6	33,4±6,5
ON477c	45,5±1,4	1810,0±101,0	2,5±0,7	42,3±12,8
ON477d	-	-	-	-
ON477e	-	-	-	-
ON477f	-	-	-	-
ON477g	-	-	-	-
ON477h	8,5±2,5	424,0±24.2	2,0±0,5	52.9±14,3
ON477i	31,8±5,3	255,6±60,0	12,8±2,1	8,0±1,4

Table 1. Kinetic and equilibrium constants for modifications ON435, ON436, ON438, ON440, ON466, ON476, ON477, and natural R06. The missing values represent the cases where SPR experiments did not show any complex formation. Constants, which were fit from full experiments (full) and simplified experiments (100 nM), are shown for R06 aptamer.

We can compare our results with those already obtained on TAR complexes with R06 modified analogs and published in [84, 90, 92, 93]. In all cases the published studies dealt with R06 analogs with all or at least many modified nucleotides and the employed modifications was isosteric, it means that the modification does not change the number of covalent bonds in an internucleotide linkage. Comparable stability was reported for analogues of R06 24-mer with all nucleotides substituted for 2′-O-methyl analogues ([90], 1.5 times higher K_d than that

for parent RNA R06 aptamer) or deoxyphosphoramidate analogues ([93], 2 times lower K_d). LNA modification was found not to lead to a stable kissing complex when used for all positions in the R06 chain [84]. Better results were obtained when LNA nucleotides were combined with DNA nucleotides; the chimeric LNA/DNA 16-mer with 8 LNA nucleotides, four at the two end base-pairs of the stem and four in the loop corresponding to U6*, C8*, A10* and G11* nucleotides of our notation, possessed K_d only three times higher than R06 [84]. Substantially better stability was found for some chimeric aptamers combining LNA and 2′-O-methyl modifications. Two aptamers with two LNA modifications (all the others of 2′-O-methyl type) in C9*/A10* and C9*/G11* positions formed kissing complexes with the equilibrium dissociation constant 5 times lower and one aptamer with a single LNA modification in C9* position 2 times lower in respect to the parent natural R06 ([92]).

Looking for the effect of various modification types and sites on kinetic constants, remarkably higher impact on the dissociation rate constants than on the association rate constants is obvious. The dissociation rate constants were found in the range of two orders of magnitude, while the largest association constant was only fifteen times larger than the smallest one. We can also notice a strong correlation between variations of the dissociation rate constants and the equilibrium dissociation constants. This clearly indicates that the less successful oligonucleotide modifications influence mainly the resistance of the kissing complex to dissociation. From the thermodynamic point of view it means reduction of the energetic favorability of the complex. On the other hand, the activation energy of the complex formation, which is crucial for the association rate constant, seems to be less influenced in case of modifications forming low stable complexes.

Despite the obvious differences for particular types of modifications we can try to evaluate the overall sensitivity of particular positions on the used modifications. For that we calculated the corresponding values of dissociation equilibrium constants over modifications ON435-ON476 by means of arithmetic and geometric averages (see Figure 45). The modification ON477 was excluded because it did not form the kissing complex for all positions. It means that Figure 45 shows the sensitivities of individual positions in respect to placing of a non-isosteric modification, which lengthen the internucleoside linkage of one covalent bond. It is worth to mention that oligonucleotides are compared according to the same position of the internucleoside linkage and not according to the position of the modified

nucleoside. For instance, for position (b) it means that 2′-deoxyribose is present at G5* and at U6* for anti-TAR oligonucleotides ON440b and ON466b (see Figure 35-Figure 37), respectively.

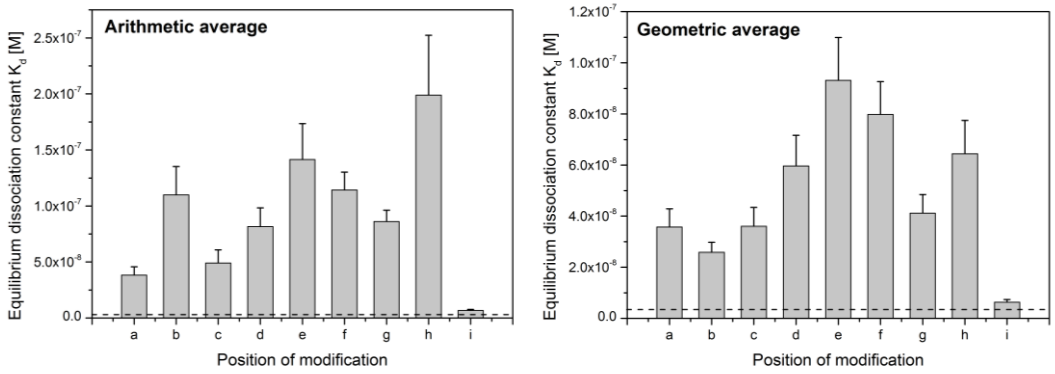

Figure 45. Dissociation equilibrium constants for individual positions averaged through modifications ON435-ON476. Error bars show the standard errors of the averages according to the precisions of particular K_d values. Dashed line presents K_d for natural R06.

We can distinguish three types of positions: i) the central part of apical loop - positions (c)-(g) of linkages between nucleosides forming canonical base-pairs with those in the apical loop of TAR, ii) the side part of apical loop - positions (b) and (h) lying between the nucleoside pairing with the TAR loop and the nucleoside forming the unusual GA base-pair closing the R06 loop, and iii) stem-loop junction -positions (a) and (i).

In the central part, the non-isosteric modifications lead to a significant lowering of the kissing complex stability. This effect is increasing for positions close to the middle one (e), when the average values of K_d are maximal. For this position and its neighbors (d-f) the modifications cause both the lowering of the association rate constant and increasing of the dissociation rate constant in respect to parent R06. It indicates that geometry of this R06 part has to be conserved and any lengthening of an internucleoside linkage results in conformation changes destabilizing the inter-molecular hydrogen bonds. The side positions (c) and (g) possess less destabilization when modified. In case of position (c) it is mainly due to a practically no effect or even increase of the association rate constant (see Figure 41), while in the case of position (g) it is due to only moderate increase of the dissociation rate constant. It is worth to say that for the ON476g modification the stability of the kissing complex is comparable with natural R06.

For the positions (b) and (h) between the nucleosides pairing with the TAR loop and the nucleosides of the unusual GA base-pair, the most characteristic is the high sensitivity of the dissociation rate constant to the type of modification. The dissociation rate constants range from 1.95×10^{-5} s^{-1} for ON476b, which is 1.3 times lower than that for R06 aptamer, to 1.48×10^{-2} s^{-1} for ON438b. High variability of k_d for these positions leads to the high variability of equilibrium constants K_a and K_d with the highest stability for ON476b (K_d = $2.9\pm0.7\times10^{-9}$ M). High sensitivity to a particular type of modification of position (b) is related to the proximity of non-canonical interactions between TAR hairpin and anti-TAR oligonucleotides. According to [87, 89], hydrogen bondings between G5*(H-O2′) on R06 aptamer and either C5 (O2p) or C4 (O3′) on TAR hairpin and between C4 (H-O2′) and either U6* (O1p) or U6* (O2p) may be formed as well as a stacking interaction between G5* and C5. Formation of these stabilizing interactions may also influence the effect of modification in position (c).

Modification at positions in the stem-loop junction causes, in general, no or at least less destabilization of the kissing complex. There is though a significant difference between the two, (a) and (i), positions, when the average stability of complexes formed by aptamers modified at position (i) is several times higher than that for position (a). It seems that this difference may also be caused by the presence of the non-canonical interactions in the close proximity of position (a). Very similar result was obtained by Di Primo et al., who studied LNA/2′-O-methyl chimeric anti-TAR oligonucleotides [92]. The LNA modification at the position on 5′ side of the apical loop possessed lower complex stability than that on 3′ side. The position (i) is in any case suitable for modifications due to its lowest sensitivity to various types of non-isosteric modifications with lengthen internucleoside linkage.

As a starting point for characterization of particular modifications, we calculated mean values of dissociation equilibrium constants as arithmetic and geometric averages through all nine positions for each modification except ON477, which did not allow a measurable complex formation when placed in the central positions (d) – (g). The results shown in Figure 46 indicate that the modifications with lengthened internucleotide linkage may be divided into three groups according to their average destabilizing effect on the kissing complex. The best results (lowest destabilization) were obtained for the modification ON476, i.e. ribonucleoside-5´-O-methylphoshonate. Medium level destabilization exhibit modifications ON435,

ON436, and ON466, i.e. ribonucleoside-3´-O-methylphoshonate, ribonucleoside-2´,3´-O-methylphoshonate, and 2´-deoxyribonucleoside-5´-O-methylphoshonate, respectively. The most destabilizing modifications are ON438 and ON440, i.e. ribonucleoside-2´-O-methylphoshonate and 2´-deoxyribonucleoside-3´-O-methylphoshonate.

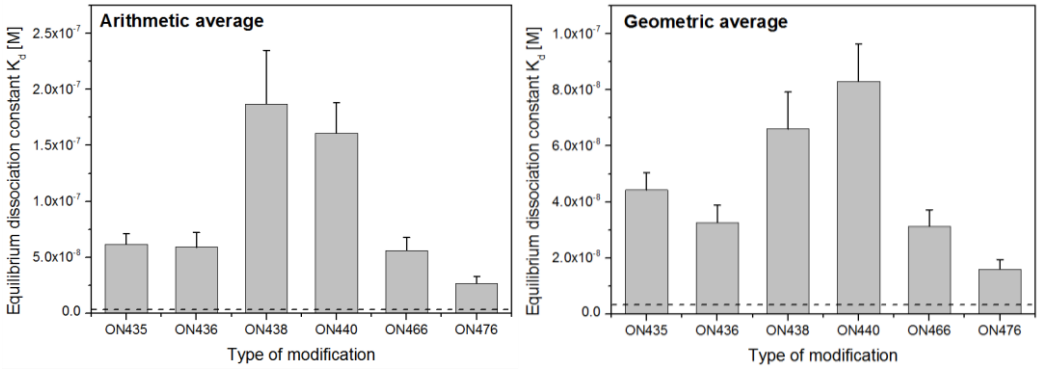

Figure 46. Dissociation equilibrium constants for individual modifications averaged through positions (a)-(i). Error bars show the standard errors of the averages according to the precisions of particular K_d values. Dashed line presents K_d for natural R06.

Our set of modifications enables to analyze in details relations between particular chemical aspects of the modified nucleotides and their effect on the stability of the kissing complex. There are two pairs of modifications that differ only in the nucleoside sugar, ribose or 2´-deoxyribose. The kinetic and equilibrium constants of 3´-O-methylphoshonate modifications, ON435 (ribose) and ON440 (deoxyribose) are compared in Figure 47. It is obvious that the higher destabilizing effect of 2´-deoxyribose → ribose substitution concerns all positions except (a) and (c), where on the opposite the 2´-deoxyribose modification is favorable. This is coherent with the general notion that the central parts of TAR and R06 loops form in the kissing complex A-type duplex, in which sugars are in C3′-endo conformation. As mentioned above, (a) and (c) positions are in the proximity of stabilizing non-canonical interactions, where the optimal sugar puckering may be different. Let us notice that the NMR determined liquid crystal structure of TAR/R06 kissing complex revealed C3′-endo conformation for all R06 and TAR-loop riboses except three riboses in the vicinity of the aptamer GA loop-closing base pair, which adopt a C4′-exo conformation (G5* of R06 aptamer and A11 of TAR) or a C2′-endo conformation (G4*) [87]. Comparison of kinetic constants reveals that in agreement

with the general tendency the destabilization is caused mainly by increase of the dissociation rate constants, which means decreased energetic favorability of the complex. Simultaneously, the association rate constants are somewhat reduced, especially for the positions (e)-(h).

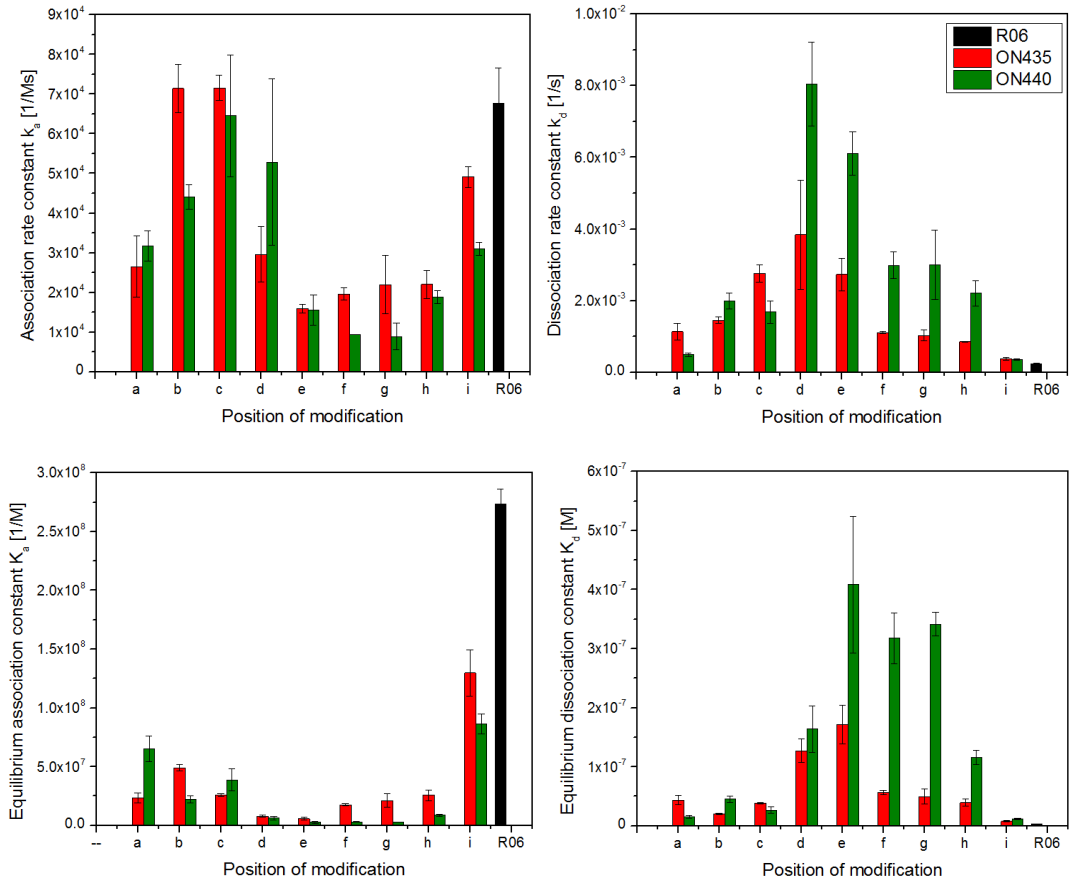

Figure 47. Kinetic and equilibrium constants for modifications ON435, ON440 and natural R06. Error bars present the standard deviations from at least three independent experiments.

Similar comparison is done for 5´-O-methylphoshonate modifications, ON476 (ribose) and ON466 (deoxyribose) in Figure 48. We can notice very similar dependence of the 2´-deoxyribose → ribose substitution on the position. For all positions this substitution increases the dissociation rate constant while the association rate constant is remarkably reduced only for (d) central position while for (c) position it is even increased. As a result, the equilibrium association constant is reduced significantly for the substitution in position (b) or (d)-(h), only small decrease was observed for positions (a) and (c), and no effect is seen for position (i).

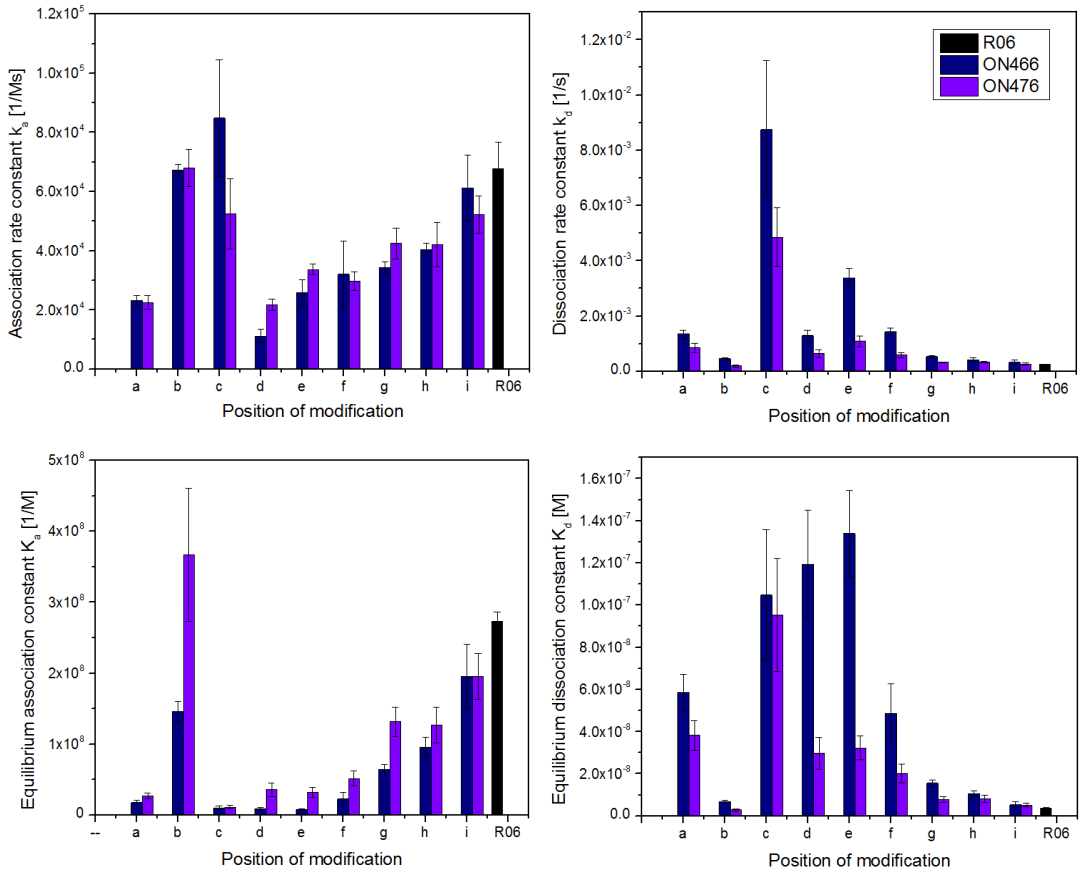

Figure 48. Kinetic and equilibrium constants for modifications ON476, ON466 and natural R06.Error bars present the standard deviations from at least three independent experiments.

It was shown (Figure 46) that 5´-O-methylphoshonate modifications (ON476 and ON466) exhibit in average higher stability than their 3´-O-methylphoshonate regioisomers. It is though worth to analyze in details how the reverse of the methylene group position in respect to phosphorus in the modified linkage effect the kissing complex stability depending on the linkage position. Figure 49 compares the kinetic and equilibrium constants for the two ribose regioisomers, ON476 (5´-O-methylphoshonate) and ON435 (3´-O-methylphoshonate). The effect of both modifications on the stability of the kissing complex is dictated invariably for all positions by affecting the dissociation rate constant, i.e. the energetic favorability of the complex.

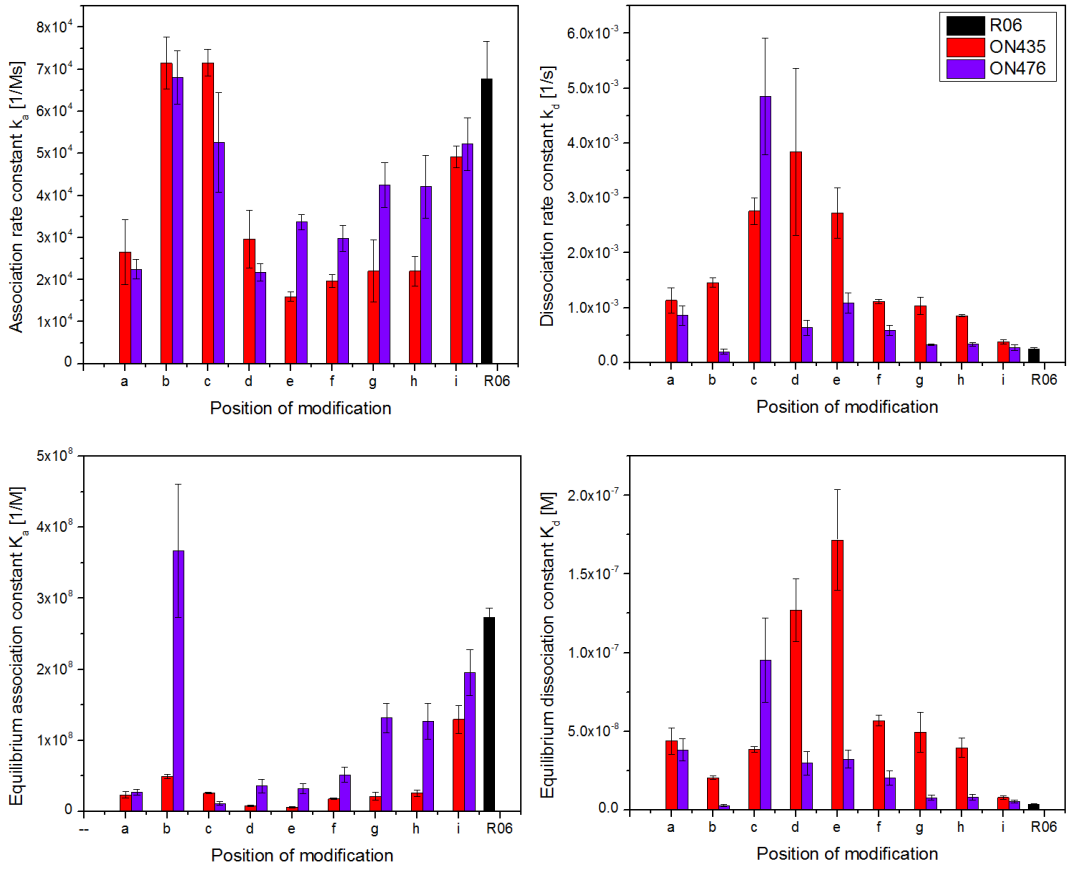

Figure 49. Kinetic and equilibrium constants for modifications ON476, ON435 and natural R06. Error bars present the standard deviations from at least three independent experiments.

5´-O-methylphoshonate modification leads to higher stability of the complex in comparison with the 3´-O-methylphoshonate. On the other hand, while in comparison with the natural RNA/RNA duplex the 5´-O-methylphoshonate modification was found to cause only relatively small decrease of the duplex stability [138], in the case of the kissing complex with TAR the stability is remarkably decreased when the modification is placed to the central part of the loop or to positions (a) or (h). The exceptions are positions (i), which we have found as insensitive to various modifications, and position (b) – the only position where the 5´-O-methylphoshonate modification increase the kissing complex stability. By far the greatest destabilization of the complex causes the 5´-O-methylphoshonate modification at position (c) when its negative effect is significantly stronger than that of the 3´-O-methylphoshonate modification. The contrast of the placements of the 5´-O-methylphoshonate linkage on the 5´ (ON476b) or the 3´ (ON476c) side of U6* nucleotide indicates importance of the proper uracil U6* position for the complex stabilization.

Our set of employed modification enables also to investigate the impact on the way how the methylphoshonate, when directed to the 3´ end, is linked to the ribose of the modified nucleotide. Figure 50 compares the kinetic and equilibrium constants for modifications ON435, ON436, and ON438 that represent 3´-O-methyl-phoshonate, cyclic 2´,3´-O-methylidenephoshonate, and 2´-O-methylphoshonate linkage, respectively. At first glance, it can be seen that on average the bad influence of the 2´-O-methylphoshonate modification on the kissing complex stability is due to the dramatic increase in dissociation rate constants when used in positions between the nucleosides pairing with the TAR loop and the nucleosides of the unusual GA base-pair, i.e. (b) and (h). If these two positions were excluded from our considerations, we could evaluate the influence of the 2´-O-methylphoshonate modification on reduction of the kissing complex stability as comparable with the other two.

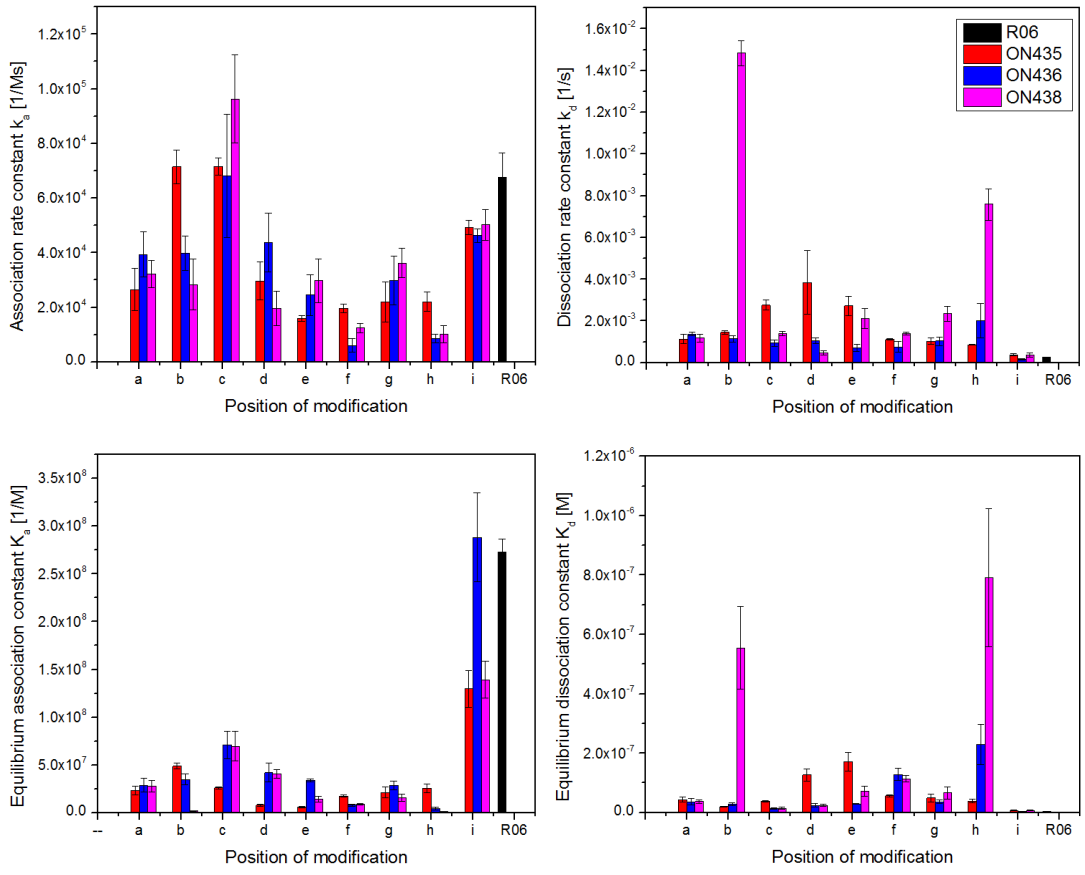

Figure 50. Kinetic and equilibrium constants for modifications ON435, ON436, ON438 and natural R06. Error bars present the standard deviations from at least three independent experiments.

Furthermore, although the cyclic 2´,3´-O-methylidenephoshonate is less flexible than the other two modifications, the modification ON436 is not less successful in terms of stability of the kissing complex. On contrary, in positions (a) and (d) it leads to a higher association rate constant and in positions (b), (c), (e), (f) and (i) to a lower dissociation rate constant than the 3´-O-methylphoshonate or 2´-O-methylphoshonate modifications. Especially for the (i) position of the 2´,3´-O-methylidenephoshonate modification, the kissing complex comparably is stable as that formed by the parent R06.

For positions inside the central part of the loop, the equilibrium constants follow the general tendency when the kissing complex stability decreases with approaching the center of the loop; the minimal stability for the 3´-O-methylphoshonate modification is found at position (e) and that for the other two modifications at position (f). On the other hand, Figure 50 reveals that the effects of modifications on the kinetic constants are more variable. For each position the set of changes of the association and dissociation rate constant caused by these three modifications represents a unique pattern. It indicates that individual nucleosides even inside the central part of the aptamer loop play specific roles in the kissing complex formation and dissociation.

Detailed consequences of the lengthened internucleoside linkage incorporation on particular interactions stabilizing the kissing complex can be revealed by means of MD simulations. They were performed for the parent TAR/R06 complex and the kissing complexes of TAR with oligonucleotides containing the most successful modification ON476 (ribonucleoside-5´-O-methylphoshonate) in positions at the junction of the loop and the closing GA base-pair (b) and (h) and in the central part of the loop, (f). Figure 51-Figure 54 shows the distances of heavy atoms pairs potentially forming important hydrogen bonds visualized within 300-500 ns trajectories. The hydrogen bond is classified as broken when the distance exceeds 2Å.

For the kissing complex of TAR and natural R06 aptamer (Figure 51), MD simulation shows stable hydrogen bonds in canonical base-pairs except infrequent instabilities of the C3*-G14* base-pair in the central part of the R06 stem. Somewhat lower stability is observed for the unusual G5*-A12* pair closing the R06 loop, which is in agreement with the previous study [85]. In contrast to the hydrogen bonds between nucleobases, the hydrogen bonds that are envisaged to provide additional

stabilization of the kissing complex, between G5* ribose of R06 and C5 phosphate of TAR and between U6* phosphate and C4 ribose, seem to be highly unstable.

The MD simulation for the most stable complex (K_d = 2.9±0.7 nM) TAR/ON476b where the 5´-O-methylphoshonate linkage is placed between G5* of the closing pair and U6*, the first nucleoside of the loop (Figure 52), shows not surprisingly effects on hydrogen bonds in the vicinity of the modification. Remarkable stabilizing effect can be seen on the G5*-A12* base-pair together with higher stability of one of hydrogen bonds between G5* ribose and C5 phosphate while the stability of the second hydrogen bond is lowered. Also the hydrogen bonds in the base pair U6*-A10 between R06 and TAR loops is partly destabilized. Simultaneously the modification practically breaks the hydrogen bonds between U6* phosphate and C4 ribose, indicating that these bonds are not important for the kissing complex stability. Very interesting effect is the noticeably decreased stability of the C4-G11 base-pair that closes the TAR loop, which is caused by a tension transferred from the modified R06 loop by the loop-loop interactions. This demonstrates that the kissing complex is not a weakly bound cluster of two rather autonomous loop-stem hairpin structures, but a 3D structure where the intermolecular and intramolecular interactions are of a comparable importance and strength.

Figure 54 shows MD simulation results for complex TAR/ON476h, where the 5´-O-methylphoshonate linkage is placed at the junction between the loop and the closing GA base-pair at 3′-end of the aptamer loop - between nucleosides G11* and A12*. The modification slightly decreases stability of hydrogen bonds connecting nucleosides of R06 loop located near the modification with nucleosides in the loop of TAR, A10*-U6, and slightly also G11*-C5, but the main effect is destabilization of the unusual GA base-pair closing the loop. On the other hand, as a result of the modification the central hydrogen bonds between TAR and R06 loops , i.e. C9*-G7, C8*-G8, and C7*-G9, became more stable.

Figure 53 shows MD simulation results for TAR/ON476f complex with the 5´-O-methylphoshonate linkage in the loop between nucleosides C9* and A10*. The modification decreases the stability of the hydrogen bonds connecting nucleosides of R06 loop located near the modification with nucleosides in the loop of TAR, A10*-U6, C9*-G7, and slightly also G11*-C5. Surprisingly the hydrogen bonds at the opposite side of the loop are also affected; the destabilization is obvious for U6*-A10 connection and hydrogen bond between phosphate of U6* and ribose of C4.

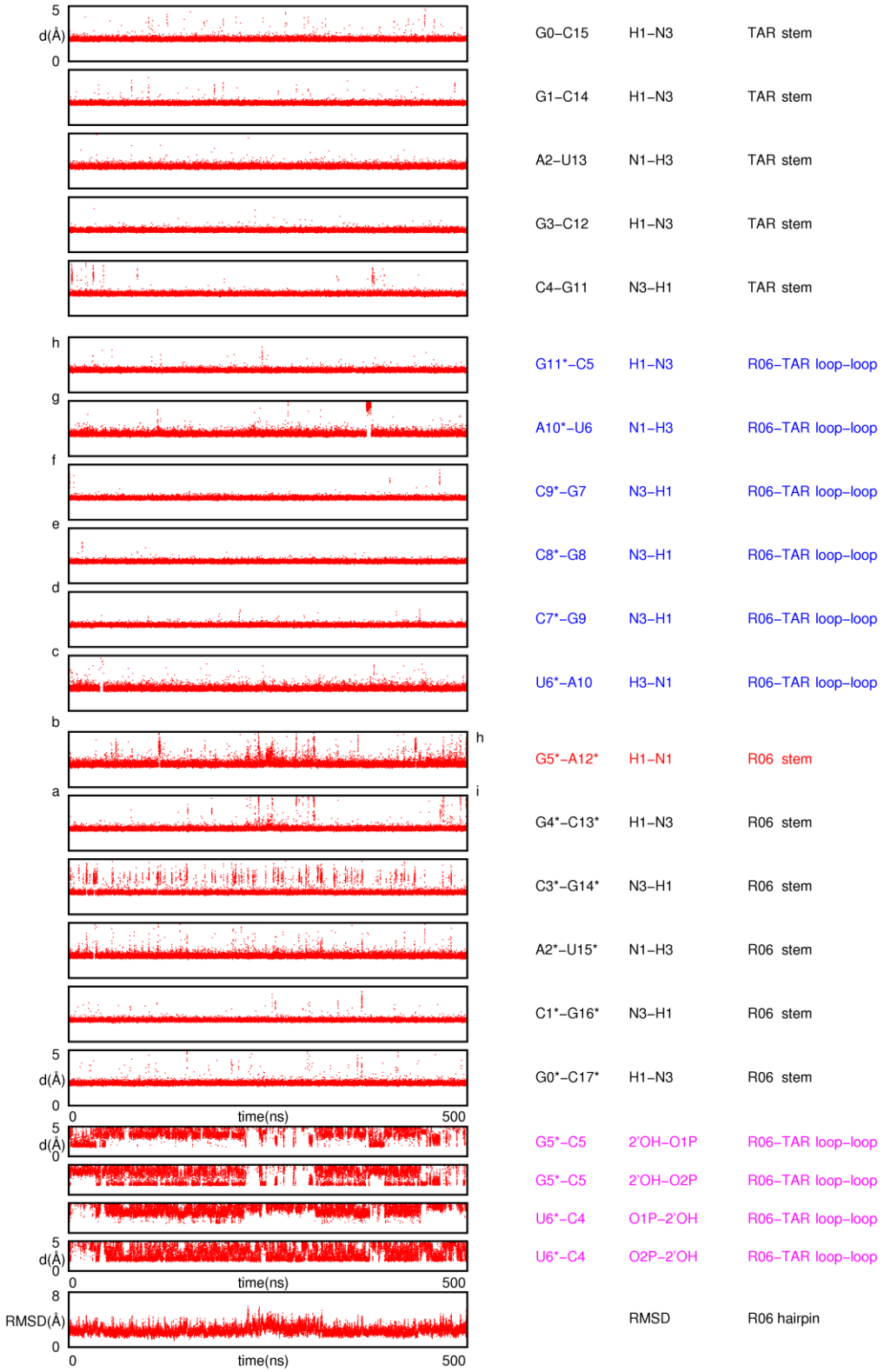

Figure 51. Results of molecular dynamic simulations for TAR and R06 aptamer. Distances of the hydrogens forming important hydrogen bonds from the hydrogen bond acceptors within 500 ns MD simulation run.

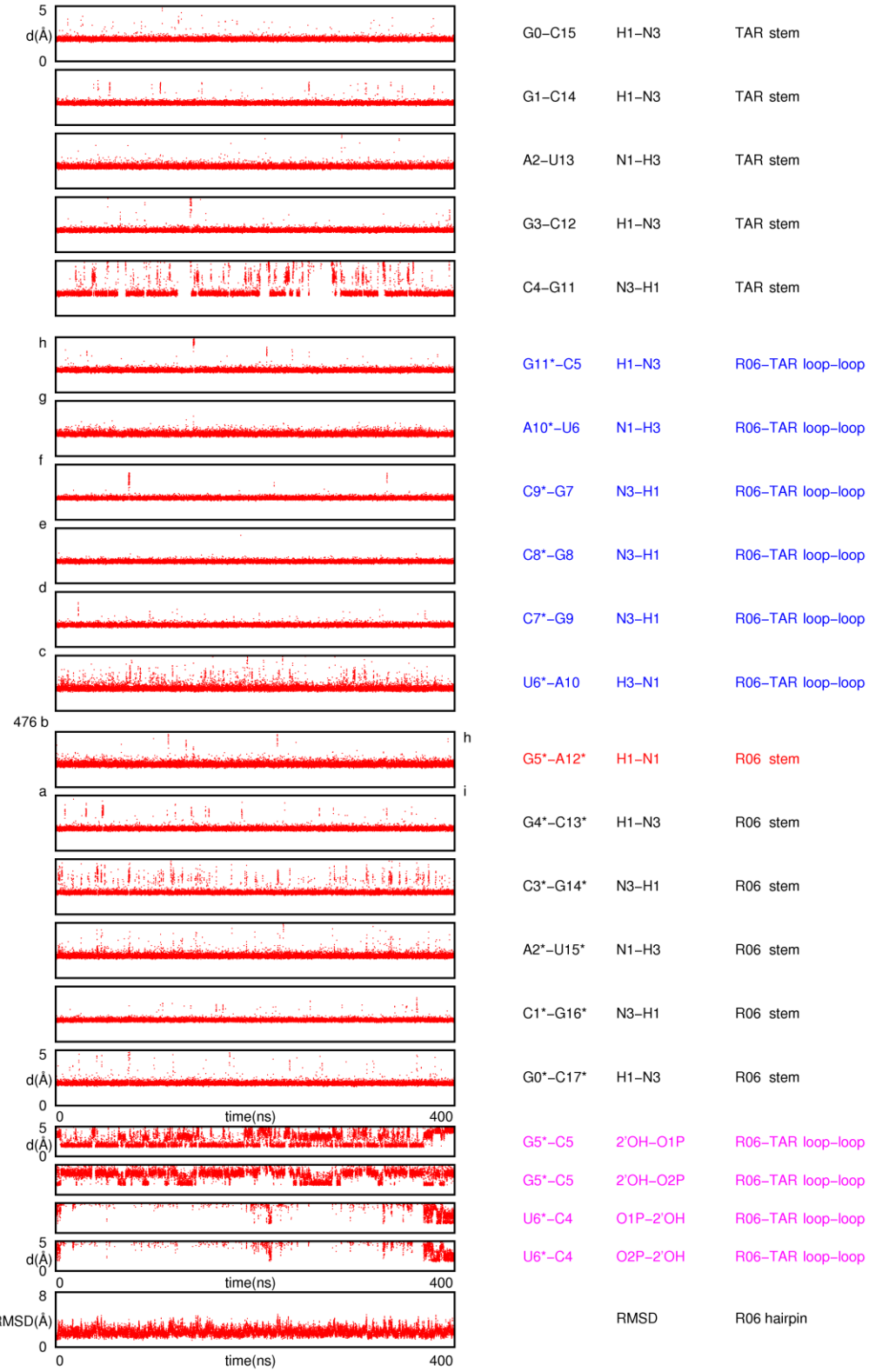

Figure 52. Results of molecular dynamic simulations for TAR and 476b. Distances of the hydrogens forming important hydrogen bonds from the hydrogen bond acceptors within 400 ns MD simulation run.

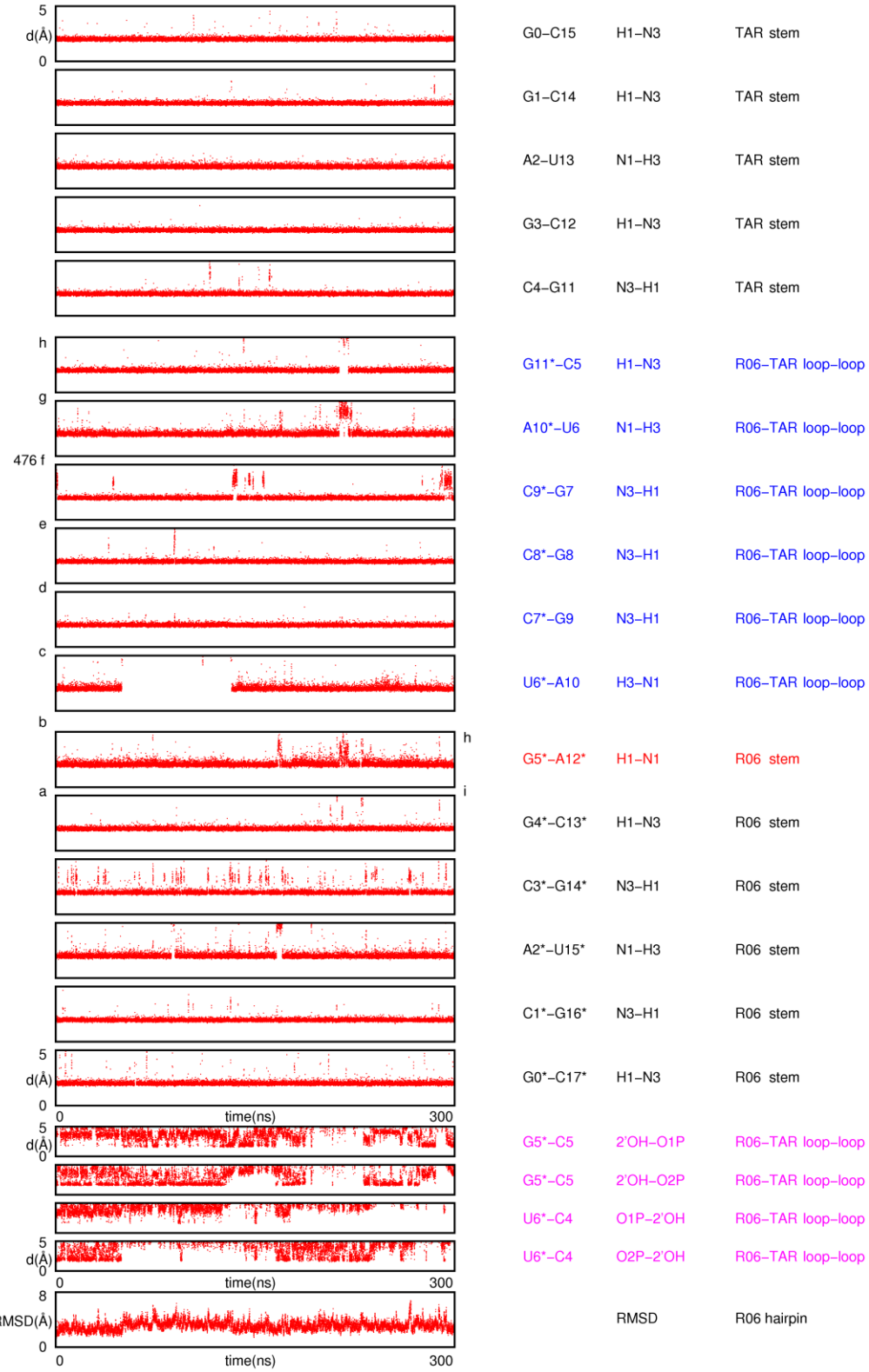

Figure 53 Results of molecular dynamic simulations for TAR and 476f aptamer. Distances of the hydrogens forming important hydrogen bonds from the hydrogen bond acceptors within 300 ns MD simulation run.

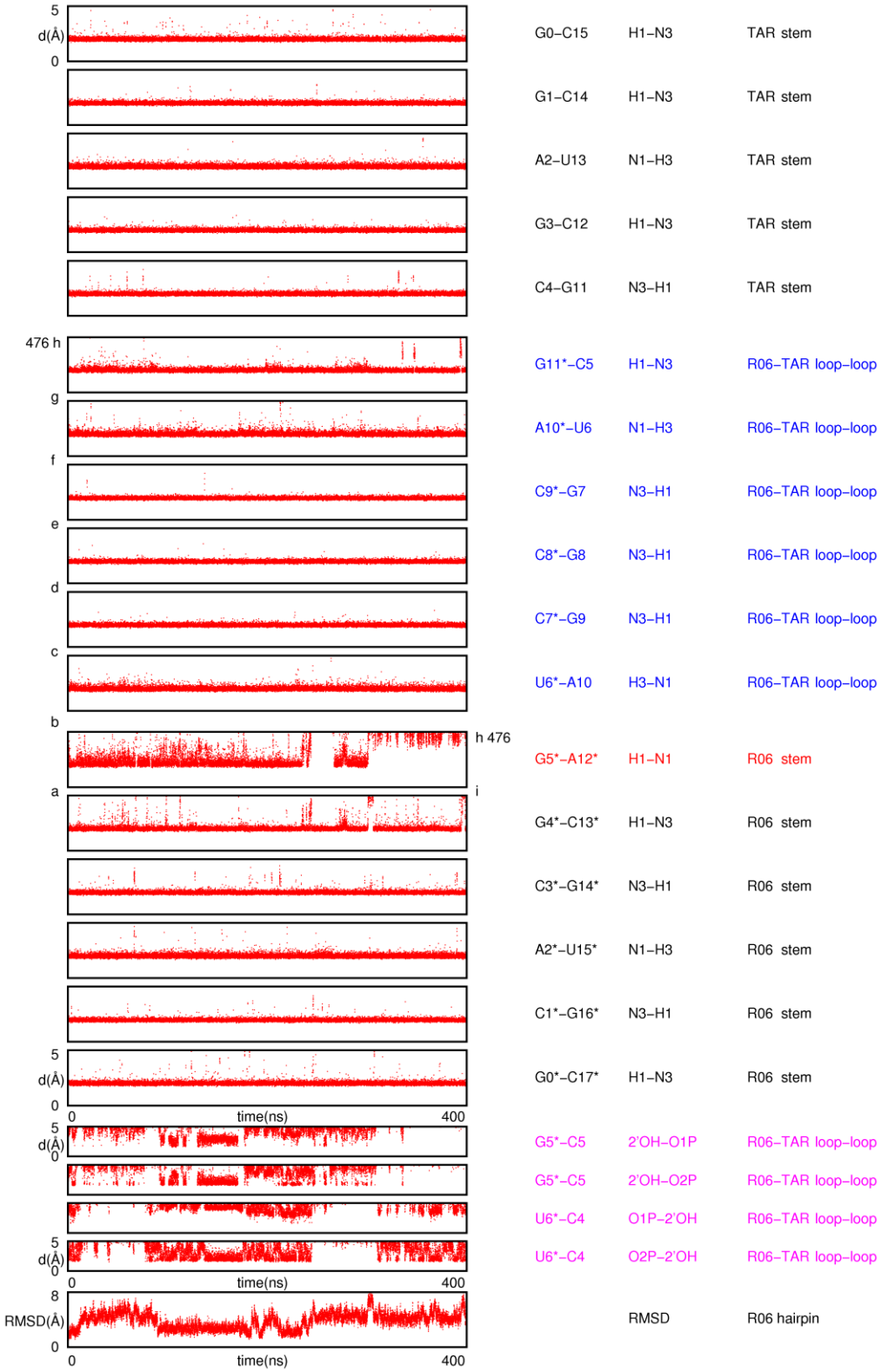

Figure 54 Results of molecular dynamic simulations for TAR and 476h aptamer. Distances of the hydrogens forming important hydrogen bonds from the hydrogen bond acceptors within 400 ns MD simulation run.

4.3.3 Conclusions - Potential new therapeutics targeting TAR hairpin in HIV virus RNA

Our study revealed that the effect of the internucleotide linkage modification in analogue of R06 aptamer is highly site specific. In fact we did not find any two positions between all linkages within the loop, the closing GA basepair, and its junctions to the stem, which would possess the same sensitivity of the TAR/anti-TAR kissing complex formation to various modifications.

We found out by far the greatest tolerance to the modification for the junction between the adenosine in the GA basepair and the stem (position (i)). All lengthened linkages with ribose and 5´-O-methylphoshonate also with deoxyribose placed at that position caused only low destabilization of the complex. On the other hand, any tested modification placed to the analogous junction at the 5´ end of the loop, i.e. the position (a) between the stem and guanosine from the GA basepair, caused significant drop of the complex stability. This linkage was also the only one, when the shortened 2´-deoxyribose-5´-hydroxyphoshonate linkage (ON477) was relatively more suitable than the lengthened modifications, except for the 2´-deoxyribose-5´-O-methylphoshonate linkage (ON440).

The linkages in the central part of the loop (positions (d), (e), and (f)) were also found as very sensitive to the modification. For these positions, the best among the tested modifications was the ribose-5´-O-methylphoshonate linkage (ON476), which is known to reduce only little stability of RNA/RNA duplex. Nevertheless, when placed in the central part of the loop, it destabilizes the kissing complex remarkably causing temporary breaking of intermolecular hydrogen bridges (as was revealed by MD simulations).

Very specific response to various kinds of modifications was found for the junctions between the loop and nucleosides in the GA basepair (positions (b) and (h)) and also the neighboring linkages toward the loop (positions (c) and (g)). In particular, in positions (b) and (h) the most successful were the 5´-O-methylphoshonate linkages, both ribose- and deoxyribose-, but the ribose being better. The ribose-5´-O-methylphoshonate linkage in position (b) was the only case when the complex stability was increased. On the other hand, positions (b) and (h) were the only ones where failed the ribose-2´-O-methylphoshonate linkage (ON438), which caused even much greater destabilization of the complex than the shortened

linkage (ON477) placed at these positions. For position (g) the 5´-O-methylphoshonate linkages were also the most suitable, while for position (c) at the opposite site of the loop the 5´-O-methylphoshonate linkages caused the largest destabilization among the lengthened linkages. On the opposite, the ribose-2´,3´-O-methylidenephoshonate (ON436) and ribose-2´-O-methylphoshonate (ON438) linkages caused the relatively lowest complex destabilization. According MD simulations, the specificity of the abovementioned positions does not seem to be dominantly given by possible additional non-canonical interactions stabilizing the complex structure, but more probably due to the fact that they influence hydrogen bondings stabilizing both the kissing complex and the GA basepair of R06.

Our results have revealed a possible way how to design a promising anti-TAR oligonucleotide: It should be a chimeric nucleotide with ribose-5´-O-methylphoshonate modifications (besides the stem) in positions (b), (g), (h) and (i). In case that the unmodified RNA sequence of the loop would not exhibit the sufficient stability against nucleases, it would be necessary to search for other, preferably isosteric, modification suitable for the central part of the loop.

5 Conclusions

This doctoral thesis was focused on the investigation of interactions involving nucleic acids with potential benefits for the development of novel therapeutic agents. SPR spectroscopy was chosen as the main tool in this research as it allows for sensitive, real-time, and label-free monitoring of molecular interactions. A substantial part of this thesis was devoted to both the improvement of the SPR biosensor instrumentation as well as the characterization of nucleic acid interactions on DNA/RNA chips. The main results of this doctoral thesis were divided into three parts.

In the first part of the doctoral thesis, a new dispersionless microfluidics was developed. This microfluidic system enabled the observation of molecular interactions occurring at a SPR chip surface without any interfering effects, such as sample dispersion and inter-sample mixing. We also demonstrated that this approach provides more robust biosensor data, and thus improves the accuracy of the analysis of interaction kinetics. The design and pilot application of the dispersionless microfluidic system resulted in two publications in scientific journals [115, 116] (Appendix II and III).

In the second part of the doctoral thesis, attention was focused on the study of nucleic acid interactions, specifically duplex and triplex formation as well as probe immobilization on the surface of an SPR chip. It was demonstrated that the cationic shielding of repulsion concerning negatively charged oligonucleotides is crucial for oligonucleotide interactions at the surface of a DNA chip, which typically contains high densities of oligonucleotide probes ($\sim 5 \times 10^{12}$ molecules/cm^2). We demonstrated a pronounced role of divalent magnesium in comparison with monovalent sodium in the shielding of oligonucleotide negative charges. In addition, this effect was found to be specific for interactions of oligonucleotides under spatially restricted conditions on the surface of a DNA chip, which differs from the conditions in a solution. We proposed an explanation of this phenomenon based on an assumption of surface restricted conditions. A detailed account of this study can be found in [123] (Appendix IV).

The third part of the doctoral thesis presents results of a comprehensive study of 63 novel chemically modified analogues based on R06 aptamer that target the TAR

hairpin of HIV virus. These modifications were assessed with respect to their potential for the construction of effective anti-TAR oligonucleotides. It was found that anti-TAR oligonucleotides that contained ribose exhibited higher stability than those with deoxyribose. Anti-TAR oligonucleotides with 5´-O-methylphosphonate modifications were observed to exhibit higher stability than those with 3´-O-methylphosphonate modifications, suggesting that the promising tested oligonucleotide was ribose-5´-O-methylphosphonate. We also found ten anti-TAR oligonucleotides that exhibited reasonable stabilities (K_d was lower than 11 nM, i.e. stability was three times lower than that of the parent RNA R06 aptamer), and one of them (ON476b with ribose-5´-O-methylphoshonate linkage in position (b)) was even more stable than the parent R06 aptamer. Furthermore, the study revealed a high sensitivity of individual positions in the R06 aptamer to substitutions with modifications. The position (i) exhibited great tolerance for any modifications, and positions (b), (g) and (h) were suitable for both ribose- and deoxyribose-5´-O-methylphoshonate modifications. In contrast, the central positions (d), (e), (f) were found not to be suitable for any modifications, as they destabilized the intermolecular hydrogen bonds. We also discussed in detail the results in the context of local nucleotide geometries and interactions of the TAR/anti-TAR complex. We found that the specificity of the abovementioned positions is not determined by additional non-canonical interactions stabilizing the complex structure, but probably rather by the fact that they influence hydrogen bondings stabilizing both the complex and the GA basepair of R06. In summary, this study suggests that promising anti-TAR oligonucleotides should contain ribose-5´-O-methylphoshonate modifications (besides the stem) in positions (b), (g), (h) and (i).

6 Bibliography

1. Zubay, G.L., W.W. Parson, and D.E. Vance, *Principles of Biochemistry*, ed. E.M. Sievers. 1995: Wm. C. Brown Publishers.
2. Watson, J.D. and F.H.C. Crick, *Molecular Structure of Nucleic Acids - a Structure for Deoxyribose Nucleic Acid.* Nature, 1953. **171**(4356): p. 737-738.
3. Rajagopal, P. and J. Feigon, *Triple-strand formation in the homopurine:homopyrimidine DNA oligonucleotides d(G-A)4 and d(T-C)4.* Nature, 1989. **339**(6226): p. 637-40.
4. Praseuth, D., A.L. Guieysse, and C. Helene, *Triple helix formation and the antigene strategy for sequence-specific control of gene expression.* Biochim Biophys Acta, 1999. **1489**(1): p. 181-206.
5. Sugimoto, N., et al., *pH and cation effects on the properties of parallel pyrimidine motif DNA triplexes.* Biochemistry, 2001. **40**(31): p. 9396-9405.
6. Huppert, J.L. and S. Balasubramanian, *Prevalence of quadruplexes in the human genome.* Nucleic Acids Research, 2005. **33**(9): p. 2908-2916.
7. Burge, S., et al., *Quadruplex DNA: sequence, topology and structure.* Nucleic Acids Research, 2006. **34**(19): p. 5402-5415.
8. Crick, F.H.C., *Codon-Anticodon Pairing - Wobble Hypothesis.* Journal of Molecular Biology, 1966. **19**(2): p. 548-&.
9. SantaLucia, J., *A unified view of polymer, dumbbell, and oligonucleotide DNA nearest-neighbor thermodynamics.* Proceedings of the National Academy of Sciences of the United States of America, 1998. **95**(4): p. 1460-1465.
10. Owczarzy, R., et al., *Predicting stability of DNA duplexes in solutions containing magnesium and monovalent cations.* Biochemistry, 2008. **47**(19): p. 5336-5353.
11. SantaLucia, J., H.T. Allawi, and A. Seneviratne, *Improved nearest-neighbor parameters for predicting DNA duplex stability.* Biochemistry, 1996. **35**(11): p. 3555-3562.
12. Sassolas, A., B.D. Leca-Bouvier, and L.J. Blum, *DNA biosensors and microarrays.* Chemical Reviews, 2008. **108**(1): p. 109-39.
13. Wang, J., *From DNA biosensors to gene chips.* Nucleic Acids Research, 2000. **28**(16): p. 3011-6.
14. Pozhitkov, A.E., D. Tautz, and P.A. Noble, *Oligonucleotide microarrays: widely applied--poorly understood.* Brief Funct Genomic Proteomic, 2007. **6**(2): p. 141-8.
15. Ji, W., et al., *A method for cross-species gene expression analysis with high-density oligonucleotide arrays.* Nucleic Acids Research, 2004. **32**(11): p. e93.
16. Uhlmann, E. and A. Peyman, *Antisense oligonucleotides: a new therapeutic principle.* Chemical Reviews, 1990. **90**(4): p. 543–584.
17. Dias, N. and C.A. Stein, *Antisense oligonucleotides: basic concepts and mechanisms.* Mol Cancer Ther, 2002. **1**(5): p. 347-55.
18. Held, D.M., et al., *HIV-1 inactivation by nucleic acid aptamers.* Frontiers in Bioscience, 2006. **11**: p. 89-112.

19. Nakano, S., et al., *Nucleic acid duplex stability: influence of base composition on cation effects.* Nucleic Acids Research, 1999. **27**(14): p. 2957-2965.
20. Levicky, R. and A. Horgan, *Physicochemical perspectives on DNA microarray and biosensor technologies.* Trends in Biotechnology, 2005. **23**(3): p. 143-149.
21. Zhang, L., et al., *Free energy of DNA duplex formation on short oligonucleotide microarrays.* Nucleic Acids Research, 2007. **35**(3).
22. Korolev, N., A.P. Lyubartsev, and L. Nordenskiold, *Application of polyelectrolyte theories for analysis of DNA melting in the presence of Na+ and Mg2+ ions.* Biophysical Journal, 1998. **75**(6): p. 3041-3056.
23. Record, M.T., *Effects of Na+ and Mg++ Ions on Helix-Coil Transition of DNA.* Biopolymers, 1975. **14**(10): p. 2137-2158.
24. Tan, Z.J. and S.J. Chen, *RNA helix stability in mixed Na+/Mg2+ solution.* Biophysical Journal, 2007: p. 227A-227A.
25. Wilson, R.W., D.C. Rau, and V.A. Bloomfield, *Comparison of Poly-Electrolyte Theories of the Binding of Cations to DNA.* Biophysical Journal, 1980. **30**(2): p. 317-325.
26. Manning, G.S., *Molecular Theory of Polyelectrolyte Solutions with Applications to Electrostatic Properties of Polynucleotides.* Quarterly Reviews of Biophysics, 1978. **11**(2): p. 179-246.
27. Tan, Z.J. and S.J. Chen, *Nucleic acid helix stability: Effects of salt concentration, cation valence and size, and chain length.* Biophysical Journal, 2006. **90**(4): p. 1175-1190.
28. Tan, Z.J. and S.J. Chen, *Electrostatic correlations and fluctuations for ion binding to a finite length polyelectrolyte.* Journal of Chemical Physics, 2005. **122**(4).
29. Piliarik, M., L. Parova, and J. Homola, *High-throughput SPR sensor for food safety.* Biosensors & Bioelectronics, 2009. **24**(5): p. 1399-1404.
30. Yu, F., D.F. Yao, and W. Knoll, *Oligonucleotide hybridization studied by a surface plasmon diffraction sensor (SPDS).* Nucleic Acids Research, 2004. **32**(9).
31. Okahata, Y., et al., *Kinetic measurements of DNA hybridisation an an oligonucleotide-immobilized 27-MHz quartz crystal microbalance.* Analytical Chemistry, 1998. **70**(7): p. 1288-1296.
32. Peterson, A.W., R.J. Heaton, and R.M. Georgiadis, *The effect of surface probe density on DNA hybridization.* Nucleic Acids Research, 2001. **29**(24): p. 5163-5168.
33. Cho, Y.K., et al., *Characterization of DNA immobilization and subsequent hybridization using in situ quartz crystal microbalance, fluorescence spectroscopy, and surface plasmon resonance.* Journal of Colloid and Interface Science, 2004. **278**(1): p. 44-52.
34. Vainrub, A. and B.M. Pettitt, *Coulomb blockage of hybridization in two-dimensional DNA arrays.* Physical Review E, 2002. **66**(4).
35. Halperin, A., A. Buhot, and E.B. Zhulina, *Sensitivity, specificity, and the hybridization isotherms of DNA chips.* Biophysical Journal, 2004. **86**(2): p. 718-730.
36. Aboul-Fadl, T., *Antisense oligonucleotides: The state of the art.* Current Medicinal Chemistry, 2005. **12**(19): p. 2193-2214.

37. Kurreck, J., *Antisense technologies - Improvement through novel chemical modifications.* European Journal of Biochemistry, 2003. **270**(8): p. 1628-1644.
38. Mansoor, M. and A.J. Melendez, *Advances in antisense oligonucleotide development for target identification, validation, and as novel therapeutics.* Gene Regulation and Systems Biology, 2008: p. 275-295.
39. Crooke, S.T., *Molecular mechanisms of action of antisense drugs.* Biochimica Et Biophysica Acta-Gene Structure and Expression, 1999. **1489**(1): p. 31-44.
40. Wu, H.J., et al., *Determination of the role of the human RNase H1 in the pharmacology of DNA-like antisense drugs.* Journal of Biological Chemistry, 2004. **279**(17): p. 17181-17189.
41. Saison-Behmoaras, T.E., et al., *Antisense PNA tridecamers targeted to the coding region of Ha-ras mRNA arrest polypeptide chain elongation.* Journal of Molecular Biology, 1999. **294**(2): p. 403-416.
42. Paterson, B.M., B.E. Roberts, and E.L. Kuff, *Structural Gene Identification and Mapping by DNA-Messenger-Rna Hybrid-Arrested Cell-Free Translation.* Proceedings of the National Academy of Sciences of the United States of America, 1977. **74**(10): p. 4370-4374.
43. Zamecnik, P.C. and M.L. Stephenson, *Inhibition of Rous-Sarcoma Virus-Replication and Cell Transformation by a Specific Oligodeoxynucleotide.* Proceedings of the National Academy of Sciences of the United States of America, 1978. **75**(1): p. 280-284.
44. Brody, E.N. and L. Gold, *Aptamers as therapeutic and diagnostic agents.* Reviews in Molecular Biotechnology, 2000. **74**(1): p. 5-13.
45. Lee, J.F., G.M. Stovall, and A.D. Ellington, *Aptamer therapeutics advance.* Current Opinion in Chemical Biology, 2006. **10**(3): p. 282-289.
46. Nimjee, S.M., C.P. Rusconi, and B.A. Sullenger, *Aptamers: an emerging class of therapeutics.* Annu Rev Med, 2005. **56**: p. 555-83.
47. Gold, L., et al., *Diversity of Oligonucleotide Functions.* Annual Review of Biochemistry, 1995. **64**: p. 763-797.
48. Osborne, S.E. and A.D. Ellington, *Nucleic acid selection and the challenge of combinatorial chemistry.* Chemical Reviews, 1997. **97**(2): p. 349-370.
49. Tuerk, C. and L. Gold, *Systematic Evolution of Ligands by Exponential Enrichment - Rna Ligands to Bacteriophage-T4 DNA-Polymerase.* Science, 1990. **249**(4968): p. 505-510.
50. Jellinek, D., et al., *Potent 2'-Amino-2'-Deoxypyrimidine Rna Inhibitors of Basic Fibroblast Growth-Factor.* Biochemistry, 1995. **34**(36): p. 11363-11372.
51. Gewirtz, A.M., C.A. Stein, and P.M. Glazer, *Facilitating oligonucleotide delivery: Helping antisense deliver on its promise - Commentary.* Proceedings of the National Academy of Sciences of the United States of America, 1996. **93**(8): p. 3161-3163.
52. Matteucci, M.D. and R.W. Wagner, *In pursuit of antisense.* Nature, 1996. **384**(6604): p. 20-22.
53. Agrawal, S., et al., *Mixed-backbone oligonucleotides as second generation antisense oligonucleotides: In vitro and in vivo studies.* Proceedings of the National Academy of Sciences of the United States of America, 1997. **94**(6): p. 2620-2625.

54. Chen, X.L., et al., *Chemical modification of gene silencing oligonucleotides for drug discovery and development.* Drug Discovery Today, 2005. **10**(8): p. 587-593.
55. Agrawal, S., *Importance of nucleotide sequence and chemical modifications of antisense oligonucleotides.* Biochimica Et Biophysica Acta-Gene Structure and Expression, 1999. **1489**(1): p. 53-68.
56. Wu, H.J., W.F. Lima, and S.T. Crooke, *Properties of cloned and expressed human RNase H1*. Journal of Biological Chemistry, 1999. **274**(40): p. 28270-28278.
57. Weiss, R.A., *How Does Hiv Cause Aids.* Science, 1993. **260**(5112): p. 1273-1279.
58. Sierra, S., B. Kupfer, and R. Kaiser, *Basics of the virology of HIV-1 and its replication.* Journal of Clinical Virology, 2005. **34**(4): p. 233-244.
59. Frankel, A.D. and J.A.T. Young, *HIV-1: Fifteen proteins and an RNA.* Annual Review of Biochemistry, 1998. **67**: p. 1-25.
60. *Overview: UNAIDS Report on the Global AIDS Epidemic*, 2012, Joint United Nations Programme on HIV/AIDS.
61. Rambaut, A., et al., *The causes and consequences of HIV evolution.* Nature Reviews Genetics, 2004. **5**(1): p. 52-61.
62. Kwong, P.D., et al., *Structure of an HIV gp120 envelope glycoprotein in complex with the CD4 receptor and a neutralizing human antibody.* Nature, 1998. **393**(6686): p. 648-59.
63. Pollard, V.W. and M.H. Malim, *The HIV-1 Rev protein.* Annu Rev Microbiol, 1998. **52**: p. 491-532.
64. Chan, D.C. and P.S. Kim, *HIV entry and its inhibition.* Cell, 1998. **93**(5): p. 681-684.
65. Adamson, C.S. and E.O. Freed, *Novel approaches to inhibiting HIV-1 replication.* Antiviral Research, 2010. **85**(1): p. 119-141.
66. Wyatt, R. and J. Sodroski, *The HIV-1 envelope glycoproteins: Fusogens, antigens, and immunogens.* Science, 1998. **280**(5371): p. 1884-1888.
67. Dorman, N. and A.M. Lever, *RNA-based gene therapy for HIV infection.* HIV Med, 2001. **2**(2): p. 114-22.
68. Sullenger, B.A. and E. Gilboa, *Emerging clinical applications of RNA.* Nature, 2002. **418**(6894): p. 252-8.
69. Joshi, P.J., T.S. Fisher, and V.R. Prasad, *Anti-HIV inhibitors based on nucleic acids: emergence of aptamers as potent antivirals.* Curr Drug Targets Infect Disord, 2003. **3**(4): p. 383-400.
70. Nielsen, M.H., F.S. Pedersen, and J. Kjems, *Molecular strategies to inhibit HIV-1 replication.* Retrovirology, 2005. **2**: p. 10.
71. Rana, T.M. and K.T. Jeang, *Biochemical and functional interactions between HIV-1 Tat protein and TAR RNA.* Arch Biochem Biophys, 1999. **365**(2): p. 175-85.
72. Gait, M.J. and J. Karn, *RNA recognition by the human immunodeficiency virus Tat and Rev proteins.* Trends Biochem Sci, 1993. **18**(7): p. 255-9.
73. Berkhout, B., R.H. Silverman, and K.T. Jeang, *Tat trans-activates the human immunodeficiency virus through a nascent RNA target.* Cell, 1989. **59**(2): p. 273-82.
74. Greene, W.C. and B.M. Peterlin, *Charting HIV's remarkable voyage through the cell: Basic science as a passport to future therapy.* Nat Med, 2002. **8**(7): p. 673-80.

75. Churcher, M.J., et al., *High affinity binding of TAR RNA by the human immunodeficiency virus type-1 tat protein requires base-pairs in the RNA stem and amino acid residues flanking the basic region.* Journal of Molecular Biology, 1993. **230**(1): p. 90-110.
76. Richter, S., Y.H. Ping, and T.M. Rana, *TAR RNA loop: a scaffold for the assembly of a regulatory switch in HIV replication.* Proc Natl Acad Sci U S A, 2002. **99**(12): p. 7928-33.
77. Edwards, T.E., B.H. Robinson, and S.T. Sigurdsson, *Identification of amino acids that promote specific and rigid TAR RNA-tat protein complex formation.* Chem Biol, 2005. **12**(3): p. 329-37.
78. Kulinski, T., et al., *The apical loop of the HIV-1 TAR RNA hairpin is stabilized by a cross-loop base pair.* J Biol Chem, 2003. **278**(40): p. 38892-901.
79. Yamamoto, R., et al., *A novel RNA motif that binds efficiently and specifically to the Tat protein of HIV and inhibits the trans-activation by Tat of transcription in vitro and in vivo.* Genes to Cells, 2000. **5**(5): p. 371-388.
80. Toulme, J.J., et al., *Modulating viral gene expression by aptamers to RNA structures.* Biol Cell, 2003. **95**(3-4): p. 229-38.
81. Duconge, F. and J.J. Toulme, *In vitro selection identifies key determinants for loop-loop interactions: RNA aptamers selective for the TAR RNA element of HIV-1.* Rna-a Publication of the Rna Society, 1999. **5**(12): p. 1605-1614.
82. Darfeuille, F., et al., *Driving in vitro selection of anti-HIV-1 TAR aptamers by magnesium concentration and temperature.* Combinatorial Chemistry & High Throughput Screening, 2002. **5**(4): p. 313-325.
83. Boiziau, C., et al., *DNA aptamers selected against the HIV-1 trans-activation-responsive RNA element form RNA-DNA kissing complexes.* Journal of Biological Chemistry, 1999. **274**(18): p. 12730-12737.
84. Darfeuille, F., et al., *LNA/DNA chimeric oligomers mimic RNA aptamers targeted to the TAR RNA element of HIV-1.* Nucleic Acids Research, 2004. **32**(10): p. 3101-3107.
85. Duconge, F., C. Di Primo, and J.J. Toulme, *Is a closing "GA pair" a rule for stable loop-loop RNA complexes?* Journal of Biological Chemistry, 2000. **275**(28): p. 21287-21294.
86. Beaurain, F., et al., *Molecular dynamics reveals the stabilizing role of loop closing residues in kissing interactions: comparison between TAR-TAR* and TAR-aptamer.* Nucleic Acids Research, 2003. **31**(14): p. 4275-4284.
87. Van Melckebeke, H., et al., *Liquid-crystal NMR structure of HIV TAR RNA bound to its SELEX RNA aptamer reveals the origins of the high stability of the complex.* Proceedings of the National Academy of Sciences of the United States of America, 2008. **105**(27): p. 9210-9215.
88. Lebars, I., et al., *NMR structure of a kissing complex formed between the TAR RNA element of HIV-1 and a LNA-modified aptamer.* Nucleic Acids Research, 2007. **35**(18): p. 6103-6114.
89. Lebars, I., et al., *Exploring TAR-RNA aptamer loop-loop interaction by X-ray crystallography, UV spectroscopy and surface plasmon resonance.* Nucleic Acids Research, 2008. **36**(22): p. 7146-7156.
90. Darfeuille, F., et al., *2 '-O-Methyl-RNA hairpins generate loop-loop complexes and selectively inhibit HIV-1 Tat-mediated transcription.* Biochemistry, 2002. **41**(40): p. 12186-12192.

91. Lebars, I., et al., *LNA derivatives of a kissing aptamer targeted to the trans-activating responsive RNA element of HIV-1*. Blood Cells Molecules and Diseases, 2007. **38**(3): p. 204-209.
92. Di Primo, C., et al., *Systematic screening of LNA/2 '-O-methyl chimeric derivatives of a TAR RNA aptamer*. Febs Letters, 2007. **581**(4): p. 771-774.
93. Darfeuille, F., et al., *Loop-loop interaction of HIV-1 TAR RNA with N3 '-> P5 ' deoxyphosphoramidate aptamers inhibits in vitro Tat-mediated transcription.* Proceedings of the National Academy of Sciences of the United States of America, 2002. **99**(15): p. 9709-9714.
94. Homola, J., *Surface Plasmon Resonance Based Sensors*. Springer Series on Chemical Sensors and Biosensors, ed. O.S. Wolfbeis. Vol. 4. 2006.
95. Homola, J., *Surface plasmon resonance sensors for detection of chemical and biological species.* Chemical Reviews, 2008. **108**(2): p. 462-493.
96. Vaisocherova, H., et al., *Ultralow fouling and functionalizable surface chemistry based on a zwitterionic polymer enabling sensitive and specific protein detection in undiluted blood plasma.* Analytical Chemistry, 2008. **80**(20): p. 7894-7901.
97. Vaisocherova, H., et al., *Functionalizable surface platform with reduced nonspecific protein adsorption from full blood plasma-Material selection and protein immobilization optimization.* Biosensors & Bioelectronics, 2009. **24**(7): p. 1924-1930.
98. Vaisocherova, H., et al., *Investigating oligonucleotide hybridization at subnanomolar level by surface plasmon resonance biosensor method.* Biopolymers, 2006. **82**(4): p. 394-8.
99. Knoll, W., M. Zizlsperger, and T. Liebermann, *Supramolecular interfacial architectures for optical biosensing.* Abstracts of Papers of the American Chemical Society, 1997. **213**: p. 219-ANYL.
100. Jung, L.S., et al., *Binding and dissociation kinetics of wild-type and mutant streptavidins on mixed biotin-containing alkylthiolate monolayers.* Langmuir, 2000. **16**(24): p. 9421-9432.
101. Lofas, S., et al., *Methods for Site Controlled Coupling to Carboxymethyldextran Surfaces in Surface-Plasmon Resonance Sensors.* Biosensors & Bioelectronics, 1995. **10**(9-10): p. 813-822.
102. Emmenegger, C.R., et al., *Interaction of Blood Plasma with Antifouling Surfaces.* Langmuir, 2009. **25**(11): p. 6328-6333.
103. O'Shannessy, D.J., *Determination of kinetic rate and equilibrium binding constants for macromolecular interactions: a critique of the surface plasmon resonance literature.* Curr Opin Biotechnol, 1994. **5**(1): p. 65-71.
104. Myszka, D.G., *Kinetic analysis of macromolecular interactions using surface plasmon resonance biosensors.* Curr Opin Biotechnol, 1997. **8**(1): p. 50-7.
105. McDonnell, J.M., *Surface plasmon resonance: towards an understanding of the mechanisms of biological molecular recognition.* Curr Opin Chem Biol, 2001. **5**(5): p. 572-7.
106. Schuck, P. and A.P. Minton, *Analysis of mass transport-limited binding kinetics in evanescent wave biosensors.* Anal Biochem, 1996. **240**(2): p. 262-72.
107. Edwards, D.A., B. Goldstein, and D.S. Cohen, *Transport effects on surface-volume biological reactions.* J Math Biol, 1999. **39**(6): p. 533-61.
108. Marrero, J.A. and A.S. Lok, *Newer markers for hepatocellular carcinoma.* Gastroenterology, 2004. **127**(5 Suppl 1): p. S113-9.

109. Kamimori, H., et al., *Evaluation of the membrane-binding properties of the proximal region of the angiotensin II receptor (AT1A) carboxyl terminus by surface plasmon resonance.* Anal Sci, 2005. **21**(2): p. 171-4.
110. Shen, B., et al., *Biosensor analysis of the molecular interactions of pentosan polysulfate and of sulfated glycosaminoglycans with immobilized elastase, hyaluronidase and lysozyme using surface plasmon resonance (SPR) technology.* J Pharm Biomed Anal, 2003. **31**(1): p. 83-93.
111. Karlsson, R. and A. Falt, *Experimental design for kinetic analysis of protein-protein interactions with surface plasmon resonance biosensors.* J Immunol Methods, 1997. **200**(1-2): p. 121-33.
112. Situma, C., M. Hashimoto, and S.A. Soper, *Merging microfluidics with microarray-based bioassays.* Biomol Eng, 2006. **23**(5): p. 213-31.
113. Jonsson, M., et al., *Quartz crystal microbalance biosensor design II. Simulation of sample transport.* Sensors and Actuators B-Chemical, 2007. **123**(1): p. 21-26.
114. Hull, R.D., R.E. Malick, and J.G. Dorsey, *Dispersion Phenomena in Flow-Injection Systems.* Anal Chim Acta, 1992. **267**(1): p. 1-24.
115. Springer, T., M. Piliarik, and J. Homola, *Surface plasmon resonance sensor with dispersionless microfluidics for direct detection of nucleic acids at the low femtomole level.* Sensors and Actuators B-Chemical, 2010. **145**: p. 588-591.
116. Springer, T., M. Piliarik, and J. Homola, *Real-time monitoring of biomolecular interactions in blood plasma using a surface plasmon resonance biosensor.* Anal Bioanal Chem, 2010. **398**(5): p. 1955-61.
117. Gong, P. and R. Levicky, *DNA surface hybridization regimes.* Proceedings of the National Academy of Sciences of the United States of America, 2008. **105**(14): p. 5301-5306.
118. Fish, D.J., et al., *DNA multiplex hybridization on microarrays and thermodynamic stability in solution: a direct comparison.* Nucleic Acids Research, 2007. **35**(21): p. 7197-7208.
119. Fotin, A.V., et al., *Parallel thermodynamic analysis of duplexes on oligodeoxyribonucleotide microchips.* Nucleic Acids Research, 1998. **26**(6): p. 1515-1521.
120. Vaisocherova, H., et al., *Surface plasmon resonance study on HIV-1 integrase strand transfer activity.* Analytical and Bioanalytical Chemistry, 2009. **393**(4): p. 1165-1172.
121. Peterson, A.W., L.K. Wolf, and R.M. Georgiadis, *Hybridization of mismatched or partially matched DNA at surfaces.* Journal of the American Chemical Society, 2002. **124**(49): p. 14601-14607.
122. Misra, V.K. and D.E. Draper, *The interpretation of Mg2+ binding isotherms for nucleic acids using Poisson-Boltzmann theory.* Journal of Molecular Biology, 1999. **294**(5): p. 1135-1147.
123. Springer, T., et al., *Shielding effect of monovalent and divalent cations on solid-phase DNA hybridization: surface plasmon resonance biosensor study.* Nucleic Acids Research, 2010. **38**(20): p. 7343-7351.
124. Jorgensen, W.L., et al., *Comparison of Simple Potential Functions for Simulating Liquid Water.* Journal of Chemical Physics, 1983. **79**(2): p. 926-935.

125. Cornell, W.D., et al., *A 2nd Generation Force-Field for the Simulation of Proteins, Nucleic-Acids, and Organic-Molecules.* Journal of the American Chemical Society, 1995. **117**(19): p. 5179-5197.
126. Cheatham, T.E., P. Cieplak, and P.A. Kollman, *A modified version of the Cornell et al. force field with improved sugar pucker phases and helical repeat.* Journal of Biomolecular Structure & Dynamics, 1999. **16**(4): p. 845-862.
127. Perez, A., et al., *Refinement of the AMBER force field for nucleic acids: improving the description of alpha/gamma conformers.* Biophys J, 2007. **92**(11): p. 3817-29.
128. Zgarbova, M., et al., *Refinement of the Cornell et al. Nucleic Acids Force Field Based on Reference Quantum Chemical Calculations of Glycosidic Torsion Profiles.* Journal of Chemical Theory and Computation, 2011. **7**(9): p. 2886-2902.
129. Pearlman, D.A., et al., *Amber, a Package of Computer-Programs for Applying Molecular Mechanics, Normal-Mode Analysis, Molecular-Dynamics and Free-Energy Calculations to Simulate the Structural and Energetic Properties of Molecules.* Computer Physics Communications, 1995. **91**(1-3): p. 1-41.
130. Phillips, J.C., et al., *Scalable molecular dynamics with NAMD.* Journal of Computational Chemistry, 2005. **26**(16): p. 1781-1802.
131. Harvey, M.J., G. Giupponi, and G. De Fabritiis, *ACEMD: Accelerating Biomolecular Dynamics in the Microsecond Time Scale.* Journal of Chemical Theory and Computation, 2009. **5**(6): p. 1632-1639.
132. *ACEMD*. Available from: http://www.acellera.com/.
133. Feenstra, K.A., B. Hess, and H.J.C. Berendsen, *Improving efficiency of large time-scale molecular dynamics simulations of hydrogen-rich systems.* Journal of Computational Chemistry, 1999. **20**(8): p. 786-798.
134. Humphrey, W., A. Dalke, and K. Schulten, *VMD: Visual molecular dynamics.* Journal of Molecular Graphics & Modelling, 1996. **14**(1): p. 33-38.
135. Pettersen, E.F., et al., *UCSF chimera - A visualization system for exploratory research and analysis.* Journal of Computational Chemistry, 2004. **25**(13): p. 1605-1612.
136. Roe, D.R. and T.E. Cheatham, *PTRAJ and CPPTRAJ: Software for Processing and Analysis of Molecular Dynamics Trajectory Data.* Journal of Chemical Theory and Computation, 2013. **9**(7): p. 3084-3095.
137. Darfeuille, F., et al., *RNA and N3 -> P5 ' kissing aptamers targeted to the trans-activation responsive (TAR) RNA of the human immunodeficiency virus-1.* Nucleosides Nucleotides & Nucleic Acids, 2001. **20**(4-7): p. 441-449.
138. Pav, O., et al., *Synthesis of oligoribonucleotides with phosphonate-modified linkages.* Organic & Biomolecular Chemistry, 2011. **9**(17): p. 6120-6126.

7 List of Abbreviations

DNA: deoxyribonucleic acid

RNA: ribonucleic acid

m-RNA: messenger ribonucleic acid

C: cytin

T: thymin

A: adenin

G: guanin

U: uracil

PB theory: Poisson-Boltzmann theory

CC model: counterion condensation model

probes: oligonucleotide immobilized on a surface of SPR chip

target: oligonucleotide which hybridizes with a probe

solid-phase (SP) hybridization: hybridization of targets to probes on a surface of DNA/RNA chip

HE: hybridization efficiency

SPR sensor: surface plasmon resonance sensor

RNAi: RNA interference

siRNA: small interfering RNA

SELEX method: System Evolution of Ligands by EXponencial enrichment

bFGF: basic fibroblast growth factor

AS-ON: anti-sense oligonucleotide

LNA: locked nucleic acid

PNA: peptide nucleic acid

MF: morpholino phosphoroamidates

HIV: human immunodeficiency virus

AIDS: acquired immunodeficiency syndrome

UNAIDS: United Nations Programme on HIV/AIDS

RT: reverse transcriptase

IN: integrase

PR: protease

CA (p24), Vif, Vpr, Nef, Vpu (Vpu for HIV-1, Vpx for HIV-2), NC (p7), MA (p17), gp120, gp41, gp160: proteins in HIV virus

Tat, Rev and Nef: regulatory proteins

gag, *pol*, *env*, *tat*, *rev*, *nef*, *vif*, *vpr*, *vpu* (HIV-1) or *vpx* (HIV-2): genes in HIV genome

TAR: trans-activation response element

RRE: Rev responsive element

PBS: primer binding site

DIS: dimerization initial site

SD: spliced donor site

CDK9: cyclin dependent kinase 9

R06 aptamer: the privileged oligonucleotide binding to TAR hairpin

$R06_{24}$, $R06_{16}$, and $R06_{8}$: R06 aptamer with the lengths of 24-mer, 16-mer, and 8-mer

MD simulation: molecular dynamic simulation

OMe analogues: 2′-O-methyl analogues

NP-DNA: deoxyphosphoramidate DNA

SAMs: self-assembled monolayers

NHS: *N*-hydroxysuccinimide

EDC: *N*-ethyl-*N'*-(3-diethylaminopropyl) carbodiimide

TEG: triethylene glycol

B-E441, BdO_{23}, BdA_{23}, TAR probe: DNA or RNA probe

E441C, CdO_{23},Mism2, Mism3,Mism4, dT_{23}, R06 aptamer: DNA targets

P_1: oligonucleotide probe

ON428g: complementary oligonucleotide to probe P_1

P_{ref}: reference probe

$Tris_{500}$, PBS, TAR buffer: buffers

ΔG_T: Gibbs energy

K: equilibrium association constant

D: Probe density

k_{BdO23}, k_{BdA23}: calibration coefficients

ON435, ON436, ON438, ON440, ON466, ON476 and ON477: modifications placed in R06 aptamer

anti-TAR oligonucleotide: 63 different oligonucleotides based on R06 aptamer with placed modifications

EDTA: Ethylenediaminetetraacetic acid disodium salt dihydrate

8 Appendices

List of appendices:

A) JOURNAL PAPERS

Appendix I

H. Vaisocherová, J. Snášel, T. Špringer, H. Šípová, I. Rosenberg, J. Štěpánek, J. Homola: Surface plasmon resonance study on HIV-1 integrase strand transfer activity, *Analytical and Bioanalytical Chemistry* **393** (2009), 1165–1172.

Appendix II

T. Špringer, M. Piliarik, J. Homola: Surface plasmon resonance sensor with dispersionless microfluidics for direct detection of nucleic acids at the low femtomole level, *Sensors and Actuators B – Chemical* **145** (2010), 588-591.

Appendix III

T. Špringer, M. Piliarik, J. Homola: Real-time monitoring of biomolecular interactions in blood plasma using a surface plasmon resonance biosensor, *Analytical and Bioanalytical Chemistry* **398** (2010), 1955-1961.

Appendix IV

T. Špringer, H. Šípová, H. Vaisocherová, J. Štepánek, J. Homola: Shielding effect of monovalent and divalent cations on solid-phase DNA hybridization: surface plasmon resonance study, *Nucleic Acids Research* **38** (2010), 7343-7351.

Appendix V

H. Šípová, T. Špringer, J. Homola: Streptavidin-enhanced assay for sensitive and specific detection of single nucleotide polymorphism in TP53, *Analytical and Bioanalytical Chemistry* **399** (2011), 2343-2350.

Appendix VI

T. Špringer, J. Homola: Biofunctionalized gold nanoparticles for SPR-biosensor-based detection of CEA in blood plasma, *Analytical and Bioanalytical Chemistry*, **404** (2012), 2869-2875.

Appendix VII

T. Špringer, M. Bocková, J. Homola: Label-Free Biosensing in Complex Media: A Referencing Approach, *Analytical Chemistry* **85** (2013), 5637–5640.

Appendix VIII

H. Šípová, T. Špringer, D. Rejman, O. Šimák, M. Petrová, P. Novák, Š. Rosenbergová, O. Páv, R. Liboska, I. Barvík, J. Štěpánek, I. Rosenberg, J. Homola: 5′-O-Methylphosphonate nucleic acids-new modified DNAs that increase the Escherichia coli RNase H cleavage rate of hybrid duplexes, *Nucleic Acids Research*, **8** (2014), 5378-5389.

Appendix IX

T. Špringer, M. L. Ermini , B.Špačková, J. Jabloňků, J. Homola: Enhancing Sensitivity of SPR Biosensors by Functionalized Gold Nanoparticles – Size Matters, *Analytical Chemistry*, **86** (2014), 10350-10356.

B) BOOK CHAPTERS

Appendix X

P. Adam, M. Piliarik, H. Šípová, T. Špringer, M. Vala, J. Homola: Surface plasmons for biodetection, in Photonic Sensing: Principles and Applications for Safety and Security Monitoring, Editors G. G. Xiao and W. J. Bock, John Wiley & Sons, September 2012.